ISSN 2730-2695

THAI GEOSCIENCE JOURNAL

Vol. 3 No. 4 July 2022

GEOLOGY FOR PEOPLE

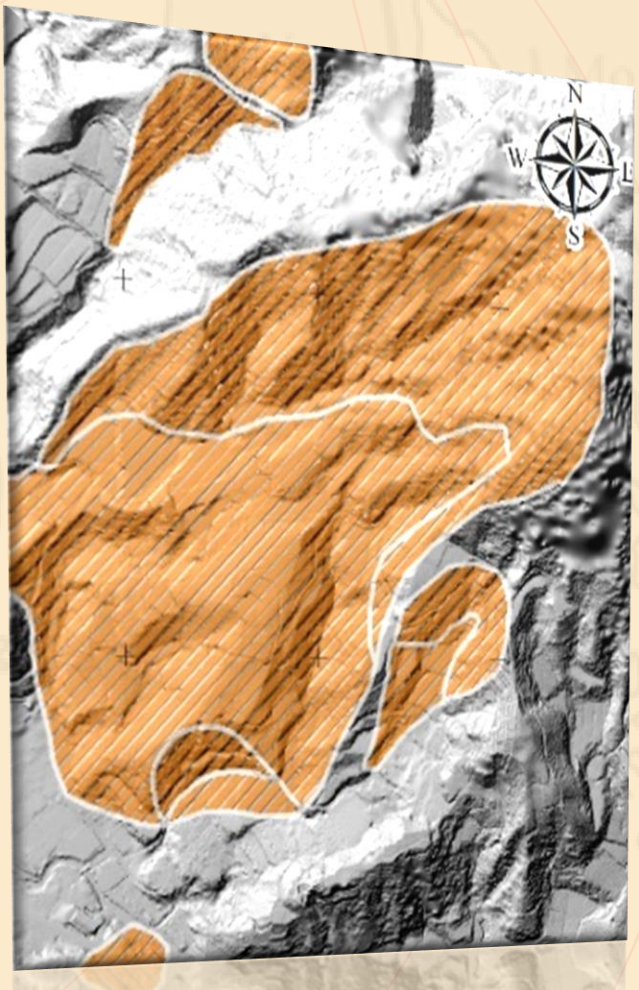

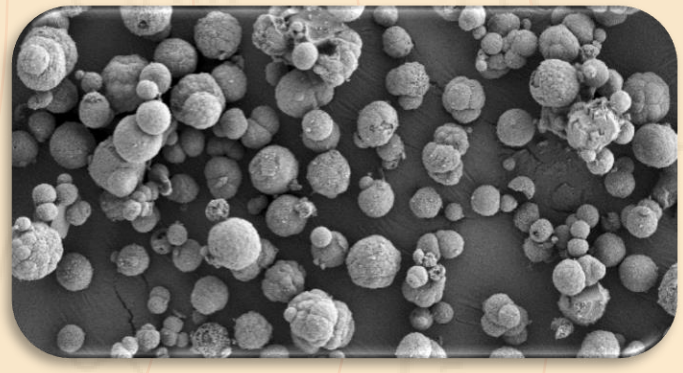

Published by
Department of Mineral Resources
Geological Society of Thailand
Coordinating Committee for Geoscience Programmes in East and Southeast Asia (CCOP)

Editorial Committee

On the cover

1) Image of Happy Geoscience Edu courses: HG-Trip. *(Yoon Jung Choi et al. p.4, fig. 3)*

2) Micrograph of PCC particles at 50 psi (*Emee Marina Salleh et al. p.9, fig. 5)*

3) Landslide inventory map of Lembah Bertam area in Cameron Highlands (*Zakaria Mohamad et al. p.31, fig.10)*

4) Regional tectonic setting of Myanmar and western Thailand. Ba Bangkok, CR Chiang Rai, HH Hua Hin, Ma Mandalay, Mo Moulmein, My Myitkyina, Np Naypyidaw, Pu Putao, Ya Yangon. (*Andrew Mitchell et al. p.37 fig. 1)*

THAI GEOSCIENCE JOURNAL

Vol. 3 No. 4
July 2022

Published By
Department of Mineral Resources • Geological Society of Thailand
Coordinating Committee for Geoscience Programmes in East and Southeast Asia (CCOP)

Thai Geoscience Journal website at http://www.dmr.go.th/tgjdmr

Preface

Thai Geoscience Journal published the first issue in July 2019 and has now reached the publication of Volume 3 Number 4. We have continued on the journal with several interesting geological articles by cooperating with the Coordinating Committee for Geoscience Programmes in East and Southeast Asia (CCOP) as co-organizers of the TGJ.

Welcome to TGJ Volume 3 Number 4 issue on July 2022. In 2022, Thailand has organized and to be the host of events related to Thailand geology, such as the revalidation of Satun Global Geopark and validation of Khorat Aspiring Geopark from UNESCO at the end of June. Geopark is one of the innovative tools for supporting a sustainable economy by using geology knowledge. In September 4th to 11th 2022, the Department of Mineral Resources of Thailand co-organized with Satun province and Satun Global Geopark will be a host of the 7th Asia Pacific Global Geoparks Network (APGN). It indicates that geology is valuable to support the Sustainable Development Goals (SDGs) in many areas in the global as the Geoparks. TGJ is glad to support this innovation in this volume as the theme of “GEOLOGY FOR PEOPLE”.

We hope that TGJ will be a small part that can support globalization and welcome all articles published on subjects of Geoscience.

Thank you very much.

(Mr. Pongboon Pongtong)
Director-General of the Department of Mineral Resources

From the editor

The Thai Geoscience journal has eventually arrived at volume 3, Number 4. We still intend to find quality articles from international researchers. In this volume, we have connected our TGJ with the Coordinating Committee for Geoscience Programmes in East and Southeast Asia (CCOP) and we have been working together on this and subsequent journal issues.

We are proud to present this volume on the theme of "GEOLOGY FOR PEOPLE" which collected geological articles related to people and society whether they be Geoscience education in Covid-19 pandemic situation, Mitigation of Carbide Lime Waste and CO_2 Gas Emission, Silica rock in crystal glass application, Landslide vulnerability and risk assessment, and Magmatic arcs and nappes in Myanmar and western Thailand.

We would like to express our appreciation to all of our TGJ Volume 3 Number 4's authors for publishing their valuable articles in TGJ. As the TGJ editor in chief, I would like to express my thanks to TGJ's honorary, advisory, associate editors, and reviewers for their kind support. Special thanks are due to the editorial secretary team who have worked very hard on every TGJ issue. We continue to strive to make TGJ a high standard international journal and welcome all researchers to be TGJ members and to be part of our geoscience community.

Thank you very much.

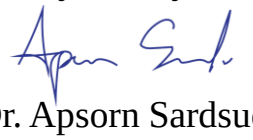

(Dr. Apsorn Sardsud)
Editor in Chief
Thai Geoscience Journal

Thai Geoscience Journal
Vol. 3 No. 4
July 2022
ISSN 2730-2695

LIST OF CONTENTS

Thai Geoscience Journal website at http://www.dmr.go.th/tgjdmr
Printed: 2twin Printing tel +66 2 185 9953, July 2022

Thai Geoscience Journal 3(4), 2022, p. 1-4

ISSN-2730-2695; DOI-10.14456/tgj.2022.6

Happy Geoscience Edu: A new geoscience education system in the time of COVID-19

Yoon Jung Choi, Sujeong Lee, Eunsu Lee, Chanung Park, and Samgyu Park*

Korea Institute of Geoscience and Mineral Resources, Daejeon, Republic of Korea
Corresponding author: samgyu@kigam.re.kr
Received 17 March 2021; Accepted 7 December 2021.

Abstract

The COVID-19 pandemic weakened many education systems worldwide. As a geoscience education center, the International School for Geoscience Resources (IS-Geo) of the Korea Institute of Geoscience and Mineral Resources (KIGAM) also faced difficulties in educating the public during the pandemic. To overcome the difficulties of a face-to-face education system, IS-Geo created a new education system brand named "Happy Geoscience Edu", which contains various home-training kits, special online courses, and small-group field training courses. Happy Geoscience Edu consists of four different courses: Happy Geoscience Box, Happy Geoscience Class, Happy Geoscience Talk, and Happy Geoscience Trip. In the 'Happy Geoscience Box' course, IS-Geo sends geoscience boxes to families with children. The box contains various geoscience experiment kits together with written instructions and scientific explanations. With this Happy Geoscience Box, parents can guide their children to run the experiments at home. 'Happy Geoscience Class' is an online education course mainly for primary to high school students. In classrooms, the students can learn geoscience experiment on a chosen topic through online lectures and follow the instructions. 'Happy Geoscience Talk' is an interactive event between KIGAM and the general public. Anyone can send their questions, within the suggested topic, to IS-Geo and then the experts from KIGAM will answer (talk) their questions via YouTube. All 'talks' are opened to the public since it aims to increase the public's attention to geoscience. 'Happy Geoscience Trip' is a small-group field training course on UNESCO Geoparks in Korea. It aims to educate local commentators and the public about the detailed geology of the Geoparks. Happy Geoscience Edu has already received positive feedbacks in Korea. We hope this can inspire the education systems in other CCOP member countries.

Keywords: coronavirus, education, E-learning, Geoscience, online education, virtual learning

1. Introduction

Coronavirus (COVID-19) pandemic has negatively affected education systems worldwide. As a geoscience education center, International School for Geoscience Resources (IS-Geo) has also faced difficulties in continuing the traditional face-to-face courses. Many institutions switched to online and virtual teaching, to narrow the education gaps in such pandemic (Ali, 2020; Daniel, 2020; Liguori & Winkler, 2020). Here we introduce a new education system "Happy Geoscience Edu" to overcome the difficulty in our education caused by the pandemic.

2. International School for Geoscience Resources (IS-Geo)

International School for Geoscience Resourses (IS-Geo), a geoscience education center of Korea Institute of Geoscience and Mineral Resources (KIGAM), was established in 2010 to spread the accumulated researches achieved by KIGAM. From 2010 to 2019, IS-Geo educated over ten thousand trainees worldwide. **Fig.1** summarizes the standard courses organized by IS-Geo. The Globalization Course is structured for international geoscience experts to learn the newest research topics in their fields. In Future Course, we teach students geoscience knowledge outside textbooks to

increase their interest in geoscience. Finally, the Communication Course is organized to raise public awareness of geoscience issues. These courses are based on face-to-face learning systems and, thus, due to the COVID-19 pandemic, it was challenging to organize IS-Geo's standard education programs.

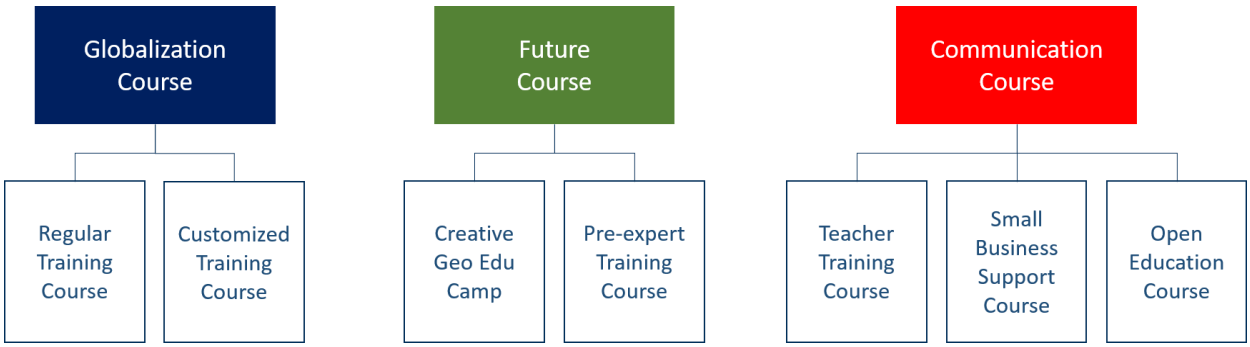

Fig. 1: Standard education programs of IS-Geo. The programs are divided into three courses depending on the education target. All courses involve traditional face-to-face learning systems.

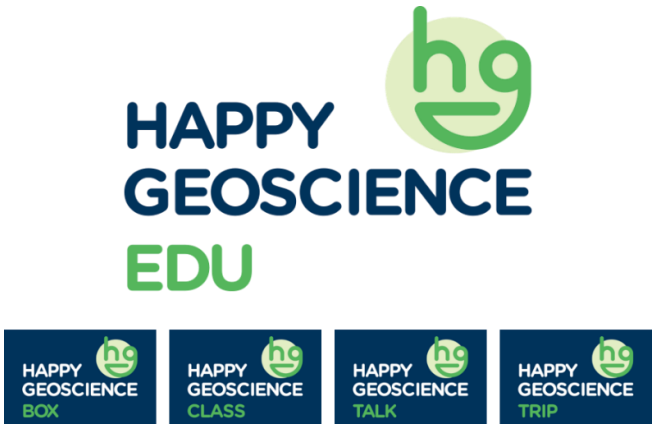

Fig. 2: Logo of the Happy Geoscience Edu.

3. Happy Geoscience Edu (HGE)

Happy Geoscience Edu (HGE) aims to overcome the education disruptions during the COVID-19 pandemic period. Unlike the traditional face-to-face education system, the HGE uses both online and offline materials to avoid direct contact between the instructor and the trainees. There are four different courses in HGE: Happy Geoscience Box (HG-Box), Happy Geoscience Class (HG-Class), Happy Geoscience Talk (HG-Talk), and Happy Geoscience Trip (HG-Trip). As summarized in **Table 1**, each HGE course has different education targets and goals.

HG-Box was organized in April 2020, just after the first COVID-19 outbreak in Korea. In HG-Box course, IS-Geo sends geoscience boxes to families with children staying at home due to the closure of schools. This box contains various geoscience experiment kits (more than nine random kits) such as earthquake detectors, fossil exploration experiments, etc. Written instructions and scientific explanations are also included in the box so the parents can guide their children to run the experiments at home. In 2020, 500 families participated in HG-Box and many participants left positive feedbacks on various social network sites.

HG-Class is an online education course for primary, middle and high school students. This course aims to increase student's interest in geoscience and teach them knowledge outside textbooks. The students can learn geoscience experiment on a chosen topic through online lectures and follow the instructions in classrooms. Teachers can guide their students based on the instruction form sent to them separately. Last year, over one thousand students from 16 schools participated in HG-Class.

HG-Talk is an interaction event between KIGAM and the general public. Anyone can send their questions, within the suggested topic, to IS-Geo and then the experts from KIGAM will answer the questions via YouTube. All 'talks' are opened to the public since the course aims to increase the public's attention to geoscience. In 2020, IS-Geo covered six different geoscience topics: paleontology, sedimentary rocks, gemstones (gem minerals), radon, landslides, and climate change. HG-Talk is available on KIGAM and IS-Geo YouTube Channel.

HG-Trip is a small group field training course on UNESCO Geoparks in Korea. It aims to educate Geopark commentators and the local people about the detailed geology of the Geoparks. HG-Trip is organized into two parts; an online theory course and an offline field course. First, the instructor, a professional geologist, explains the background geology of the Geopark through online lectures. Then, the participants are invited to the Geoparks for a field trip with the instructor. Unlike other HGE courses, the HG-trip could not avoid face-to-face meetings due to the field trip. Therefore, all participants should wear masks during the whole fieldwork. Last year we organized three HG-Trip courses, twice in Hantangang River Geopark, and once in Jeju Geopark. Approximately thirty local commentators participated in each course.

Table 1: Summary of the Happy Geoscience Edu courses.

	HG-Box	**HG-Class**	**HG-Talk**	**HG-Trip**
Target	Families with children	Students	General public	Geopark commentators
Aim	Distribute home-geoscience kits	Encourage students to study geoscience	Raise public attention to geoscience	Educate Geopark commentators
Online materials	No	Yes	Yes	Yes
Offline materials	Yes	Yes	No	Yes
Instructor	Parents	Online instructor	KIGAM's experts	Professional Geologists
Who can apply?	Parents	Teachers	Anyone	Commentators

4. Conclusions

As a government funded organization, the participation of Happy Geoscience Edu is free of charge. Due to high demand, the participants of the HGE courses are selected on a first--come, first-served basis. Happy Geoscience Edu has already received positive feedbacks in Korea. IS-Geo will continue to organize education programs to increase geoscience awareness. We hope our work can inspire the education systems in other CCOP member countries.

Fig. 3: Image of Happy Geoscience Edu courses: A) HG-Box, B) HG-Class, C) HG-Talk and D) HG-Trip.

Reference

Ali, W. (2020). Online and remote learning in higher education institutes: A necessity in light of COVID--19 pandemic. *Higher education studies*, *10*(3), 16--25.

Daniel, J. (2020). Education and the COVID-19 pandemic. *Prospects*, *49*(1), 91-96.

Liguori, E., & Winkler, C. (2020). From offline to online: Challenges and opportunities for entrepreneurship education following the COVID-19 pandemic.

Thai Geoscience Journal 3(4), 2022, p. 5-11

ISSN-2730-2695; DOI-10.14456/tgj.2022.7

Mitigation of carbide lime waste and CO_2 gas emission from acetylene gas industry: feasible technique of high-grade PCC production

Emee Marina Salleh[1*], Rohaya Othman[1], Siti Noorzidah Mohd Sabri[1]

[1]Mineral Research Centre, Department of Mineral and Geoscience Malaysia, Jalan Sultan Azlan Shah, 31400 Ipoh, Perak, Malaysia

Corresponding author: emeemarina@jmg.gov.my

Received 17 March 2021; Accepted 1 December 2021.

Abstract

The global acetylene gas market is currently witnessing stable growth. Owing to its high flame--temperature properties, acetylene gas is extensively used for numerous metalworking applications including oxy-acetylene cutting, heat treating, soldering, brazing and welding. Acetylene gas is a colourless combustible gas that is produced through the combination of calcium carbonate ($CaCO_3$) and water. However, the gas manufacturing results in a production of carbide lime as a by-product that is classified as a scheduled waste in Malaysia under Environmental Quality Act: EQA 1974 (SW 427). In addition to the abundant carbide lime waste, the acetylene manufacturing also causes an increase in carbon dioxide (CO_2) gas emission that trap heat in the atmosphere. This phenomenon has become a crucial environmental concern as the rise of CO_2 gas emission leads to global warming. In mitigating the accumulative wastes, this current work was performed by revolutionising the carbide lime waste that is rich in calcium hydroxide ($Ca(OH)_2$) of 25 to 30% and CO_2 gas waste as a main precursor of carbonate (CO_3^{2-}) ions in producing high--grade precipitated calcium carbonate (PCC). The high-grade PCC was produced using these industrial wastes as primary starting materials via a feasible carbonation technique. In increasing the PCC yield, the production of PCC was initiated via forming an ionic solution by extracting Ca^{2+} ions from carbide lime waste using a promoter agent. The current outcome signified that ~20 g of high-grade PCC with a purity of 98% was produced for every 1 litre of ionic solution. Interestingly, miscellaneous functional morphologies namely rhombohedral and spherical structures of PCC were formed, attributable to various processing parameters. Effectively, the PCC production was completed within less than 10 minutes per litre of ionic solution which significantly offered a fast-rate process. The conducted feasible carbonation technique provides high potential in converting the harmful industrial wastes to profitable products. Via this technique, the production of high-grade PCC as a main product with zero waste, not only reduces the waste management cost but also increases the industrial profits. Remarkably, the recycling of abundant carbide lime waste and CO_2 gas usage in producing high-grade-high-profit PCC results in zero waste production, and thus may help in preserving environmental sustainability.

Keywords: carbide lime waste, feasible carbonation, Precipitated calcium carbonate, waste mitigation

1. Introduction

In the fabrication industry, acetylene gas is needed for applications that involve metal including welding, cutting, and heat treating. Owing to its properties, acetylene forms an important part of numerous crucial processes in industries that make it an extremely useful gas (Han et al., 2006). However, the production of acetylene results in a formation of massive carbide lime as by-product. In Malaysia, the carbide lime waste is classified as a scheduled waste under the Environmental Quality Act; EQA 1974 (SW 427). The carbide lime waste is environmentally hazardous which is attributable to its high alkalinity with a pH of ~12.5, unpleasant odour and it can cause irritation to skin and throat (Salleh et al., 2021). In 2018, almost 20,000 tonnes of carbide lime has been produced from the Malaysian

acetylene gas industry and this statistic keeps increasing year by year. This condition makes the carbide lime an avoided by-product where the industry has to pay a high cost for water treatment in disposing of the scheduled waste. Consequently, vast amounts of carbide lime waste require urgent utilisation to avert handling and disposal difficulties. **Fig. 1** shows a dumping site of carbide lime waste from Malaysian acetylene gas manufacturing.

Fig. 1: Abundant carbide lime waste at Malaysian acetylene gas manufacturing.

In addition to the production of carbide lime waste, the manufacturing of acetylene gas has also caused an increase in carbon dioxide (CO_2) gas emission. Currently, the emission of CO_2 gas into the atmosphere has increased to over 400 parts per million (ppm) due to human activities and industries causing a climate change phenomenon. The climate change encompasses not only the rising average temperatures that is referred to as global warming but also extreme weather events, shifting wildlife populations and habitats, rising seas, and a range of other impacts (Rattapong et al., 2019). Globally, the output of greenhouse gases is a source of severe concern. According to this scenario in the acetylene industry, this innovation is introduced by recycling the CO_2 gas in order to minimize its emission into the atmosphere.

In mitigating the accumulative wastes, the carbide lime waste that is rich in calcium hydroxide ($Ca(OH)_2$) up to 25% to 30% and CO_2 gas were targeted to be the main precursor in producing a more profitable product, i.e. precipitated calcium carbonate (PCC). By utilising those wastes as the main precursors, it not only enhances the production of a profitable product via a feasible technique but it can significantly revolutionise its usage.

Consequently, this approach can offer a promisingly high return to industry especially the acetylene gas manufacturers (due to the relatively high amount of the waste) and can preserve the environmental sustainability by converting the industrial waste to wealth.

PCC is the most extensively used mineral filler in numerous commercial applications which is due to its large range of properties, thus makes it highly applicable in fulfilling various needs. There are a number of uses of PCC as a mineral filler in wide-range industrial applications including papermaking, paint, rubber and plastic, sealants, pharmaceutical and skincare products (Han et al., 2007; Ana et al., 2010; Ligia et al., 2017). There are several approaches in synthesizing PCC and commercially, the carbonation process is the most commonly used technique (Hadiko et al., 2005; Catagay et al., 2018). Carbonation is a complex process and involves simultaneous dissolution of calcium hydroxide ($Ca(OH)_2$) and carbon dioxide (CO_2) as well as the crystallization of calcium carbonate ($CaCO_3$) (Yong et al., 2005, Othman et al., 2015). The carbonation reaction is generally performed in a series of reactors under closely controlled operating conditions to produce the PCC with

required morphology and particle size distribution (Santos et al., 2012; Onimisi et al., 2016). Since the reaction between Ca^{2+} and CO_3^{2-} ions is the main approach to synthesize PCC, the generation of CO_3^{2-}dominates the reaction during the process (Shirsath et al., 2015; Sun et al., 2017). It is well known that CO_2 gas can be used as raw material to provide CO_3^{2-} and then react with Ca^{2+} obtaining PCC (Walsh and Mann, 1995; Hadiko et al., 2005). Hence, this current work was mainly focused on producing high-grade precipitated calcium carbonate (PCC) by recycling industrial wastes from acetylene gas industries i.e. carbide lime and CO_2 gas. Inclusively, this research methodology in utilising industrial waste as a promising industrial raw material will lead to green environment as well as will generate more utilisation of mineral resources efficiently.

2. Research Methodology

2.1 Materials

Carbide lime waste was acquired from an acetylene gas manufacturer (MCB Industries, Sdn. Bhd., Taiping, Perak). Quicklime which also used as a controlled starting material was obtainedfrom Simpang Pulai quarry in Malaysia. Sucrose that acts as a promoter agent was purchased from a local company and compact CO_2 gas of 99% purity was supplied by Linde Malaysia Sdn. Bhd.

2.2 PCC Production via Continuous Carbonation Technique

Ionic solution containing calcium ions (Ca^{2+}) was prepared using carbide lime waste (or quicklime) as starting materials with the addition of 10 wt.% of the promoter agent. 1 litre of Ca-rich ionic solution was continuously supplied and simultaneously, CO_2 gas was introduced in order to provide an effective carbonation process. Prior to the PCC production using carbide lime waste, high-purity quicklime was utilised in order to ensure the capability of the studied technique using ionic solution. The presence of both Ca-rich ionic solution as liquid droplets and CO_2 gas under high pressure in the carbonation reactor might enhance the precipitation mechanism of PCC.

In order to investigate an effect of CO_2 gas flow on the PCC formation, an atomizing air pressure was varied at 10, 20, 30, 40 and 50 psi. In addition, liquid air pressure and cylinder air pressure were kept constant at 30 psi and 45 psi, respectively. 1 litre of PCC slurry was collected from the carbonation process. The synthesized PCC was then filtered and washed using warm water to remove the excess promoter agent. The filtrate was dried in an oven at 60 °C for 24 hours. The time taken for the carbonation process and weight of the PCC yield was measured. **Fig. 2** shows a research flow of producing high-grade PCC from calcium-based mineral.

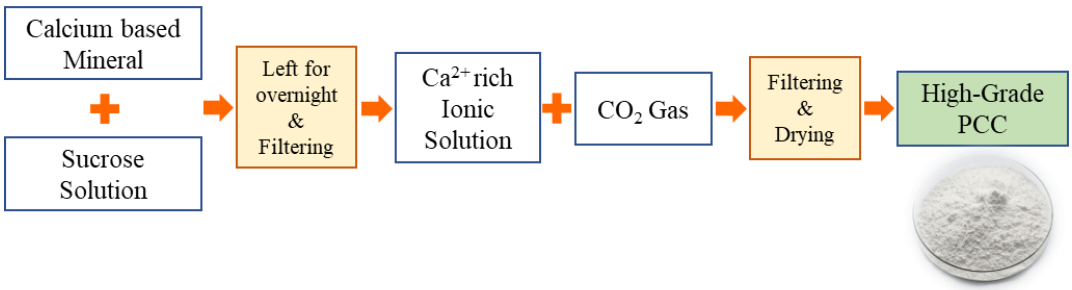

Fig. 2: A research flow of producing high-grade PCC from calcium-based mineral.

2.3 Characterization of Produced PCC

The morphology of the synthesized PCC was evaluated using Field Emission Scanning Electron Microscope (FESEM) *Supra 40V Zeiss, Germany*. The particle size distribution of the PCC was measured using Laser Particle Size Analyzer.

3. Results and Discussion

Fig. 3 shows the effect of atomizing air pressure on carbonation time and the weight of produced PCC. The carbonation time gradually increased which as a function of atomizing air pressure. This phenomenon was attributed to the longer time was required in order to achieve a complete precipitation reaction at higher CO_2 gas feeding (Catagay et al., 2018). In addition to the increasing carbonation time, the PCC yield was also increased with increasing atomizing air pressure up to 40 psi. However, above that pressure, the PCC yield was slightly reduced. This situation suggested that the applied atomizing air pressure provided different effect on the both carbonation time and PCC yield.

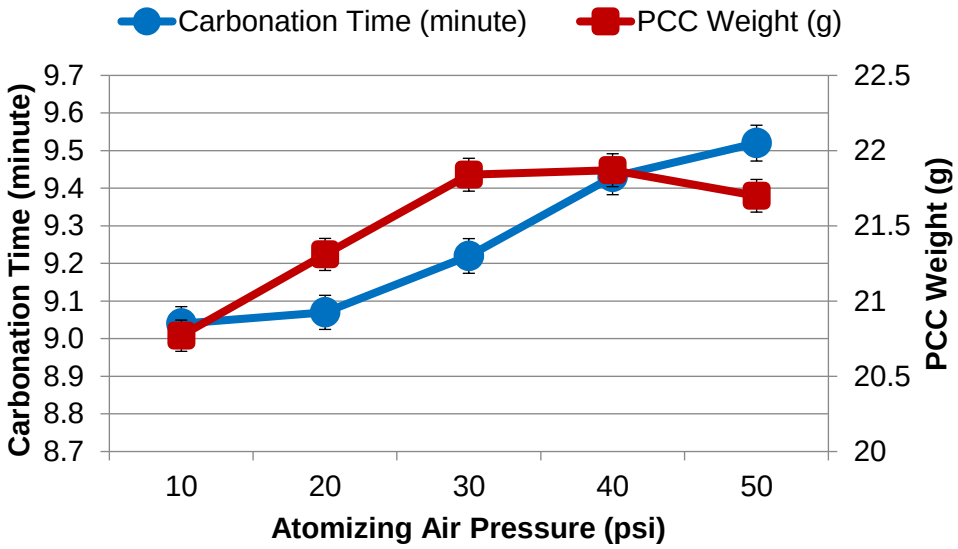

Fig. 3: Carbonation time and weight of PCC yield at various atomizing air pressure.

Fig. 4 displays the size distribution of PCC particle at various atomizing air pressures. The PCC particle sizes were between 11 µm to 18 µm. As can be seen, the coarsest PCC particles (17.938 µm) were obtained at 30 psi which might be due to the particle intergrowth phenomenon that occurred during the carbonation reaction (Sun et al., 2017). The fluctuating particle size distribution of the produced PCC suggested the particle growth occurred differently under various CO_2 feeding pressure.

Fig. 5 illustrates the morphologies of PCC particles at different atomizing air pressures. At 30 psi, the PCC particles existed in a form of rhombohedral structure. According to the micrograph, there was a formation of inter-growth particles which resulted in enlargement of particles size as reported previously. Interestingly, at higher atomizing air pressure of 50 psi, the PCC particles were dominantly spherical. This current finding signified that various morphologies of produced PCC might be acquired by varying the atomizing air pressure (which was denoted to CO_2 gas feeding) during the precipitation process.

In ensuring the capability of this currently used technique, the research work was performed by recycling carbide lime waste from the acetylene gas industry as a primary starting material. **Table 1** shows a comparative study on PCC production from high-grade quicklime and low-grade carbide lime waste. According to the findings, the carbonation time for producing PCC using carbide lime waste (6 to 18 minutes) was slightly longer than the time taken by utilising quicklime (about 9 minutes) as a main source of Ca^{2+} ions. In addition, the PCC yield produced from carbide lime waste was between 9 to 12 g at different atomizing air pressure. The attained yield was considerably lower than the quicklime based PCC which was about 21g. This phenomenon was attributed to the lower calcium content in the carbide lime waste which was only 25% to 30% of calcium hydroxide as compared to the purely quicklime (99.9 purity) (Han et al., 2006).

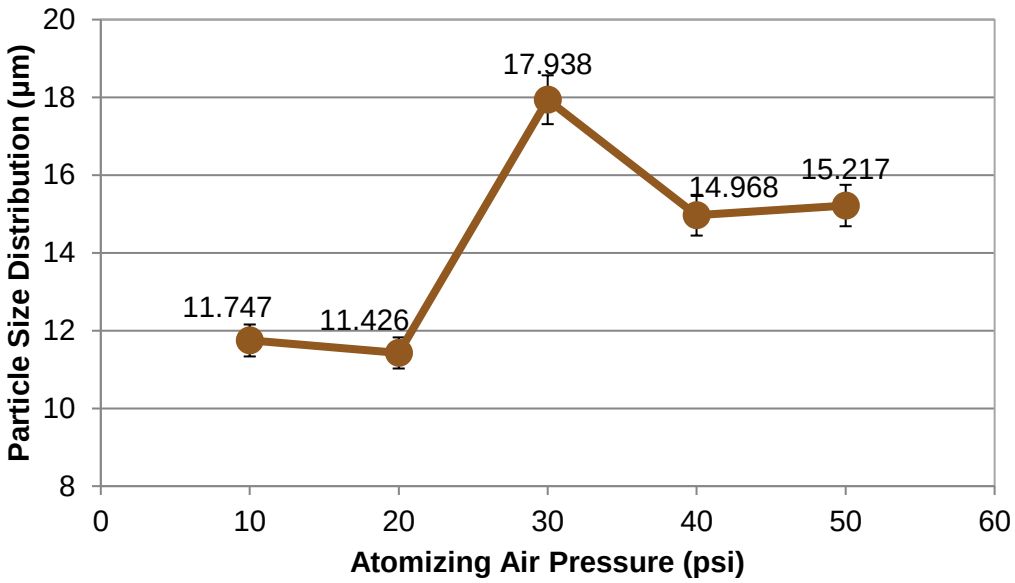

Fig. 4: Particle size distribution of produced PCC at various atomizing air pressure.

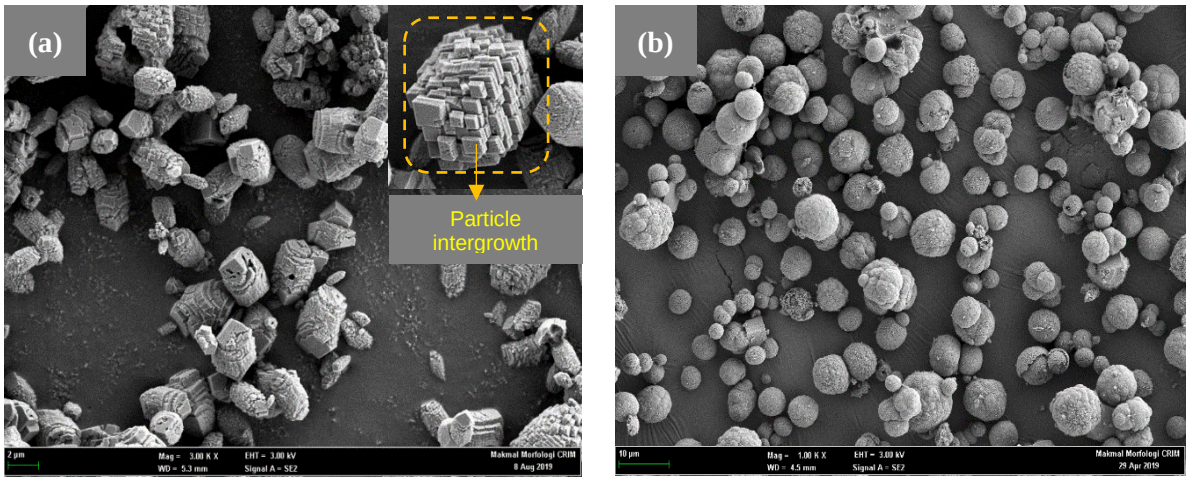

Fig. 5: Micrograph of PCC particles at (a) 30 psi and (b) 50 psi.

Interestingly, via this currently used technique, the produced PCC from carbide lime waste showed markedly high purity of about 98% that represented the high-grade PCC. This finding might help industrial players in converting the massive waste into more profitable product i.e. high-grade PCC.

4. Conclusions

According to the findings, the currently used technique showed high potential in converting the harmful carbide lime waste to profitable products of PCC. The carbonation time gradually increased as a function of atomizing air pressure and the weight of PCC also increased with increasing atomizing air pressure up to 40 psi. The size distribution of PCC particles were between 11 µm to 18 µm. According to morphological study, various structures of PCC particles were formed at different atomizing air pressures. At low pressure of 30 psi, there was intergrowth of rhombohedral PCC particles. Meanwhile at higher pressure of 50 psi, the PCC particles formed in more spherical structures. Effectively, the utilisation of ionic solution as a feed stock showed high potential in extracting Ca^{2+} ions even from the industrial waste for producing high-grade PCC. By employing this technique, the produced PCC from carbide lime

Table 1: Carbonation time and weight of produced PCC from different starting materials at various.

Starting Materials	Atomizing Air Pressure (psi)	Carbonation Time (minutes)	PCC Yield (g)
Carbide Lime Waste	10	14.53	12.2
	20	18.21	10.5
	30	6.18	9.3
Quicklime	10	9.04	20.8
	20	9.07	21.3
	30	9.22	21.9

waste showed markedly high purity of about 98% that represented the high-grade PCC. Profitably, CO_2 gas was used as main source of CO_3^{2-} ions, thus can mitigate its excessive emission into the atmosphere. Consequently, the recycling of abundant carbide lime waste and CO_2 gas from acetylene gas industry might not only reduce the waste management cost but might also increase the industrial profit and importantly, this scenario might help to sustain the natural resources and preserve the environmental sustainability.

Acknowledgement

This work was supported by the Ministry of Energy and Mineral Resources and MCB Industries Sdn. Bhd. The authors would like to thank the Mineral Research Centre, Department of Mineral and Geoscience Malaysia and the Rock Based Technology Section for technical support.

References

Ana M.L.P., Roberta P., Carlos G.G, Lourdes F.V., & C. Domingo.(2010). A breakthrough technique for the preparation of high-yield precipitated calcium carbonate. *The Journal of Supercritical Fluids*, *52*, 298-305.

Cagatay M.O., & Batur E. (2018). Influence of pH on morphology, size and polymorph of room temperature synthesized calcium carbonate particles, *Powder Technology*, *339*, 781-788.

Hadiko G., Han Y., Fuji M., & Takahashi M. (2005). Synthesis of hollow calcium carbonate particles by the bubble templating method, *Materials Letters*, *59*, 2519-2522.

Han J.T., Xu X., & Cho K. (2007). Sequential formation of calcium carbonate superstructure: From solid/ hollow spheres to sponge-like/solid films. *Journal of Crystal Growth*, *308*, 110–116.

Han Y.S., Hadiko G., Fuji M., & Takahashi M. (2006). Influence of initial $CaCl_2$ concentration on the phase and morphology of $CaCO_3$ prepared by carbonation, *Journal of Materials Science*, *41*, 4663–4667.

Ligia M.M.C., Gabriel M.O., & Rafael S. (2017). Precipitated calcium carbonate nano-microparticles: applications in drug delivery. *Advances in Tissue Engineering & Regenerative Medicine Open Access*, *3*, 336–340.

Onimisi J.A., Roniza I., Kamar S.A., Norlia B., & Hashim H. (2016). A novel rapid mist spray technique for synthesis of single phase precipitated calcium carbonate using solid-liquid-gas process. *Korean Journal of Chemical Engineering*, *34*, 1-5.

Othman A., Isa N., & Othman R. (2015). Preparation of precipitated calcium carbonate using additive and without additive. *Jurnal Teknologi*, *77*, 49-53.

Rattapong T., Ratchanon P., Pornpote P., and Benjapon C. (2019). Computational fluid dynamics of sulfur dioxide and carbon dioxide capture using mixed feeding of calcium carbonate/calcium oxide in an industrial scale circulating fluidized bed boiler. *Applied Energy*, *250*, 493-502.

Salleh E.M., Othman R., Mahim Z., & Mohd Sabri SN. (2021). Effect of Liquid Feeding Rate on Carbonation of Precipitated Calcium Carbonate via Continuous Method. *Journal of Physics: Conference Series*, 2080 012017.

Santos R.M., Pieter C., & Tom V.G. (2012). Synthesis of pure aragonite by sonochemical mineral carbonation. *Chemical Engineering Research and Design*, *90*, 715-725.

Shirsath S.R., Sonawane S.H., Saini D.R., and Pandit A.B. (2015). Continuous precipitation of calcium carbonate using sonochemical reactor. *Ultrasonics Sonochemistry*, *24*, 132-139.

Sun J., Wang L., & Zhao D. (2017). Polymorph and morphology of CaCO3 in relation to precipitation conditions in a bubbling system, *Chinese Journal of Chemical Engineering*, *25*(9) 1335-1342.

Walsh D., & Mann S. (1995). Fabrication of hollow porous shells of calcium carbonate from self-organizing media. *Nature*, *377*, 320-323.

Yong S.H., Hadiko G., Fuji M., and Takahashi M. (2005). A Novel Approach to Synthesize Hollow Calcium Carbonate Particles. *Chemistry Letters*, *34*, 152-153.

Thai Geoscience Journal 3(4), 2022, p. 12-19

ISSN-2730-2695; DOI-10.14456/tgj.2022.8

Properties and behavior of silica rock from east coast Malaysia region in crystal glass application

Syarifah Aminah Ismail*, Mohd Idham Mustaffar

Mineral Research Centre, Mineral and Geoscience Department Malaysia, Jalan Sultan Azlan Shah, 31400 Ipoh, Perak, Malaysia

**Corresponding author: syarifahaminah@jmg.gov.my, idham@jmg.gov.my*

Received 17 March 2021; Accepted 3 July 2021.

Abstract

Crystal glass is defined as colorless and translucent glass, which is generally applied as tableware utensils and art products, in compliance with the ASTM C162-56 standard method. Traditionally, crystal glass was manufactured using silica sand with SiO_2 purity of not less than 99.5 %. In this research, local silica rock acquired from the east coast of Malaysia region was utilized in the production of crystal glass. Previous studies revealed that raw silica rocks possess a good quality, but still inadequate to comply with the minimum requirements for crystal glass making. The purpose of this study was to improve the quality of silica rock via a physico-chemical method that comprised simultaneous attrition scrubbing and acid treatment. In this method, variable citric acid concentrations of less than 1 %, and constant scrubbing time and speed of agitation of 20 minutes and 1250 rpm, respectively were implemented. Markedly, citric acid was found effective in improving the purity of SiO_2, where 99.8 % purity was successfully achieved at 0.75 % acid concentration. XRD analysis revealed trigonal crystals system of SiO_2 in the silica rock samples. By implementing the novel crystal glass formulation, crystal glass with density of ≥ 2.40 g/cm^3, Vickers hardness of 550 ± 20 kg.f/cm^2, and refractive index of ≥ 1.5 was successfully produced, which complied with the standard requirements of BS 3828:1973.

Keywords: Glass application, Physical-chemical method, silica rock

1. Introduction

Glass is an important material owing to its attractive appearance and versatile usage. The main composition of glass includes sand, lime (alkaline earth oxide), sodium or potassium oxide (alkali oxide) and other elements, where each component has its own contribution to the overall properties of the glass. Particularly, potassium contributes to enhance the light refraction and transparency of glass, making it more appealing. In addition, zinc is commonly added into the composition for chemical durability and safety in the glass products. In general, glass is categorized into four distinct groups, namely borosilicate, glass, crystal glass, and lead crystal. Composition in crystal glass, which contains 10 % of metal oxides, is highly priced due to the quality of its raw material. Small impurities such as iron could affect the crystal glass color, hence high purity sand (silica oxide) is commonly used to over--come this drawback. The crystal glass from local silica sand has been reported with hardness values between 517 kg./cm^2 to 520 kg./cm^2 (Mohamad Haniza Mahmud and Abdul Hadi Abdul Rahman, 2016), which are still acceptable but it requires improvement for crystal glass quality. In enhancing the properties of silica, several methods were suggested in the literature, including the use of ultrasound for surface cleaning of silica (Farmer and Jameson, 2000), acid leaching (Khalifa and Ezzaouia, 2019), and reverse flotation technique (Yuan and Chen, 2018).

In this current research, crystal glass from local silica rock which is from argillaceous rock, volcanic and limestone formation was prepared via a physico-chemical method using low concentrations of organic acid (less than 1%). Attrition scrubbing was conducted with citric acid as the chelating agent, which has the capability to recover silica content and remove

impurities such as iron. Moreover, in comparison to other conventional acids, e.g. sulfuric acid, hydrochloric acid, or nitric acid, the cost of citric acid is much lower (Bouabdallah and Chaib, 2015). Citric acid is a natural acid with low molecular weight. It is considered as a non-persistent biodegradable product (Romkens and Draaisma, 2002) with a half-life in soil suspension of close to 8 days (Brynhildsen and Rosswall, 1997). These characteristics make citric acid as potentially the sole medium for the effective recovery of silica oxide even at a concentration as low as 0.05 mol/L, with no risk for pollution or post-treatment requirement (Larba and Tifouti, 2013).

However, to the best of the authors' knowledge, no studies are available concerning the use of silica rock for crystal glass fabrication. In view of that, this present work reveal the implementation of a new source of silica rock from the east coast Malaysia region for crystal glass manufacturing, by considering its lower density, refractive index, and Vickers hardness than those of silica sand.

2. Methodology

2.1 Field investigation and sample collection

Fig. 1 shows the maps of silica rock deposit for this study located in Lojing, Gua Musang, Kelantan. The potential silica rock deposit an area of about 34.69 acres. Outcrop mapping and rock blocking were carried out using transverse methods with the aid of compasses, measuring tapes, GPS devices, and topographic maps (1:50,000 scale to base map). Based on visual observation, the silica rock samples were characterized with light greyish color and rough surface, as illustrated in **Fig. 2**. Different quartz colorations were observed due to various contents of SiO_2 and impurities. Gua Musang formation comprises of argillaceous rock, volcanic and limestone. The quartz ridge or dyke is believed to be a late phase magma residue that intruded into metasedimentary rocks and shifted by fault zone at the boundary between the Gua Musang Formation and the Silurian-Devonian metamorphic rock in the Late Triassic period (Ngah, 1986 and Foo, 1973).

2.2 Experimental work

In this study, 30 kg of silica rock samples was collected from Lojing in Gua Musang, Kelantan. The samples were analyzed using X-ray fluorescence (XRF) in order to identify the elemental composition prior to attrition scrubbing treatment. From the analysis, the samples showed the presence of SiO_2, Fe_2O_3, Cr_2O_3, and Al_2O_3 (Table 2). The process of attrition scrubbing is commonly employed for ion reduction instead of SiO_2 content enhancement. However, this process is important since the presence of Fe_2O_3 and other impurities could influence the quality of crystal glass. (Nishkov and Grigorova, 2011).Therefore, an optimization of the final product of crystal glass after attrition scrubbing process was carried out in this study.

The silica rock samples were sieved in order to obtain a fraction of particle size that is less than 600 µm. The samples were subsequently subjected to attrition scrubbing operation using a laboratory "Denver flotation cell" with a Perspex container, as shown in **Fig. 3**.

Optimization of the scrubbing process was performed by studying the effect of varying acid concentrations. The scrubbed silica rocks were deslimed and thoroughly washed using water prior to mixing for palletizing processes. In this study, the crystal glass formulation employed is shown in Table 1.

Table 1: Crystal glass formulation.

Component	Percentage
SiO_2	60-65
Na_2O	11-4
K_2O	6-8
BaO	6-8
Ba_2O_3	1-4
CaO	7-10
Sb_2O_3	1-3
Al_2O_3	1-3
Na_2SiO_3	2-5

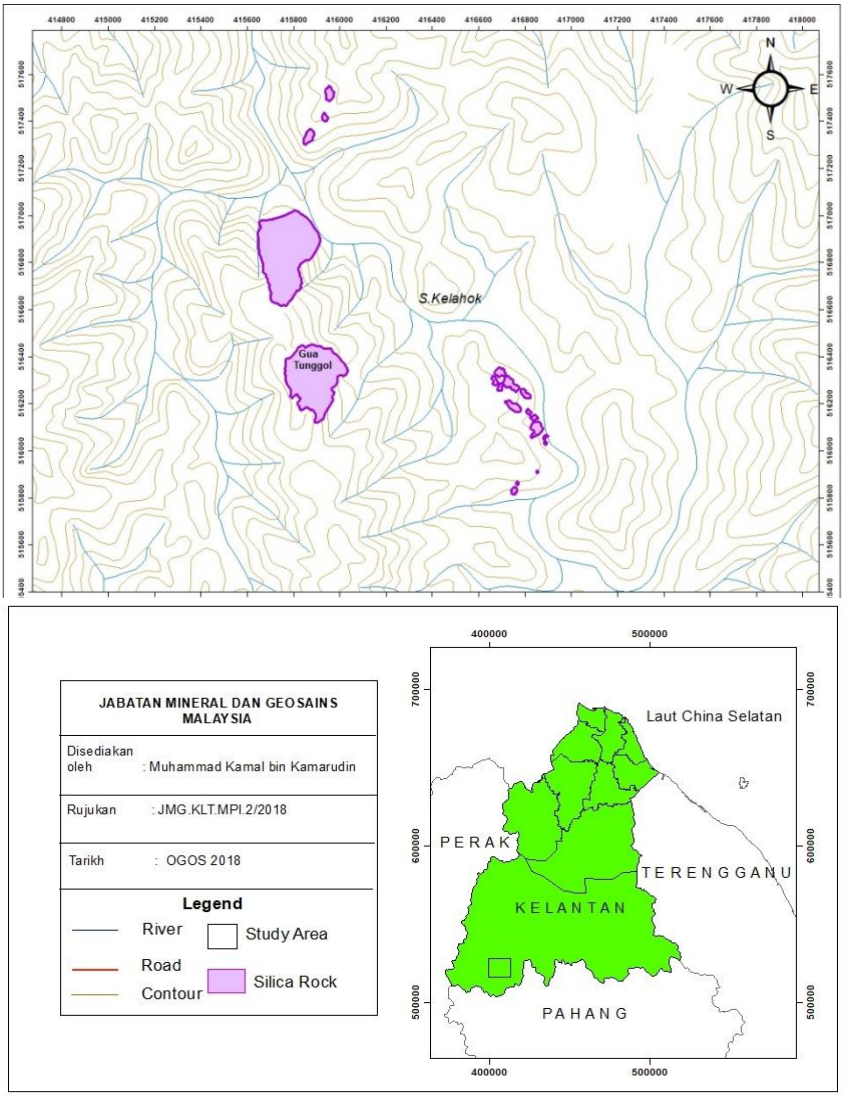

Fig. 1: Maps of silica rock deposit intruded into Gua Musang Formation in Lojing, Kelantan.

Fig. 2: Coarse-grained light grey silica rock.

Fig. 3: Assembled impeller system.

A complete chemical analysis was carried out on the raw silica rock samples using X-ray fluorescence (XRF), Shimadzu XRF-1700 instrument. Meanwhile, phase analysis was conducted on the raw and post-treatment samples via X-ray diffraction (XRD) using D8 Advance instrument, Bruker.

3.1 Phase identification

Fig. 4 illustrated XRD pattern of the raw silica rock. The characteristic peak of α-quartz (JCDS 00-046-1045) appeared as the major constituent, confirming its abundant content in crystallized silica rocks within the east coast Malaysia region. The intense peaks at 2θ = 20.860° and 26.640° indicated the presence of crystalline silica in the sample. Furthermore, the raw silica rock, which was free from any treatment, was characterized with trigonal silica phase.

3.2 Chemical composition

Major elemental quantification was made on 18 samples of silica rock through XRF analysis. The chemical composition of the silica rock (Table 2) revealed high and consis--tent percentages of SiO_2 with an average of over 98.12 wt. %, indicating the quartz-rich nature of the samples. The silica rock was characterized with low percentages of alumina (Al_2O_3) and manganese oxide (MnO) of <0.41 wt.% and <0.01%, respectively. These properties were indicative of the extra-siliceous content within the silica rock (Tsai, 2004). Minor oxides of Fe_2O_3, Na_2O, K_2O, and TiO_2 also presented at low percentages which was not exceeding 0.6 wt. %. For this chemical analysis, the average loss on ignition (LOI) value was 0.30%.

3.3 Attrition scrubbing of the silica rock sample

3.3.1 Effect of acid concentration

Table 3 illustrated the chemical analysis of the raw silica rock. The raw sample composed of 98.75% SiO_2, 0.410% Fe_2O_3, 0.175% TiO_2, and 0.492% of other compounds. As commonly reported, a high-grade silica must contain 99% or above SiO_2 and is free of inclusions, coating, and stains of any heavy mineral (Andrews, 1984).

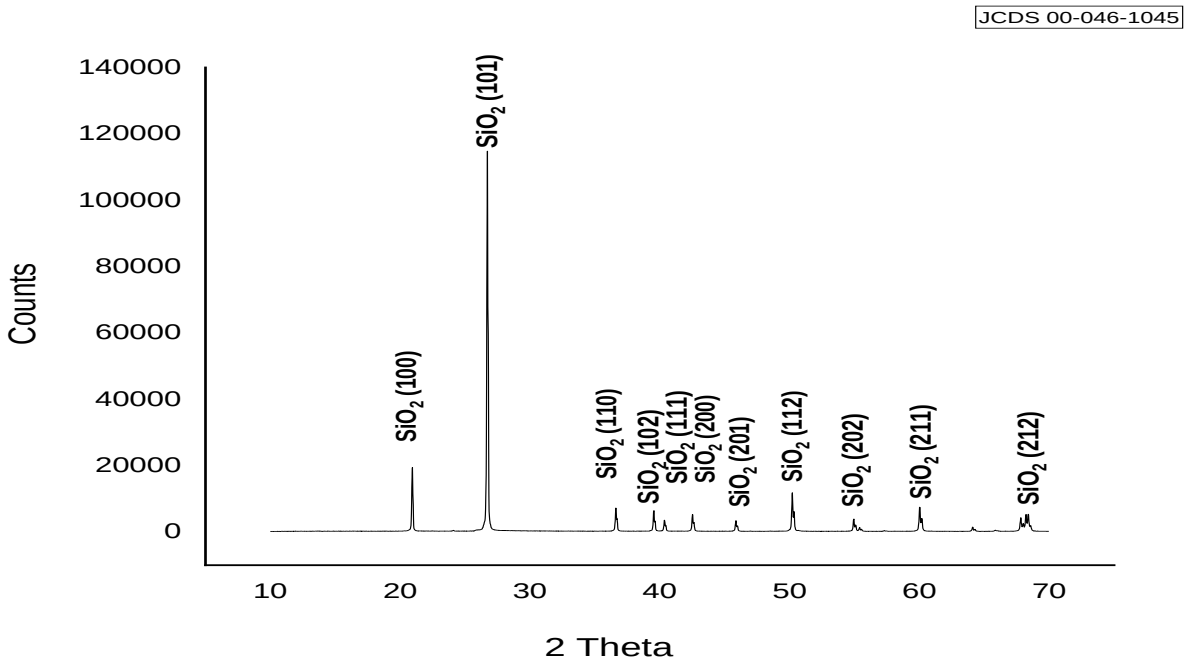

Fig. 4: XRD pattern of the raw silica rock sample.

Table 2: Chemical composition of the raw silica rock sample.

Sample No.	Chemical Composition										
	SiO_2	Al_2O_3	Fe_2O_3	TiO_2	K_2O	Na_2O	MgO	CaO	MnO	P_2O_5	LOI
1	98.00	0.57	0.09	<0.01	0.12	<0.01	0.05	<0.01	<0.01	0.01	0.31
2	98.00	0.60	0.06	<0.01	0.13	<0.01	0.05	0.01	<0.01	0.02	0.29
3	98.20	0.55	0.07	<0.01	0.09	<0.01	0.04	<0.01	<0.01	0.01	0.22
4	96.90	1.07	0.22	<0.01	0.27	0.01	0.08	<0.01	<0.01	0.02	0.40
5	96.90	1.01	0.06	0.01	0.27	0.02	0.08	<0.01	<0.01	0.01	0.39
6	98.10	0.60	0.22	<0.01	0.10	0.01	0.06	<0.01	<0.01	0.01	0.28
7	98.90	0.24	0.04	0.02	<0.01	0.01	0.03	<0.01	<0.01	0.02	0.35
8	99.00	0.23	0.02	<0.01	<0.01	<0.01	0.03	<0.01	<0.01	0.02	0.08
9	99.00	0.24	0.02	<0.01	<0.01	<0.01	0.03	<0.01	<0.01	0.02	0.22
10	98.70	0.27	0.04	<0.01	<0.01	<0.01	0.03	<0.01	<0.01	0.02	0.14
11	99.10	0.22	0.02	<0.01	<0.01	<0.01	0.03	<0.01	<0.01	0.02	0.11
12	98.70	0.35	0.07	<0.01	0.02	0.01	0.03	<0.01	<0.01	0.01	0.20
13	98.90	0.26	0.02	<0.01	<0.01	<0.01	0.03	<0.01	<0.01	0.02	0.19
14	99.00	0.25	0.02	<0.01	<0.01	<0.01	0.03	<0.01	<0.01	0.02	0.33
15	98.60	0.39	0.14	<0.01	0.05	<0.01	0.05	0.01	<0.01	0.01	0.28
16	96.20	0.27	0.29	0.08	0.01	0.01	0.32	0.16	<0.01	0.02	0.75
17	96.90	0.17	0.30	0.02	0.02	0.05	0.08	0.03	<0.01	0.01	0.33
18	97.00	0.04	0.14	0.05	<0.01	0.03	0.25	0.02	0.01	0.01	0.47
Avg.	98.12	0.41	0.10	0.04	0.11	0.02	0.07	0.05	0.01	0.02	0.30

Table 3: Chemical compositions of the raw and treated silica rocks.

Compound	Raw (%)	$C_6H_8O_7$ treated (%)
SiO_2	98.75	99.87
Fe_2O_3	0.410	0.114
Al_2O_3	0.175	-
TiO_2	0.067	-
Others	0.492	0.026

In this research work, acid concentration was varied at five concentration levels i.e. 0.25%, 0.5%, 0.75%, 1.0 %, and 1.5%. The maximum recovery of silica was achieved at 99.87 % with 0.75% $C_6H_8O_7$ addition, as displayed in **Fig. 5**. This condition was attributed to the increasing concentration of complex ions such as citrate or oxalate, which increased the soluble fraction. However, a decrease in the purity of SiO_2 was observed with a further increase in $C_6H_8O_7$ concentration than the optimum, which can be explained by the diffusion rate factor.

This scenario was due to the collapse of the SiO_2 structure at concentrations beyond the optimum (Al-Zahrani, 2009). The diffusion rate of SiO2 ions from solid into the solution increased as the concentration and diffusion rate of hydronium ions increased, until a maximum recovery was reached at 0.75 % $C_6H_8O_7$. Recovery of SiO_2 purity decreased from 99.87% to 98.73% when reached at 1% $C_6H_8O_7$. It can be observed that a further increment of the acid concentration did not improve the purity of the silica (Shin and Lee, 2014).

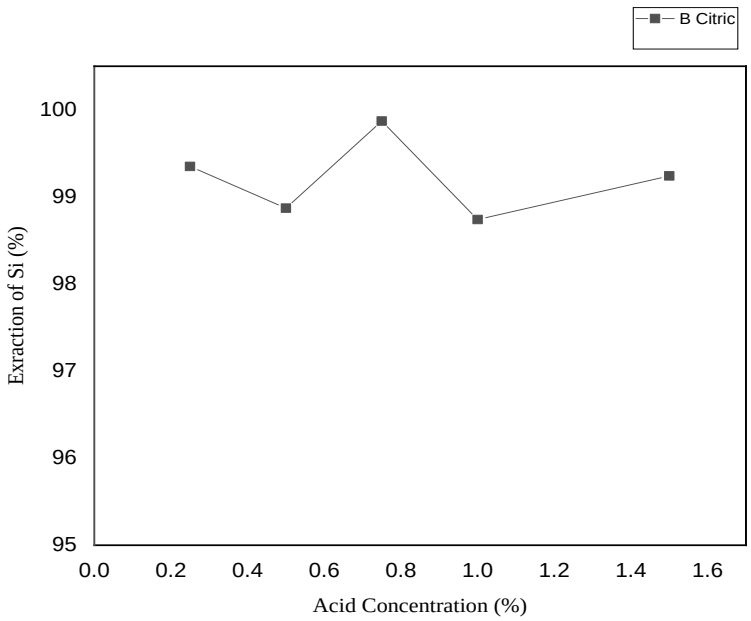

Fig. 5: Effect of acid concentration on silica recovery.

3.4 Crystal glass properties

3.4.1 Refractive index

Five samples, namely Sample A, Sample B, Sample C, Sample D, and Sample E represent the silica rock samples treated using various acid concentrations of 0.25%, 0.5%, 0.75%, 1.0 %, and 1.5%, respectively. The refractive indices of all samples, as well as the raw silica rock, were as indicated in Table 4. The difference in the values of refractive index amongst particular crystal glass was influenced by the purity of SiO_2 composition and the content of metallic oxides. In general, the refractive index of the crystal glass from the silica rock was higher than ≥1.50, thus fulfilling the specification for crystal glass application in accordance to the BS 3828:1973.

Table 4: Refractive index, density, and Vickers hardness of different crystal glass types.

Acid concentration (%)	Refractive Index	Density (g/cm^3)	Vickers hardness $kg.f/cm^2$
Raw sample	1.5280	2.5949	486.0300
Sample A	1.5274	2.6273	437.2000
Sample B	1.5258	2.6298	414.2200
Sample C	1.5261	2.6326	466.7000
Sample D	1.5273	2.6180	483.9000
Sample E	1.5240	2.6130	476.2700

3.4.2 Density

As specified in the BS 3828:1973, there are four (4) accepted values of density of crystal glass, which are based on the percentage of metallic oxides. A full lead crystal (30% lead oxide content) should have a density of greater than or equal to 3.00 g/cm3, while an acceptable crystal glass with the lowest content of lead oxide (less than or equal to 10%) is classified with a minimum density value of 2.40 g/cm3. The results of the density tests were summarized in Table 4, where all the density values were in the range of full lead crystal and crystal glass with at least 10% of BaO, PbO, and K_2O contents, either individually or grouped. In other words, the crystal glass produced from scrubbed silica rock demonstrated a comparable crystal glass specification by BS 3828:1973. However, the difference in the density value was due to several factors including the structure, bonding, and chemical composition of the glass material itself (Schubert, 1997). Furthermore, the density properties of the crystal glass were also influenced by the cooling process. Rapidly cooled samples exhibited slightly lower density values as compared to the slowly cooled samples, as a result of less melting time needed to densify its structure upon freezing.

3.4.3 Vickers hardness

Table 4 presented the Vickers hardness of Sample A, Sample B, Sample C, sample D, and Sample E. From the results, it can be concluded that the hardness of the crystal glass produced from east coast Malaysian silica rock is lower within the range of 414.22 kg.f/cm2 to 486.03 kg.f/cm2 than the required hardness by the BS 3828:1973 of 550 ± 20 kg.f/cm2. It was concluded that the crystal glass produced from silica rock was comparatively softer than that fabricated from traditional silica sand (Mohamad Haniza Mahmud and Abdul Hadi Abdul Rahman, 2016). Moreover, the surface hardness of the glass could generally affect the cutting and engravement process.

4. Conclusion

The properties and behavior of the silica rock acquired from the east coast of Malaysia region were investigated in the application of crystal glass. The maximum SiO_2 content of 99.76% of the silica rock samples was achieved from a purification process using 0.75% $C_6H_8O_7$ acid concentration with 20 minutes of scrubbing time, and attrition scrubbing agitation of 1250 rpm. The silica rock meet the grade B specification in which the purity is more than 99.5% with small amount of impurities such as iron oxide (0.015%), alumina (0.05%), chromium (2ppm) and titanium oxide (0.05%). Intense peaks of crystalline structured corresponding to α-quartz were observed from the XRD analysis on the treated silica rock at 2θ of 20.860º and 26.640º accordingly. The studied silica rock was found suitable for crystal glass application, at the provided density (≥ 2.40 g/cm3), Vickers hardness (550 ± 20 kg.f/cm2) and refractive index (≥ 1.5) and were in compliance with the standard requirements of BS 3828:1973.

Acknowledgements

The authors would like to express their highest gratitude to the Senior Director of Mineral Research Centre of Mineral and Geoscience Department Malaysia, Dr. Nazwin Ahmad, as well as Che Abdul Rahman Jaafar, and Dato' Ahmad Zukni Ahmad Khalil, Director of Mineral and Geoscience, Perak, for their continuous support in the completion of this research and technical paper. In addition, the authors would like to thank the supporting staff of Mineral Research Centre.

References

Al-Zahrani, A. A. (2009). Extraction of alumina from local clays by hydrochloric acid process. *Engineering Sciences*, *20*(2).

Andrews, W. H. (1984). Uses and Specifications of Silica sand. *Res. Counc. Alberta, Bull.; (Canada)*, *71–4*, 49–66.

Bouabdallah, S., Bounouala, M., Idres, A., & Chaib, A. (2015). Iron removal process for high-purity silica production by leaching and magnetic separation

technique. *Naukovyi Visnyk Natsionalnoho Hirnychoho Universytetu*, *5*, 47–52.

Brynhildsen, L., & Rosswall, T. (1997). Effects of metals on the microbial mineralization of organic acids. *Water, Air, and Soil Pollution*, *94*(1), 45–57. https://doi.org/10.1007/BF02407092

Farmer, A. D., Collings, A. F., & Jameson, G. J. (2000). The application of power ultrasound to the surface cleaning of silica and heavy mineral sands. *Ultrasonics Sonochemistry*, *7*(4), 243–247. https://doi.org/10.1016/S1350-4177(00)00057-2.

Foo, K. Y. (1973). *Summary of The Geology and Mineral Resources the State of Kelantan*.

Khalifa, M., Ouertani, R., Hajji, M., & Ezzaouia, H. (2019). Innovative technology for the production of high-purity sand silica by thermal treatment and acid leaching process. *Hydrometallurgy*, *185*, 204–209.

Larba, R., Boukerche, I., Alane, N., Habbache, N., Djerad, S., & Tifouti, L. (2013). Citric acid as an alternative lixiviant for zinc oxide dissolution. *Hydrometallurgy*, *134–135*, 117–123. https://doi.org /10.1016/j.hydromet.2013.02.002.

Mohamad Haniza Mahmud, Mohd Idham Mustaffar, & Abdul Hadi Abdul Rahman. (2016). Development of Lead Free Crystal Glass Using Silica Sand from Gong Belibis Setiu, Terengganu. *Journal of Geological Resource and Engineering*, *4*(3), 137–141. https://doi.org/10.17265/2328-2193/2016.03.004.

Ngah, D. S. (1986). *Potential Mineral Resources in Kelantan*.

Nishkov, I., Valchev, A., Marinov, M., Grigorova, I., & Nishkov, I. (2011). *Low Iron Silica Sand for Glassmaking*. *III* (January 2011), 755–760. https:// www.researchgate.net/publication/306056275.

Römkens, P., Bouwman, L., Japenga, J., & Draaisma, C. (2002). Potentials and drawbacks of chelate-enhanced phytoremediation of soils. *Environmental Pollution (Barking, Essex : 1987)*, *116*(1), 109–121. https://doi.org/10.1016/s0269-7491(01)00150-6.

Schubert, U. (1997). Book Review: Introduction to glass science and technology. By J. E. Shelby. *Angewandte Chemie International Edition in English*, *36*(20), 2248–2249. https://doi.org/10.10 02/anie.199722481.

Shin, D., Jeong, J., Kim, B., Ilyas, S., & Lee, J. (2014). Lead trace removal from waste electronic scraps by organic acids. *Materials Transactions*, *55*(3), 586–590.

Tsai, M. S. (2004). The study of formation colloidal silica via sodium silicate. *Materials Science and Engineering B: Solid-State Materials for Advanced Technology*, *106*(1), 52–55. https://doi.org/10.1016/ j.mseb.2003.08.052.

Yuan, Y., Zhang, L., Guan, J., Zhang, C., Wu, J., & Chen, Z. (2018). Contribution on fluid inclusion abundance to activation of quartz flotation. *Physicochemical Problems of Mineral Processing*, *54*.

Thai Geoscience Journal 3(4), 2022, p. 20-35

ISSN-2730-2695; DOI-10.14456/tgj.2022.9

Landslide vulnerability and risk assessment: A guideline for critical infrastructure in Malaysia

Zakaria Mohamad [1*], Muhammad Zulkarnain Abd Rahman [2], Zamri Ramli [3], Mohd Faisal Abdul Khanan [2], Zainab Mohamed [4], Rozlan Ahmad Zainuddin [5], Rozaimi Che Hasan [6], Mohd Asraff Asmadi [2], Nurul A'dilah Sailey [1], Muhamad Farid Mohamed Dali [1]

[1] *Geomapping Technology (GMT) Sdn. Bhd., Bandar Baru Bangi, Malaysia*
[2] *Faculty of Built Environment and Surveying (FBES), Universiti Teknologi Malaysia (UTM), Johor Bahru, Malaysia*
[3] *Department of Mineral and Geoscience Malaysia (JMG), Putrajaya, Malaysia*
[4] *Universiti Teknologi Mara Shah Alam (UiTM), Shah Alam, Malaysia*
[5] *Ganding Asli Runding Sdn. Bhd., Petaling Jaya, Malaysia*
[6] *Razak Faculty of Technology and Informatics (RFTI), Universiti Teknologi Malaysia (UTM), Kuala Lumpur, Malaysia*
*****Corresponding author: dzakaria17@gmail.com*
Received 17 March 2021; Accepted 20 July 2022.

Abstract

Landslide vulnerability is a crucial element that connects hazard and risk for a specific element-at-risk. Currently, landslide vulnerability study in Malaysia is limited and attention is given to susceptibility and hazard assessments. Ideally, vulnerability assessment should address various aspects of element-at-risk including physical, social, economic, and environmental. In 2018, a guideline for landslide vulnerability and risk assessment for critical infrastructure in Malaysia was developed for the Construction Research Institute of Malaysia (CREAM). The guideline aimed at developing large-scale landslide vulnerability and risk assessment methods for local authorities as a level of basic and supporting information for land-use plan, landslide mitigation purposes, and risk assessment for any development of the critical infrastructure (CI) i.e. road, dam, building and electricity pylon. The aim of this study is to develop a simple methodology to support more detailed on-site landslide vulnerability and risk assessment. Using a case study from the Cameron Highlands District in northern Malaysia remotely sensed and field data were combined to create a detailed landslide inventory and element-at-risk mapping. Due to the limited landslide damage records, a vulnerability model was developed using the qualitative indicator-based method (IBM). The indicators and the corresponding sub-indicators are divided into four clusters i.e. 1) the susceptibility of element-at-risk (C), 2) surrounding environment (E), 3) intensity of landslide hazard (I), and 4) affected community (P). Suitable indicators and sub-indicators were selected and proposed based on a thorough literature review and a series of focus group discussions (FGD) with agencies involved with landslide hazard management in Malaysia. The FGD sessions also focused on experts assigning scores for each indicator and sub-indicator based on their relationship to the likelihood of landslide vulnerability. The final scores were then converted to final weighting values and a landslide vulnerability map was generated by combining the individual vulnerability cluster maps i.e. C, E, I and P. The resulting landslide vulnerability index was classified into five classes; very high, high, medium, low, and very low with a clear definition of the potential damage to CI and the community. Using a qualitative risk-matrix approach a landslide risk map was generated by combining the landslide hazard and vulnerability maps and was then validated against past landslide event in the Bukit Antarabangsa, Selangor, Malaysia. The results confirm good agreement between the derived vulnerability and risk maps and actual landslide damage in the area. The methodology proposed here is however strongly dependent on several key elements including, the quality of landslide hazard map, the landslide inventory map and the experience of the experts.

Keywords: geospatial, Landslide vulnerability and risk, LiDAR

1. Introduction

Risk can be defined as ‘‘the expected number of lives lost, persons injured, damage to property and disruption of economic activity due to a particular damaging phenomenon for a given area and reference period’’ (Varnes et al., 1984). On a simpler note, International Union of Geological Sciences similarly defines landslide risk as a measure of the probability and severity of an adverse effect to health, property and the environment (Cruden and Fell, 1997). Both definitions highlight three different impacts of landslide risk including, critical physical infrastructure, socio-economic and environment. Therefore, any map of landslide risk should typically present the subdivision of the terrain into zones that are characterized by different probabilities of losses that might occur due to landslides of a given type within a given period of time.

Two common methods are available for landslide risk assessment, qualitative or quantitative. Qualitative risk analysis refers to an analysis that uses word form (descriptive) or numerical scales to describe the magnitude of potential consequences and the likelihood that those consequences will occur. Whereas quantitative risk analysis is based on numerical values of the probability, vulnerability, and consequences, resulting in a numerical value of risk (Cruden and Fell, 1997; Technical Committee on Risk Assessment and Management, 2004; UN-ISDR, 2004; Fell et al., 2008). Depending on the completeness of data, a semi-quantitative approach can be devised to provide an indicative probability via qualitative terms given to a team of expert for a heuristic assessment (Van Westen et al., 2006).

Vulnerability is a fundamental component in risk assessment, which defines the relationship between level of potential damage for specific hazard intensity and element-at-risk (Dai et al., 2002; Uzielli et al., 2008; Kappes et al., 2012). It can be defined as the degree of loss to a given element at risk or set of elements at risk resulting from the occurrence of a natural phenomenon of a given magnitude and expressed on a scale from 0 (no damage) to 1 (total damage). Furthermore, vulnerability can be defined in a more integrative approach as “a characteristic of human behavior, social and physical environments, describing the degree of susceptibility (or resistance) to the impact of e.g., natural hazards’’ (Kappes et al., 2012). Although previous studies have shown that there is no general or universal approach in vulnerability assessment (Fuchs et al., 2011) and idea vulnerability assessment should account for various criteria including physical, economic, environmental, institutional, and human factors. Papathoma-Köhle et al. (2015) has defined three dominant approaches to express the vulnerability of element-at-risk i.e., vulnerability matrices, vulnerability indicators (Birkmann et al., 2013) and vulnerability curves (Totschnig et al., 2011). These approaches can be further classified into qualitative, semi-quantitative and quantitative vulnerability assessment methods.

Previous studies have shown that landslide vulnerability assessment can be accomplished using qualitative, semi-quantitative and quantitative approaches. The qualitative approach requires suitable vulnerability values for a specific element-at-risk based on the landslide type (Cardinali et al., 2002; Kappes et al., 2012). The vulnerability values (between 0.0 and 1.0) are assigned by experts based on their experience and historical records of landslide degree of damage. Vulnerability matrix and indicator-based vulnerability assessment are flexible and require less landslide damage information compared to the quantitative approach. Furthermore, the matrix and indicator-based methods are easy to use and comprehend by decision makers.

However, there is no direct (quantified) relationship between hazard intensities and degree of damage (Uzielli et al. 2008) and instead relies on expert judgments. Meanwhile, the semi-quantitative approach is more flexible with reduced level of generalization and subjectivity (Dai et al., 2002). For instance, based on this method, the damage matrices are populated by classified intensities and stepwise levels of damage. In a previous study by Frédéric et al. (1996), damage matrices were developed based on damaging factors and the resistance of the elements at risk to the impact of landslides. The

applicability of this method requires statistical analysis of detailed records on landslides and their consequences (Dai et al. 2002). It still requires detailed information on the impact of a specific landslide hazard towards a specific element-at-risk. Finally, the quantitative vulnerability assessment approach requires detailed and complex information applied on the local scale or individual infrastructure (Fuchs et al., 2011, Kaynia et al., 2008, Li et al., 2010b, Uzielli et al., 2008) and is usually employed by engineers involved in the technical decision making where a more explicit objective output is required. The results can be directly used in a quantitative risk assessment with detailed analysis on the uncertainty analysis of the vulnerability assessment.

In Malaysia, landslide vulnerability studies are still very limited. This is due to insufficient of landslide inventory and damage records among agencies related to landslide hazard management. In 2018, the Construction Research Institute of Malaysia (CREAM) has proactively created national guidance for landslide vulnerability and risk assessments for critical infrastructure in Malaysia. This guideline includes the role of geospatial technology and in deriving important indicators and sub-indicators for the vulnerability model and the in the mapping aspect of landslide risk for different critical infrastructure types in Malaysia.

In this paper, we present a more detailed methodology for landslide vulnerability and risk mapping based on the qualitative approach and illustrate its use in an area of the Cameron Highlands District in northern Malaysia. The vulnerability model was developed using indicator method, in which the indicators are carefully selected and combined based on different critical infrastructure and landslide types in Malaysia. The guideline can be used by various agencies and authorities to evaluate the vulnerability and risk of existing and future infrastructures under their jurisdiction. The outcome of this analysis can be used to further decrease the risk and vulnerability of the infrastructure towards landslide hazard. Furthermore, the guideline comes with a simple non-geospatial tool to support on-site landslide vulnerability and risk assessment.

2. Materials and method

The methodology of assessing and developing the parameters/indicators of landslide vulnerability assessment and risk index of critical infrastructures can be divided into 4 main stages namely, 1) data acquisition and pre-processing of geospatial data, 2) improvements of landslide vulnerability cluster, indicators, sub-indicators and weighting values, 3) landslide vulnerability and risk mapping in Cameron Highlands and 4) evaluation of the landslide vulnerability and risk assessment method (Fig. 1).

2.1 Description of study area

The study site is at Lembah Bertam located in Cameron Highlands, which cover about 3.66 km2 and 5.00 km2 respectively. Generally, geology of Cameron Highlands divided into two main lithologies, namely granite and schist. Granite made up most of the Cameron Highland (84.65% area) meanwhile shicst are found on west of Cameron Highlands as roof pendant (15.35% area). Granite of Cameron Highland is part of Main Range Granite dated Triassic Age around 207-230 million years ago (Bignell & Snelling, 1997). Main Range Granite formed Titiwangsa Range, where Cameron Highland is located. Generally, Main Range Granite are described as medium to coarse grained biotite granite with feldspar megacryst (Krahenbuhl, 1991) which can be found in the study area. Granite in Cameron Highlands had been jointed and faulted due to tectonic stress. Weathering profile of the granite is described as Grade I that is light grey, and Grade II with slightly brown. Grade IV-VI granite formed the residual soil has reddish brown in colour due to existence of iron element from biotite that has been weathered. However, the weathering of the granite is no continuous from the surface downward, in fact, it is controlled by geological structure such as faults and joints that allow the existence of fresh rock boulders inside the weathered granite.

Schist in Cameron Highlands formed as roof pendant, which is a body of schist left

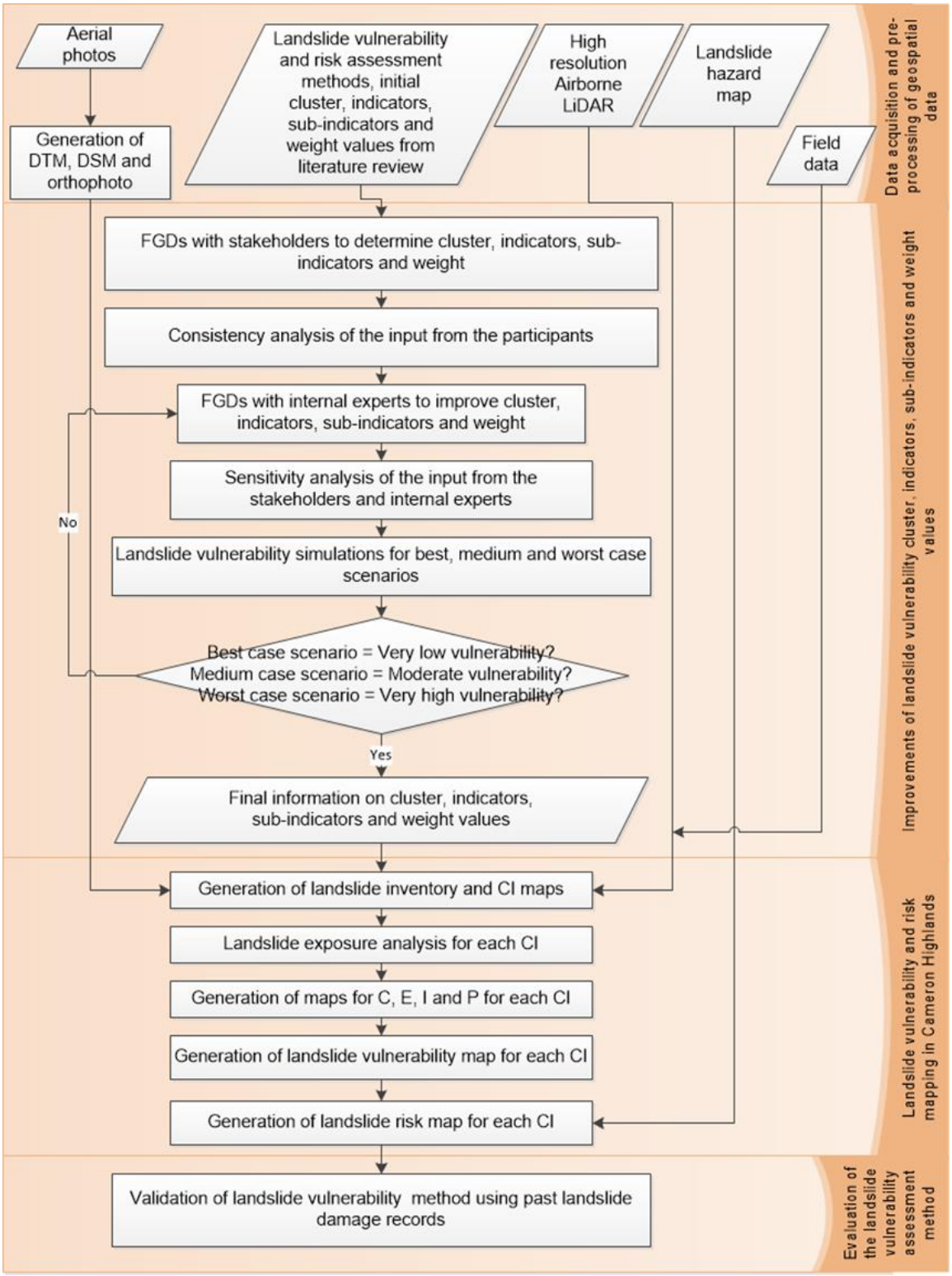

Fig. 1: Overall methodology of landslide vulnerability and risk assessments (DTM – digital terrain model; DSM – digital surface model; LiDAR – light detection and ranging; FGD – focus group discussion; CI – critical infrastructure; C - susceptibility of element-at-risk; E - surrounding environment; I - intensity of landslide hazard; and P - affected community.

islanated on the intrusive granite body. Schist that found in the study area is quartz mica schist. the age of the schist is interpreted around Palaeozoic due to younger intrusive granite is defined as Triassic. Distribution of schist is limited to west part of Cameron Highlands. The difference of lithology between granite and schist can be identified by the different soil properties. Weathered schist did not form rounded rock boulders like granite, but the the boulders are in tabular shape with darker reddish soil colour. Schist residual soil colours are the oxidation product of iron element in biotite.

Cameron highlands is undergoing rapid development that involves land clearing for hotels, residential area, shop lots, agricultural activities etc. This has become one of the main causes for landslides occurrences in Cameron Highlands.

2.2 Acquisition and pre-processing of geo--spatial data

The first stage focuses on data acquisition that includes geospatial and non-geospatial data. The geospatial data includes high--resolution aerial photographs and airborne LiDAR survey at Lembah Bertam, Cameron Highlands. The LiDAR and aerial photos were processed to produce digital terrain model (DTM), digital surface model (DSM) and orthophotos with 0.5-m spatial resolution. In addition, several other ancillary data were also obtained from different agencies for example landslide hazard map, high resolution DTM and orthophotos from the Mineral and Geoscience Department of Malaysia (JMG). The landslide hazard map was produced using high-resolution airborne LiDAR data and the final map was classified into 5 hazard classes namely, very high, high, moderate, low and very low with its spatial resolution of 0.5 m. All the data were compiled into the same map projection system and datum and stored in the GIS database. Several field visits were made in Lembah Bertam to collect information related to landslide inventory and characteristics of critical infrastructures. The field data was used to support parameterization of landslide vulnerability indicators and sub-indicators especially for the information that cannot be directly measured from the remotely sensed data. Furthermore, intensive literature review is used to define the suitable landslide vulnerability and risk assessment method for the scenario in Malaysia.

2.3 Determination of landslide vulnerability cluster, indicators and sub-indicators

Based on the proposed method for landslide vulnerability and risk assessments, the second stage focuses on determination and improvements of landslide vulnerability clusters, indicators, sub-indicators and weighting values. The landslide vulnerability model for different element-at-risk i.e., building, road, electricity dam and electricity pylon were developed based on their vulnerability cluster (C, E, I and P), indicators and sub-indicators. Cluster C determines the susceptibility of infrastructure towards landslide. Cluster E reflects the impact of surrounding environment either in reducing or increasing the vulnerability of the critical infrastructure towards landslide. Furthermore, cluster I and P represent intensity of landslide hazard and the impact to the surrounding people respectively. Each indicator under specific cluster consists of several sub-indicators.

This process was conducted via few series of expert focus group discussions (FGD) with different stakeholders. Each participant is required to fill a specially designed survey form for landslide vulnerability and risk assessments and was followed by detailed explanation on the concept of landslide vulnerability and risk assessment including a step-by-step explanation on the procedure in determining the clusters, indicators, sub-indicators and the weighting values.

A series of sensitivity analysis based on one-at-a-time (OAT) method were carried out to determine the consistency of inputs from stakeholders, the sensitivity of each indicator and cluster and reliability of the vulnerability index, based simulation of different landslide vulnerability scenarios (worst, medium and best-case scenarios). The consistency analysis was aimed at analyzing the consistency of weighting values assigned by the stakeholders

for the indicators and sub-indicators through the analysis of standard deviation value of weight between participants. A separate sensitivity analysis focused on analyzing the sensitivity of each indicator and sub-indicator towards the estimation of landslide vulnerability value (index) based on the one-at-a-time (OAT) method. A series of sensitivity analysis based on one-at-a-time (OAT) method, were then carried out to determine the sensitivity of each cluster, indicators and sub-indicators leading to a final value of landslide vulnerability for each CI. This method varies the value of a specific indicators and sub-indicators (V) while the rest of sub-indicators remains unchanged (Equation 1).

$$V = \{a_1, a_2, a_3, a_4 \ldots . a_n\} \quad (1)$$

where V is the set of specific vulnerability value (a) estimated for each indicator by varying the indicators and sub-indicator values and n is the number of possible vulnerability scenarios or simulations.

The Sen_{Ind} is defined as the sensitivity of the estimated vulnerability value with the weight changes of sub-indicators (Equation 2) and is estimated by the standard deviation of the estimated vulnerability value produced by the simulation. Higher Sen_{Ind} value indicates a more sensitive indicator compared to an indicator with a lower index value. The sensitivity index for the cluster (Sen_{Clus}) determines the sensitivity of the estimated value with the changes of weight in the indicators (Equation 3). Sen_{Clus} is estimated by the average of the Sen_{Ind} for indicators that belong to a specific cluster. Higher Sen_{Clus} values indicate a more sensitive cluster compared to other cluster with lower index value.

$$Sen_{Ind} = \sqrt{\frac{\sum_{i=1}^{n}(a_i - mean(a))^2}{n}} \quad (2)$$

where *n* is the number of indicators for each cluster.

$$Sen_{Clus} = \frac{\sum_{i=1}^{m} Sen_{Ind_i}}{m} \quad (3)$$

where *m* is the number of clusters.

In addition, several simulations on the vulnerability calculation were made for three different scenarios i.e. best-case, moderate-case and the worst-case landslide vulnerability. The simulation analyzes the reliability of weighting values given by the stakeholders and internal experts (for each CI and landslide type). The best-case landslide scenario, with the combination of indicators with the lowest weight is expected to produce the very low landslide vulnerability. The moderate landslide vulnerability scenario with the combination of moderate weight of indicators is expected to produce "moderate vulnerability" and in the worst-case landslide scenario with the highest vulnerability values is classified as "very high vulnerability".

2.4 Landslide vulnerability and risk mapping

The landslide vulnerability mapping in--volves generation of several maps representing different clusters, indicators, sub-indicators and weighting values as defined in the landslide vulnerability. The vulnerability index for CI is defined as in Equation 4.

$$V = \sum_{i=1}^{m} w_i \times S_j \quad (4)$$

where w_i is the *i-th* weight of m indicators under different indicator groups and S_i is *i-th* score for a specific class of the indicators. The weight for each group ranges from 0.1 (low influence to increase vulnerability) to 1.0 (high influence to increase vulnerability).

The C cluster map is based on interpretation and classification of high resolution orthophoto, LiDAR -derived DTM and intensive fieldwork in the study area and characterized based on the indicators and sub-indicators in this cluster. The map for cluster E accounts for the surrounding environment that might increase and decrease the impact of landslide hazard. The P

cluster map considers the impact of CI's vulnerability on the people. For example, the P map for building consists of density residents for each building. The I map reflects the intensity of landslide hazard estimated based on the landslide characteristics obtained from the landslide inventory map. The landslide inventory map has been produced based on the expert interpretation of high-density airborne LiDAR data and orthophoto. Exposure map is developed by delineating possible run-out area for each landslide body and each zone (i.e. landslide body and run-out zones) has different value of landslide hazard intensity. The exposed CI is determined by overlaying the exposure map with the CI in the study area. The maps for each cluster should be developed for each CI. Finally, the C, E, I and P maps for each CI have been used to produce landslide vulnerability map.

The landslide vulnerability map is classified into 5 classes, i.e. very high, high, moderate, low and very low. The landslide risk map is produced based on the matrix combination of landslide vulnerability and hazard classes. The landslide hazard map of the study area is obtained from the JMG, which was produced using high resolution remote sensing and geospatial modelling approaches. The landslide map was already classified to similar classes. Finally, the risk map is produced by crossing both vulnerability and hazard maps and classified into 5 classes, i.e. very high, high, moderate, low and very low landslide risk areas.

2.5 Validation of landslide vulnerability and risk results

Evaluation of the landslide vulnerability and risk assessment method is then carried out over other area with detailed records on landslide disaster. The records are used to parameterize each indicator and sub-indicator in the landslide vulnerability. The estimated landslide vulnerability value and class for building can then be compared with the damage records and damage descriptions in the report.

3. Results and discussion

3.1 Landslide vulnerability indicators

The landslide vulnerability clusters, indicators (C, E, I and P) and the specific sub-indicators (or classes) have been assigned with suitable weighting values obtained from expert input. Figure 2 to Figure 5 show the sensitivity analysis of FGD with the stakeholders regarding the indicators and clusters for each of the critical infrastructure. In the first and second FGD sessions the discussions were only focussed on the rotational and translational landslides.

The final weight for each indicator and its sub-indicator is then used to estimate the landslide vulnerability for each CI based on three different landslide scenarios. The first scenario takes into account the best case, in which a very low landslide vulnerability value is expected. The second scenario focuses on simulating landslide vulnerability in which a medium value of landslide vulnerability is expected. Finally, the highest vulnerability value is expected for the worst-case scenario of landslide vulnerability.

Discussion during the FGD sessions allowed substantial improvement and modifications of the proposed indicator, sub-indicator as well as their corresponding weighting values. The final set of clusters, indicators, sub-indicators and their weights were generated based on the output of the FDG with the stakeholders and internal experts. The indicators, sub-indicators were fine-tuned based on the locality of the particular environment. **Fig. 6** to **Fig. 9** show the list of recommended cluster indicators and sub--indicators for the guidelines of landslide vulnerability and risk assessment for critical infrastructure in Malaysia.

3.2 Landslide vulnerability and risk assessments in Lembah Bertam, Cameron Highland

The landslide inventory map was produced based on the manual interpretation of DTM derived from the LiDAR data. The elevation model from LiDAR has been used to delineate the area of landslide, possible area of landslide runout and detailed characteristics of each landslide as required by the landslide intensity

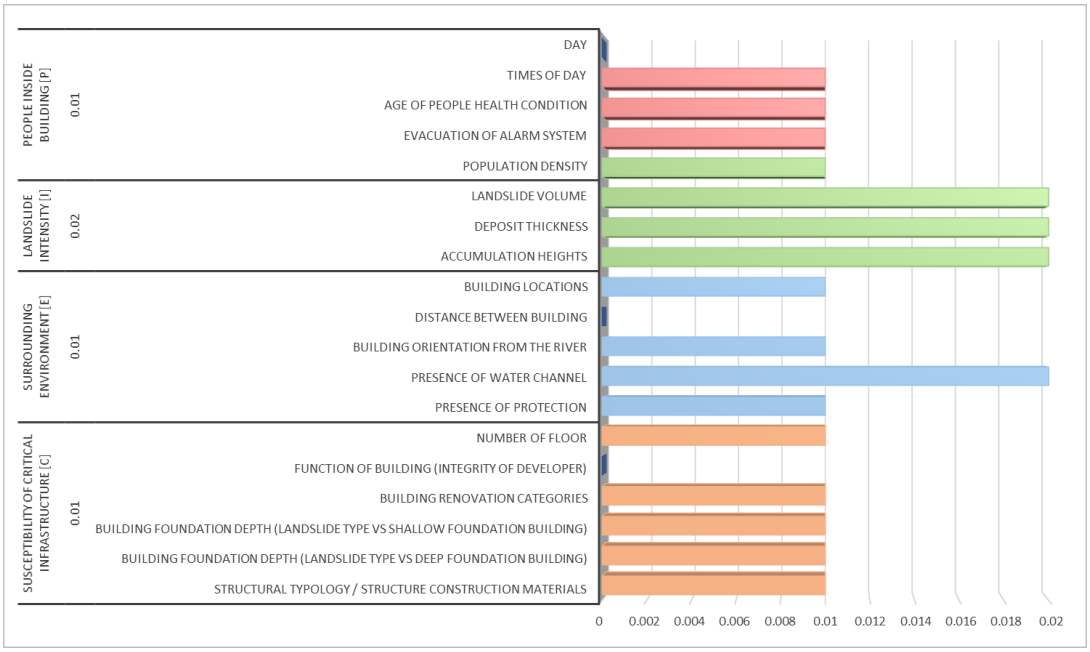

Fig. 2: Sensitivity of cluster (Sen_{Clus}) and Sensitivity of indicator (Sen_{Ind}) calculated for each indicator for building and rotational/translational landslide.

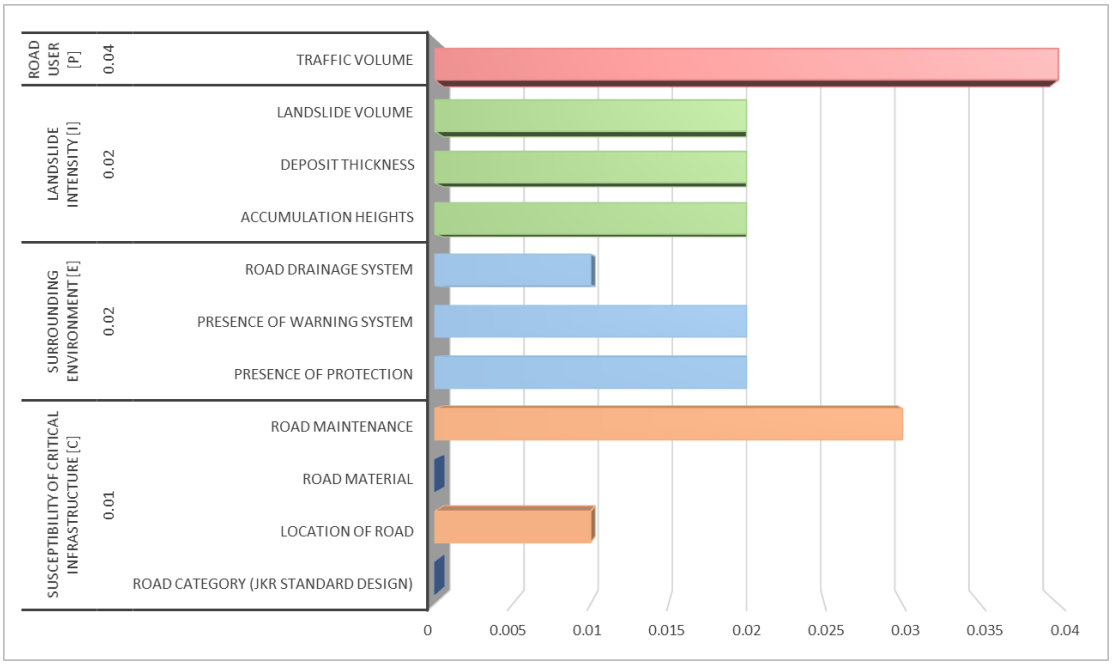

Fig. 3: Sensitivity of cluster (Sen_{Clus}) and Sensitivity of indicator (Sen_{Ind}) calculated for each indicator for road and rotational/translational landslide.

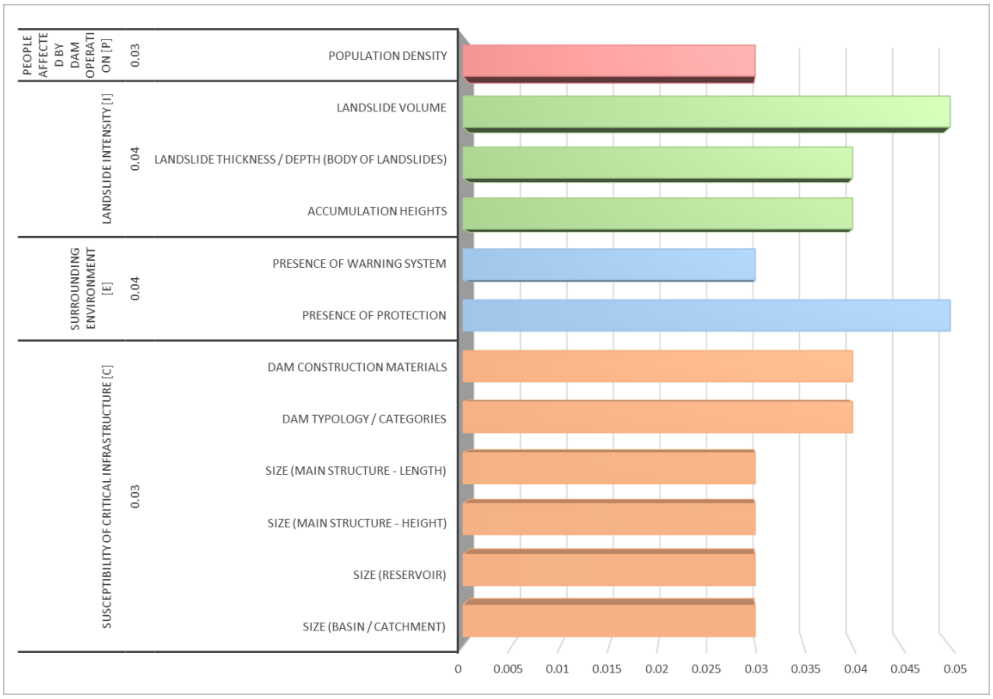

Fig. 4: Sensitivity of cluster (Sen_{Clus}) and Sensitivity of indicator (Sen_{Ind}) calculated for each indicator for dam and rotational/translational landslide.

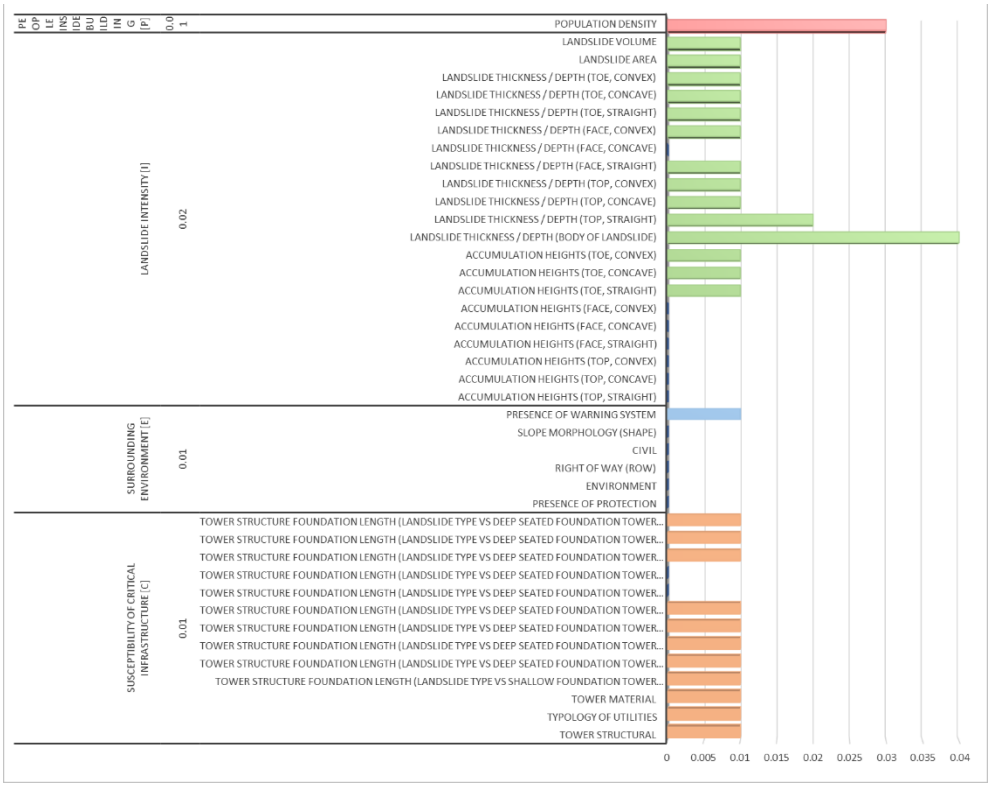

Fig. 5: Sensitivity of cluster (Sen_{Clus}) and Sensitivity of indicator (Sen_{Ind}) calculated for each indicator for pylon and rotational/translational landslide.

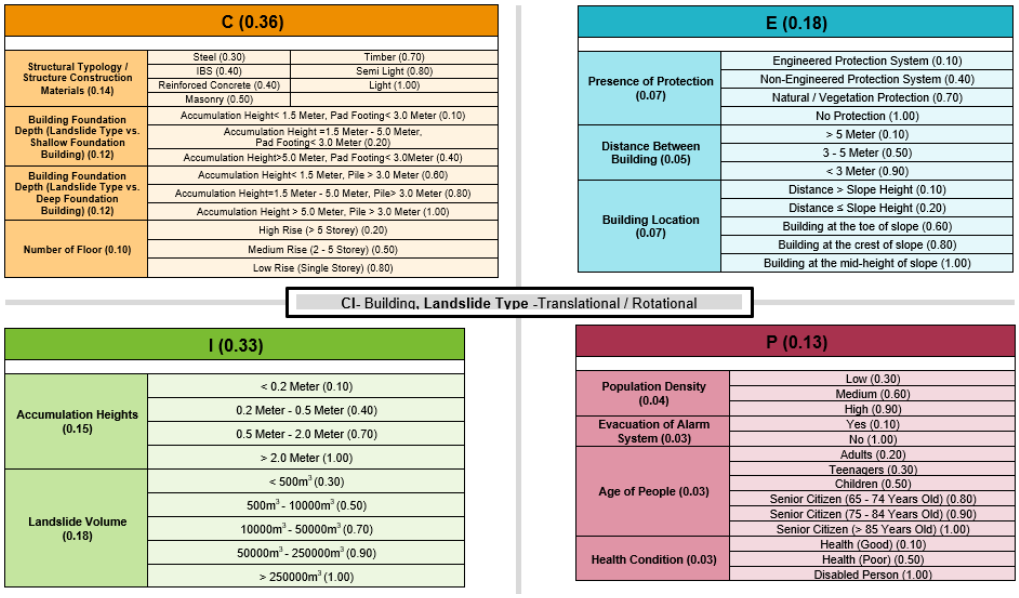

Fig. 6: Clusters, indicators and sub-indicators (C, E, I and P) and its weighting values for critical infrastructure (building) with translational/rotational as the type of landslide.

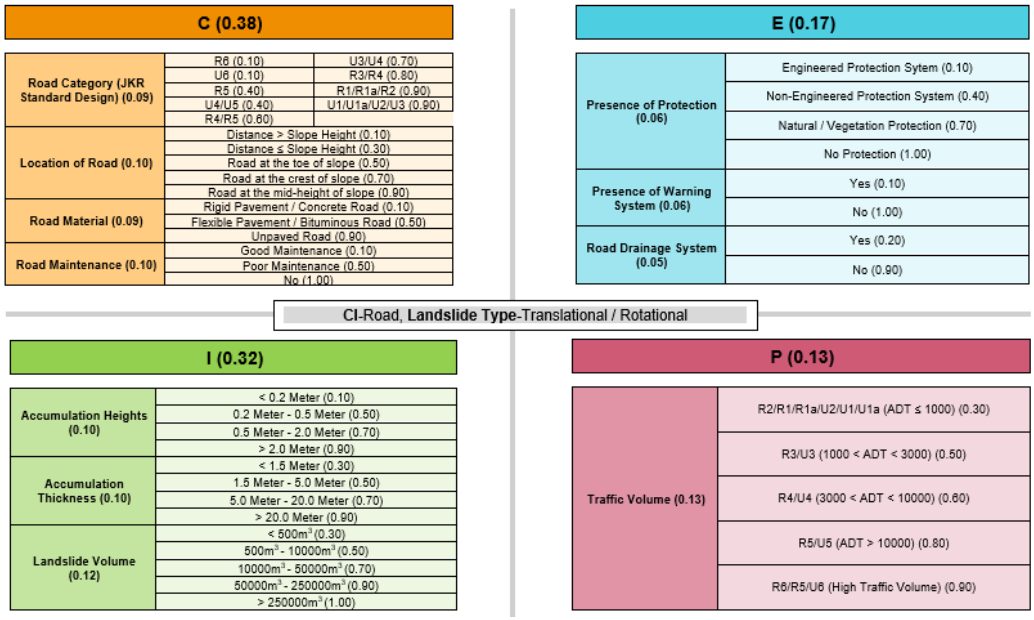

Fig. 7: Clusters, indicators and sub-indicators (C, E, I and P) and its weighting values for critical infrastructure (road) with translational/rotational as the type of landslide.

(I) indicator i.e. landslide volume, landslide velocity and accumulation height. There are in total about 54 landslides identified at Lembah Bertam. In order to identify the location of CI affected by the landslide area, the expert-based landslide runout area was developed based on the geomorphologic and topographic features of the suspected area. The resulted landslide inventory map for the Lembah Bertam area is shown in Fig. 10.

The landslide vulnerability maps for the respective CI were then generated by combining all cluster maps C, E, I and P spatially. The resulting landslide vulnerability index for each of CI was categorized into its specific vulnerability class as shown in Fig.11(a). Most of the critical infrastructures are at moderate vulnerability while the dam remains under low vulnerability class. The landslide risk map was generated by the com-

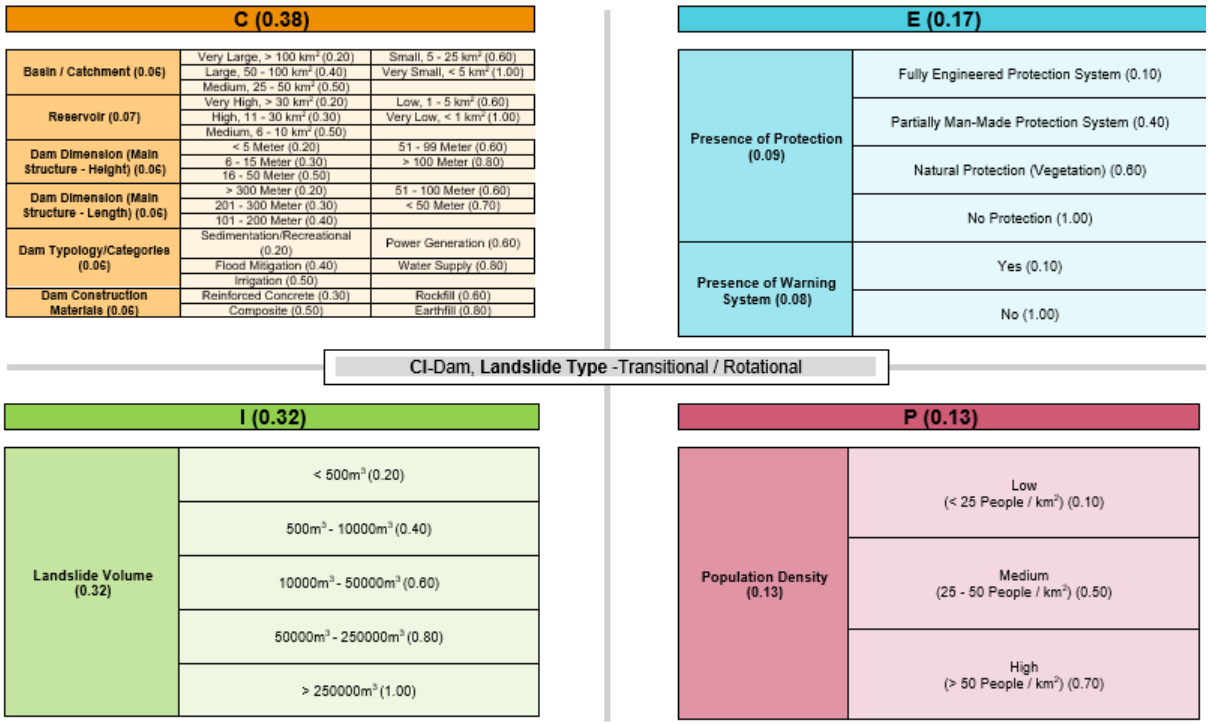

Fig. 8: Clusters, indicators and sub-indicators (C, E, I and P) and its weighting values for critical infrastructure (dam) with translational/rotational as the type of landslide.

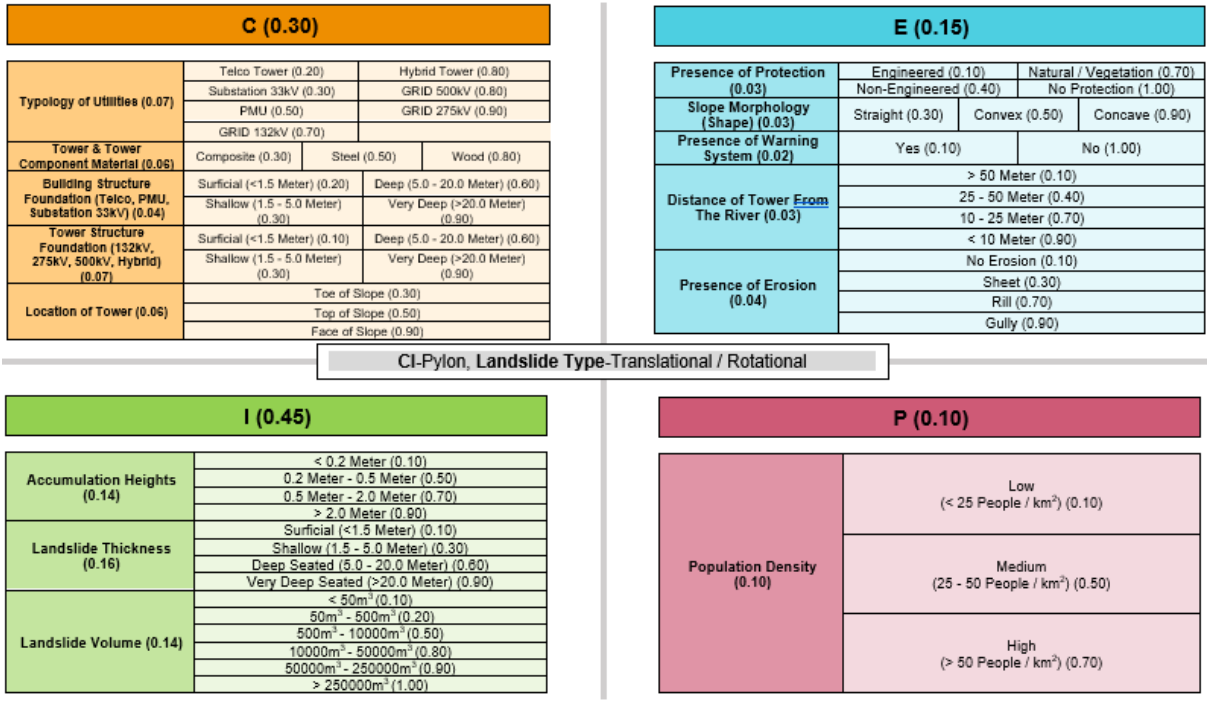

Fig. 9: Clusters, indicators and sub-indicators (C, E, I and P) and its weighting values for critical infrastructure (TNB powerline) with translational/rotational as the type of landslide.

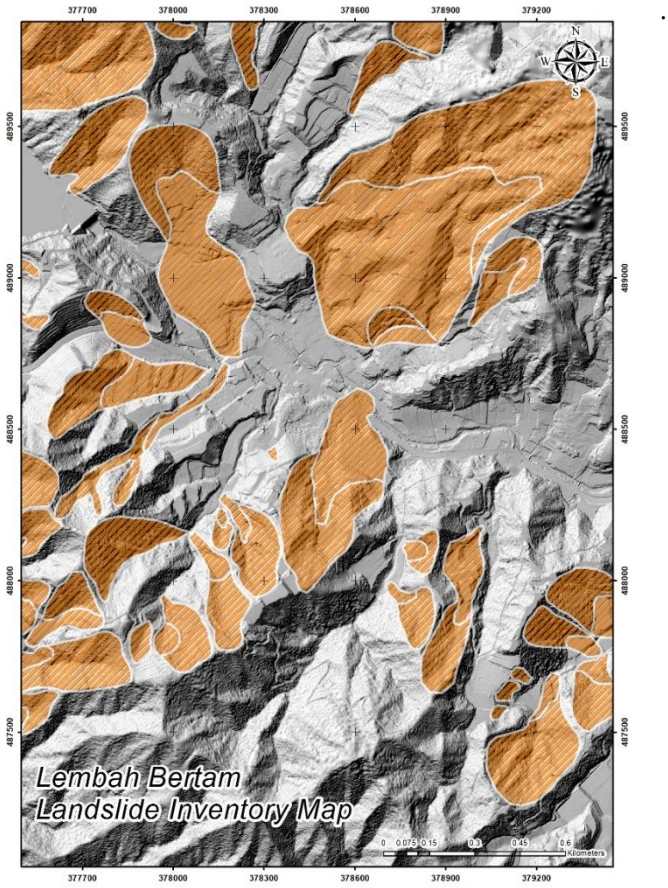

Fig. 10: Landslide inventory map of Lembah Bertam area in Cameron Highlands.

-bination of landslide hazard and landslide vulnerability maps. Fig. 11(b) shows the land-slide risk map of the same area for the respective CI. Similarly, as the vulnerability map, the landslide risk map has only five classifications from very low until very high.

This study validated the vulnerability model by estimating the landslide vulnerability index and class at Taman Bukit Mewah, Bukit Antarabangsa by using a landslide vulnerability assessment tool (Fig.12). The indicators and sub--indicators were extracted from the Slope Engineering Branch (CKC), (Public Works Department, 2008) official report and resulted an estimated of vulnerability index 0.75 (high vulnerability index) (Table 1). The class of vulnerability for this particular assessment is described as structural breaks, partly destructed, reconstruction of destructed parts, death is highly likely (severe injury) and evacuation necessary. Based on the vulnerability class descriptions, the vulnerability model success-fully meets the expectation as described in the official report.

4. Conclusion

The establishment of clusters, indicators and sub-indicators with weighting values for CI were initially based on published literature since Malaysia has yet to compile national records of damage caused by the landslide events requiring this study to carry out semi-quantitative approach. The proposed landslide vulnerability assessment requires determination of 4 groups of indicators i.e. susceptibility of CI (C), effect of surrounding environment or mitigation measures (E), susceptibility of people inside the residential building (P) and intensity of landslide hazard (I). Initially, each group of indicators are treated equally with 25% weighting value, in which all the group of

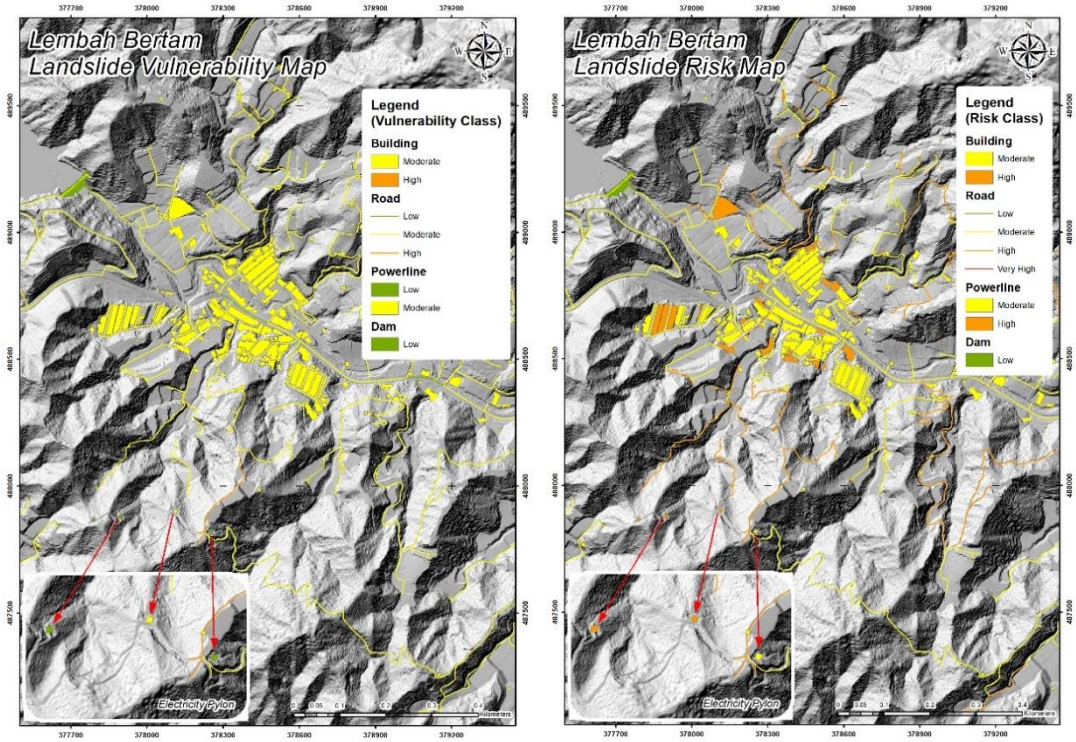

(a) **(b)**

Fig. 11: (a) Landslide vulnerability and (b) landslide risk maps for Lembah Bertam, Cameron Highlands.

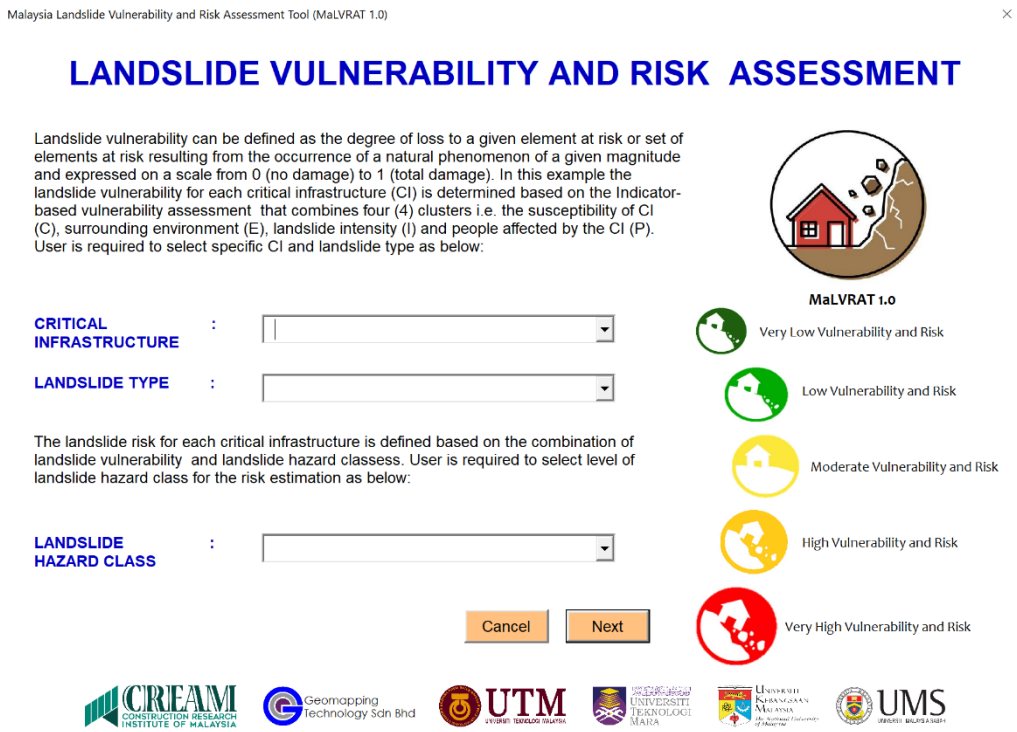

Fig. 12: Landslide vulnerability assessment tool.

Table 1: Landslide validation at Taman Bukit Mewah, Bukit Antarabangsa.

Scenario: Taman Bukit Mewah, Bukit Antarabangsa, Hulu Kelang, Selangor (6th December 2008)
Landslide type: Translational/Rotational
CI: Building
Susceptibility of CI (C) (0.36): • *Building typology (0.14)*: Reinforced concrete structure (0.40) • *Building Foundation Depth (Landslide Type Vs Deep Foundation Building (0.12)*: Accumulation height/landslide depth > 5 meter, shallow foundation (pad footing) (1.00) • *Number of floor (0.10)*: Medium rise (2 - 5 storey) (0.50) **Surrounding Environment (E) (0.18)**: • *Presence of protection (0.07)*: No protection (1.00) • *Distance between building (0.05)*: 3-5 meter (0.50) • *Building location (0.07)*: Building is located at the toe of slope (0.60) **Landslide intensity (I) (0.33)**: • *Accumulation height (0.15)*: > 2.0 meter (1.00) • *Landslide volume (0.18)*: 50,000 - 250,000 meter3 (0.90) **People inside the building (P) (0.13)**: • *Population density (0.04)*: High (0.90) • *Evacuation of alarm system (0.03)*: No (1.00) • *Age of people (0.03)*: Adults (0.20) • *Health condition (0.03)*: Health (Good) (0.10) ***Estimated vulnerability value***: 0.75
Class of vulnerability: High vulnerability
Class of vulnerability: Structural breaks, partly destructed, reconstruction of destructed parts, death is highly likely (severe injury) and evacuation necessary.

indicators have the same degree of influence on the final vulnerability value. Based on the FGD discussions, a total of 23 survey forms were completed with determined weighting values for each indicator and sub-indicator depending on the critical infrastructure given.

The results of the FGD shows that the expert panels tend to give similar scores to all indicators and sub-indicators. However, providing clear instructions to the panels during the FGD will minimize the generalization of giving the weighting values. The weighting values assigned for each indicator and sub-indicator should have good distribution between 0.1 and

1.0. The landslide vulnerability assessment based on different scenarios were conducted by using the data from FGD and internal experts' inputs show that further improvements should be made on the indicators, sub-indicators and more importantly on the weighting values.

In conclusion, the study has successfully achieved the objectives to assess and develop the parameters-indicators of landslide vulnerability assessment of critical infrastructures (CI) and assigning level for each parameter is addressed. The landslide vulnerability indicators, sub-indicators and its corresponding weights were tested in Lembah Bertam, Cameron Highland and evaluated for the Bukit Antarabangsa 2008 landslide event where detailed records from the disaster showed convincing results supported from various remotely sensed data, field data and other ancillary geospatial data.

Acknowledgement

This study is ostensibly supported by the Construction Research Institute of Malaysia (CREAM)- Construction Industry Development Board (CIDB) and Mineral and Geoscience Department (JMG) Malaysia in providing the landslide hazard map, geospatial data and non-geospatial data. We also would like to express our utmost gratitude to the specialized local experts from various backgrounds in helping us on improving indicators and sub-indicators weights during the FGD sessions.

References

Bignell, J.D., Snelling, N.J., (1977). *Geochronology of Malayan granites*. Overseas Mineral 490 Resources 47, Institute of Geological Science, London.

Birkmann, J., Cardona, O. D., Carreño, M. L., Barbat, A. H., Pelling, M., Schneiderbauer, S., … Welle, T. (2013). *Framing vulnerability, risk and societal responses: the MOVE framework*. *Natural Hazards, 67*, 193-211

Cardinali, M., Reichenbach, P., Guzzetti, F., Ardizzone, F., Antonini, G., Galli, M., … Salvati, P. (2002). A geomorphological approach to the estimation of landslide hazards and risks in Umbria, Central Italy. *Nat. Hazards Earth Syst. Sci., 2*, 57-72.

Cruden, D. M. and Fell, R. (eds.): *Landslide risk assessment. Proceedings International Workshop on Landslide Risk Assessment, Honolulu*, 19–21 February 1997, Balkema, Rotterdam, 371, 1997.

Dai, F. C., Lee, C. F. & Ngai, Y. Y. (2002). Landslide risk assessment and management: an overview. *Engineering Geology, 64*, 65-87.

Fell, R., Corominas, J., Bonnard, C., Cascini, L., Leroi, E. & Savage, W. Z. (2008). Guidelines for landslide susceptibility, hazard and risk zoning for land use planning. *Engineering Geology, 102*, 85 98.

Frédéric, L., P. Asté, J. & Leroi, E. (1996). *Vulnerability assessment of elements exposed to mass-movement: Working toward a better risk perception*.

Fuchs, S., Kuhlicke, C. & Meyer, V. (2011). Editorial for the special issue: vulnerability to natural hazards—the challenge of integration. *Natural Hazards, 58*, 609-619.

Kappes, M. S., Papathoma-Köhle, M. & Keiler, M. (2012). Assessing physical vulnerability for multi--hazards using an indicator-based methodology. *Applied Geography, 32*, 577-590.

Kaynia, A. M., Papathoma-Köhle, M., Neuhäuser, B., Ratzinger, K., Wenzel, H. & Medina-Cetina, Z. (2008). Probabilistic assessment of vulnerability to landslide: Application to the village of Lichtenstein, Baden-Württemberg, Germany. *Engineering Geology, 101*, 33-48.

Krahenbuhl, R., (1991). Magmatism, tin mineralization and tectonics of the Main Range, Malay Peninsula: Consequences for the plate tectonic model of Southeast Asia based on Rb-Sr, K-Ar and fission track data. *Geological Society of Malaysia Bulletin 29*, 1–100.

Li, Z., Nadim, F., Huang, H., Uzielli, M., & Lacasse, S. (2010). Quantitative vulnerability estimation for scenario-based landslide hazards. *Landslides. 7*. 125--134. 10.1007/s10346-009-0190-3.

Papathoma-Köhle, M., Zischg, A., Fuchs, S., Glade, T. & Keiler, M. (2015). Loss estimation for landslides in mountain areas – An integrated toolbox for vulnerability assessment and damage documentation. *Environmental Modelling & Software, 63*, 156-169.

Public Works Department. (2008). *Final landslide investigation report: investigation of slope failure at Taman Bukit Mewah, Bukit Antarabangsa, Hulu Klang, Selangor, 6 December 2008*, Slope Engineering Branch (CKC), Public Works Department (JKR) Malaysia.

Technical Committee on Risk Assessment and Management. (2004). *Glossary of Risk Assessment Terms. Version 1 [Online]*. International Society of Soil Mechanics and Geotechnical Engineering TC32.

Available: http://www.engmath.dal.ca/tc32/2004Glossary_Draft1.pdf [Accessed].

Totschnig, R., Sedlacek, W. & Fuchs, S. (2011). A quantitative vulnerability function for fluvial sediment transport. *Natural Hazards, 58*, 681-703.

UN-ISDR. (2004). *Terminology of disaster risk reduction* [Online]. United Nations International Strategy for Disaster Reduction, Geneva, Switzerland Available: http://www.unisdr.org/eng/library/lib-terminology-eng%20home.htm [Acc. July 29, 2018].

Uzielli, M., Nadim, F., Lacasse, S. & Kaynia, A. M. (2008). A conceptual framework for quantitative estimation of physical vulnerability to landslides. *Engineering Geology, 102*, 251-256.

Van Westen, C., Van Asch, T. W. & Soeters, R. (2006). Landslide hazard and risk zonation—why is it still so difficult? *Bulletin of Engineering geology and the Environment, 65*, 167-184.

Varnes, D. J. and IAEG Commission on Landslides and other Mass Movements: *Landslide hazard zonation: a review of principles and practice*. UNESCO Press, Paris, 63, 1984.

Thai Geoscience Journal 3(4), 2022, p. 36-62

ISSN-2730-2695; DOI-10.14456/tgj.2022.10

Magmatic arcs and nappes in Myanmar and western Thailand related to Neo-Tethys closure and Indian Ocean subduction

Andrew Mitchell[1]*, Kyaw Min Htun[2], Myint Thein Htay[2], and Nyunt Htay[3]

[1]*Consultant, Myanmar Precious Resources Group, Yangon, Myanmar*
[2]*Myanmar Precious Resources Group, Yangon, Myanmar*
[3]*No 176, Marga Street, Zegon West Block, Yangon, Myanmar*
**Corresponding author: andrewmitch999@aol.com*
Received 31 March 2022; Accepted 31 July 2022.

Abstract

Our tectonic interpretation of western Myanmar and westernmost Thailand adopts proposed restorations of ca 450 km post-Eocene dextral displacement on the Sagaing Fault and argues that in the Early Jurassic Neo-Tethys lay between convergent subducting oceanic basins, one offshore Sibumasu on the Asian plate, and one offshore a narrow continental Victoria-Katha Block. With basin closures ophiolitic nappes obducted from Neo-Tethys over-rode turbidites on the Asian and Victoria-Katha Blocks' passive margins, translating the turbidites landward as flysch (deformed or tectonised turbidite) nappes. On the Asian margin crustal thickening in the E-vergent orogen formed the Yinmabin Schist, re-thrust eastwards over the flysch before orogenic polarity reversed and the eastward-subducting Neo-Tethys generated the Early Cretaceous W-facing Mondaung Arc in Myanmar and Thailand. We suggest that on the Victoria-Katha Block's eastern margin ophiolite obduction was followed by reversal in orogenic polarity, westward subduction of Neo-Tethys and Late Cretaceous Popa-Loimye arc magmatism which ended soon after 90 Ma with Neo-Tethys closure, thrusting of the Victoria-Katha Block onto Asia and formation of a suture zone which probably continues into the Nujiang-Bangongco zone in China. Subsequent back-thrusting translated metamorphic rocks on the Asian margin westwards, over-riding the Neo-Tethys suture zone and *Orbitolina* Limestone on the Victoria-Katha Block as seen in the Shwebo Basin and north of Mogok. Following crustal shortening, partial melting and intrusion of Western Tin Belt granites at ca 70-44 Ma, orogenic polarity again reversed and eastward subduction of the proto-Indian Ocean generated Late Eocene and younger magmatic rocks of the Popa-Loimye Arc. We argue that most of the copper, gold, tin, tungsten, antimony, jadeite and gemstones in Myanmar west of the Palaeo-Tethys are related to the above orogenic events, although the formation of sapphire, ruby, Shante district gold and Monywa copper were accompanied by dextral displacement on the Sagaing Fault.

Keywords: arc reversals, convergent subduction zones, divergent flysch nappes, Mayathein back--thrust, metamorphic nappes, Neo-Tethys closure, Western Tin Belt.

1. Introduction

Most ideas on the tectonic evolution of Myanmar west of the Palaeo-Tethys and western-most Thailand infer that since the late Early Cretaceous a Zone 1, Shan Thai (Bunopas, 1981) or Sibumasu Block, part of Asia by the Late Triassic, occupied the Shan Scarps, Tanintharyi and much of the Shan Plateau (**Fig. 1**). This Block since the mid-Albian was bordered to the west by a variably-defined West Burma, West Myanmar or Victoria-Katha Block beneath which eastward subduction of a Tethyan or proto-Indian Ocean generated the Popa--Loimye or Western Myanmar (**Fig. 2**) magmatic arc (e.g. Mitchell, 1979; Deng, Wang, Li, Li, & Wang, 2014; Zhang et al., 2018; Li et al., 2020; Mitchell, Myint Thein Htay, & Kyaw Min Htun, 2021) and many of Myanmar's abundant mineral deposits (e.g. Mitchell, 1986; Gardiner, Robb, & Searle, 2014; Gardiner et al., 2016; Wang, Deng, Carranza, & Santosh, 2014). Significant

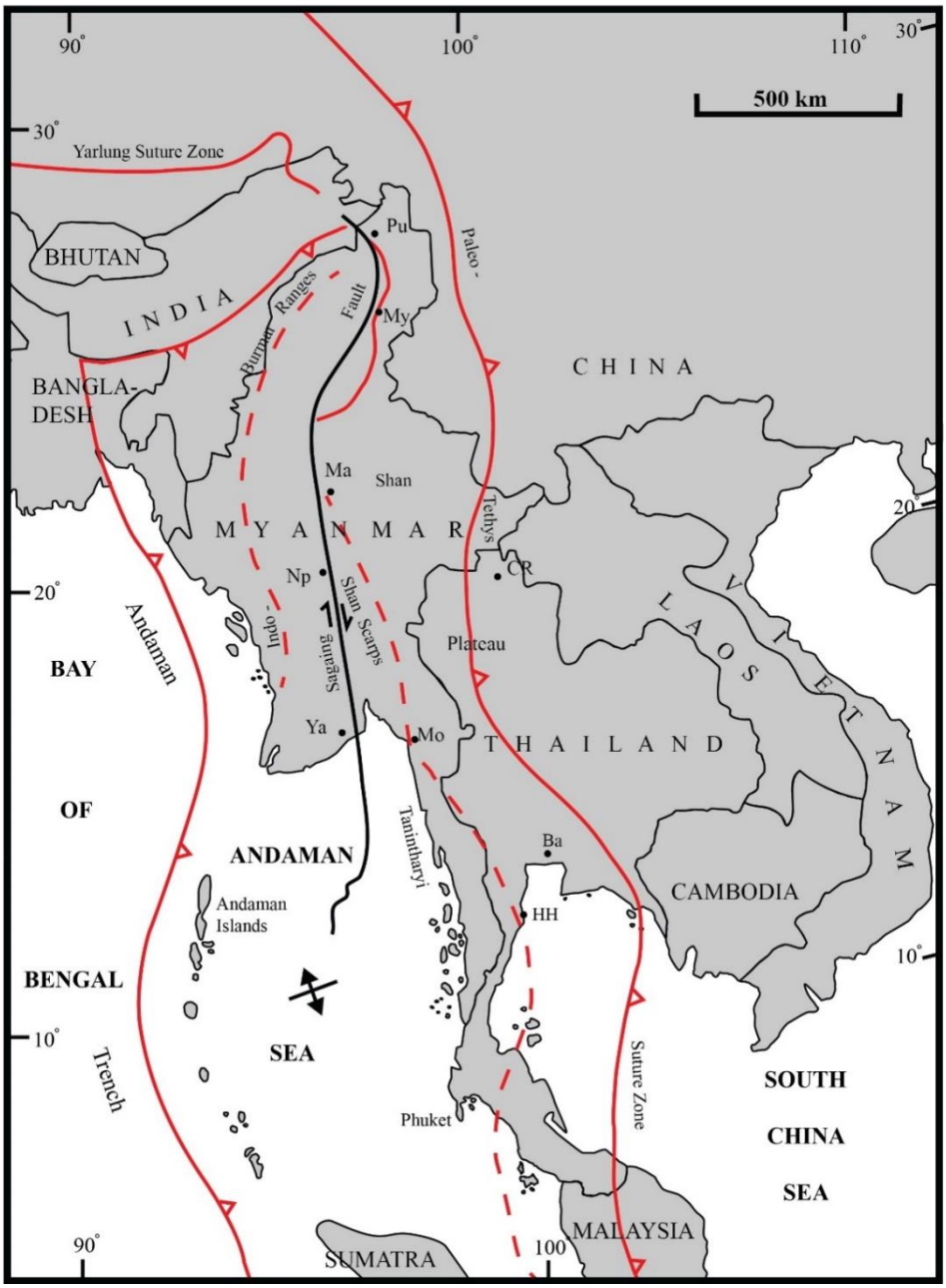

Fig. 1: Regional tectonic setting of Myanmar and western Thailand. Ba Bangkok, CR Chiang Rai, HH Hua Hin, Ma Mandalay, Mo Moulmein, My Myitkyina, Np Naypyidaw, Pu Putao, Ya Yangon.

variations of this model are those of Westerweel et al., (2019) and Morley, Chantraprasert, Kongum & Chenoll, (2021) who have proposed generation of the Popa-Loimye arc in mid--Tethys and its accretion to Asia along a Late Palaeogene dextral strike-slip fault.

For pre-Albian tectonics west of the Palaeo-Tethys there is no near-consensus comparable to that for the subsequent period. Many authors have invoked accretion to Sibumasu of a western Burma (Myanmar) block or ribbon continent. Proposed mechanisms include dextral strike-slip emplacement on a pre-Jurassic fault along (Metcalfe, 2013) or near (Barber, Khin Zaw, & Crow, 2017) the Late Cenozoic Sagaing Fault, and eastward (Mitchell, 1979; Li et al., 2018) or westward subduction (Mitchell, Tin Hlaing & Nyunt Htay, 2010; Mitchell, Chung, Thura Oo, Lin, & Hung, 2012; Mitchell, Myint Thein Htay, & Kyaw Min Htun, 2018) and closure of an ocean basin along the western margin of the Mogok Metamorphic Belt and Shan Scarp (**Fig. 3**). The Shan Scarp

and Nwalabo Fault zone of Garson, Amos, & Mitchell (1976) are the proposed continuation of Jin's (1996) Nujiang Fault, the Nujiang-Luxi suture zone of Cai & Li (2001) in Yunnan. Ridd (2017a) proposed dextral strike-slip emplacement of his Irrawaddy Block along this zone in the Mesozoic and Palaeogene, and Metcalfe (2011) favoured eastward subduction beneath a coherent Greater Sibumasu which extended westwards to the Indo-Burman Ranges. Gardiner et al. (2018) illustrated collision of an amalgamated east and west Sibumasu with the small Tengchong block of Deng et al. (2014) in the Early Cretaceous, and Zhang et al. (2018) argued for post-Triassic subduction beneath Sibumasu, by then part of Asia, and accretion to its western margin of imbricated flysch units successively younger to the west. The term flysch in this paper is taken from the intensively studied Swiss Alps where it refers to turbidites deposited in a subducting ocean basin and deformed before and during ocean closure. Other previous reconstructions for Myanmar and Thailand west of the Palaeo-Tethys include proposed links between the Upper Triassic flysches of the Tethyan Himalaya, Tagaung-Myitkyina Belt and Indo-Burman Ranges (e.g. Mitchell, 1984; Cai, Ding, & Yao, 2020; Peng et al., in press).

We here adopt the restoration (**Fig**. **3**) of a long-proposed dextral displacement on the Sagaing Fault, most recently estimated at 486 km (Morley & Arboit, 2019) since the mid--Oligocene. In northern Myanmar where the Fault is oblique to the regional trend, restoration of ca 450 km displacement implies that Neo--Tethyan oceanic rocks in the Tagaung-Myitkyina Belt northeast of the fault continued southwestwards into the northeastern end of the Indo-Burman Ranges and Central Lowlands west of the fault, forming a single Late Triassic and Jurassic ocean (Mitchell and Garson, 1981; Mitchell et al., 2021). We also adopt earlier proposals that by the end-Triassic or Early Jurassic the Victoria-Katha block, much of which now lies west of the Sagaing Fault, was off-shore Gondwana, more specifically Australia (Cai et al., 2020), and separated from the continent by an incipient proto-Indian Ocean and from Sibumasu by Neo-Tethys. We argue that oceanic basins on the Victoria-Katha and Sibumasu plates subducted on convergent zones beneath Neo-Tethys, from which ophiolite nappes were obducted on to the Victoria-Katha and Sibumasu Block margins. Subsequent reversals in orogenic polarity and closure of Neo-Tethys were followed by latest Cretaceous back-thrusting and generation of the Western Tin Belt in Myanmar and southwestern Thailand. The main structural belts in Myanmar and westernmost Thailand are shown in **Fig. 2.**

2. The Victoria-Katha Block west and east of the Sagaing Fault

The Victoria-Katha Block (Mitchell et al., 2021) includes the Kanpetlet Schist and Naga Metamorphics in the Indo-Burman Ranges, the anticlinal core of the Jade Mines Uplift east of the southern Naga Hills, the basement of the Myanmar Central Depression between the Indo--Burman Ranges and Sagaing Fault, the Katha--Gangaw Range and Tagaung Myitkyina Belt, and possibly part of the Kumon Range (**Fig. 2).**

2.1 Indo-Burman Ranges:

We describe first the Chin Hills and Rakhine Yoma in the south of the Ranges (**Fig. 4a)**, based largely on the mapping by United Nations (1979a, b, c), and then describe the Naga Hills (**Fig**. **4b**) of Aitchison et al. (2019) in northwestern Myanmar and adjacent India.

2.1.1. Eastern Belt in the Chin Hills

Pre-Campanian rocks are confined to the Eastern Belt (United Nations 1979a) of the Ranges. In the southern Chin Hills the Kanpetlet Schists of Brunnschweiler (1966) were described by United Nations (1979a) as a 30 km wide belt of muscovite and biotite schist with local meta-pillowed basalts, the Hilawng Volcanics of Kyaw Win (unpub.report, 1969), and formed the core of the S-plunging Mindat Anticline (**Fig**. **4a**). The Schist is overlain to the east and west by the highly-deformed quartzose turbidites and mudstones of the flysch-like Pane Chaung Group (**Fig. 5**) which in the northern Chin Hills includes extensive broken beds. Upper Triassic *Daonella* first reported by Theobald (1871) established the age of the Group, although flysch of this age was not

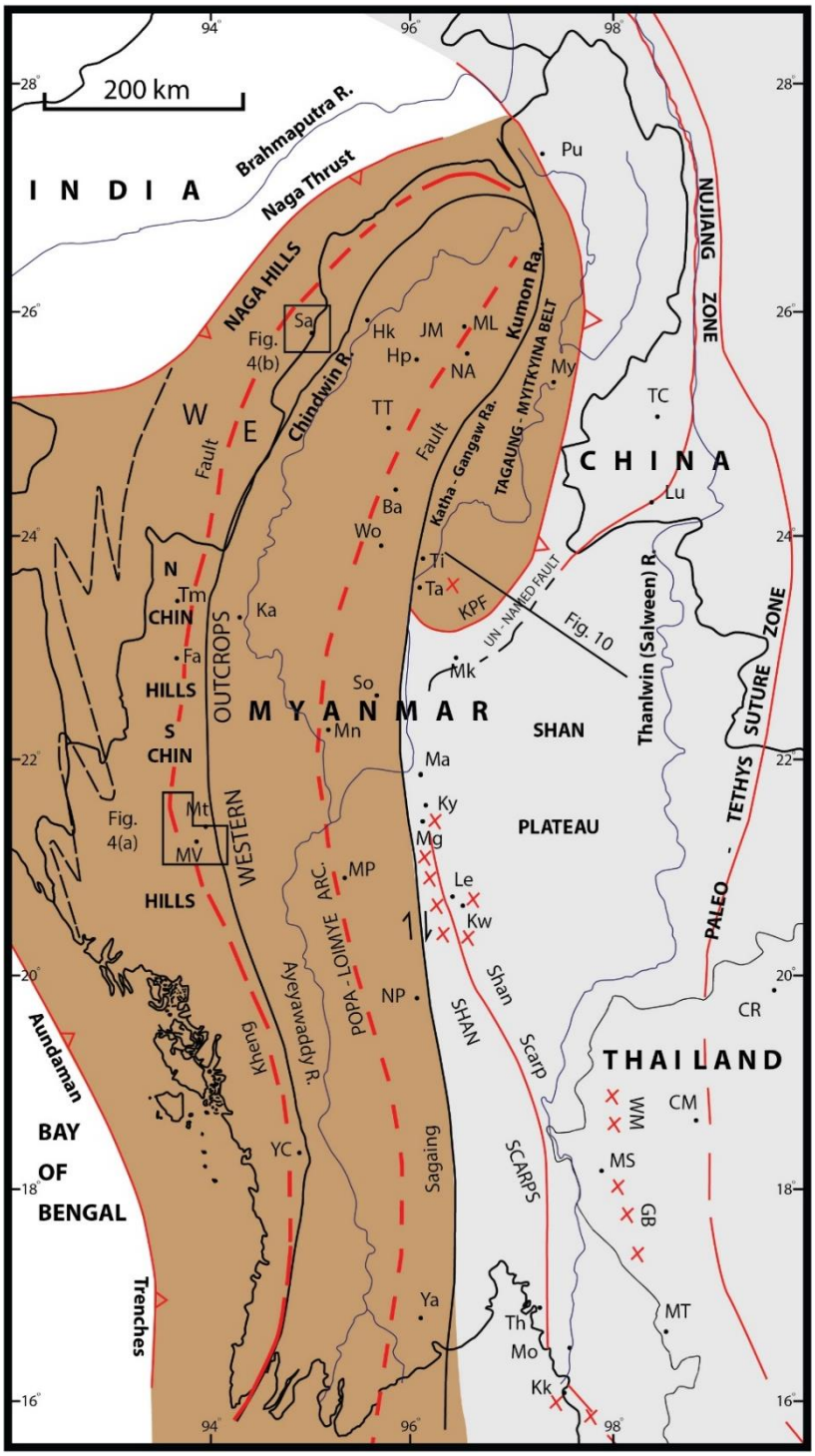

Fig. 2: Structural belts and locations in Myanmar and northwestern Thailand N of 16 deg N, partly from Myanmar Geosciences Society 2014. Ba Banmauk, CM Chiang Mai, CR Chiang Rai, E Eastern Belt Indo-Burman Ranges (IBR), Fa Falam, Hk Hkamti, Hp Hpakant, JM jade mines, Ka Kalemyo, KPF Kyaukpyu Fault, Kw Kalaw, Kk Kyaikkami, Ky Kyaukse, Le Lebyin, Lu Luxi, Ma Mandalay, Mg Mondaung, My Myitkyina, Mk Mogok, ML Mt Loimye, Mn Monywa, Mo Moulmein, MP Mt Popa, MS Mae Sariang, Mt Mindat, MT Mae Sot, MV Mt Victoria, NA Nanyaseik, NP Nay Pyi Daw, Pu Putao, Sa Mt Saramati, So Shwebo, Ta Tagaung, TC Teng Chong, Th Thaton, Ti Tigyaung. Tm Tiddim, TT Taungthonlon, Ya Yangon, YC Yethawa Chaung, W Western Belt IBR, WMGB Western Marginal Granite Belt, Wo Wuntho. Mondaung Arc shown by red crosses.

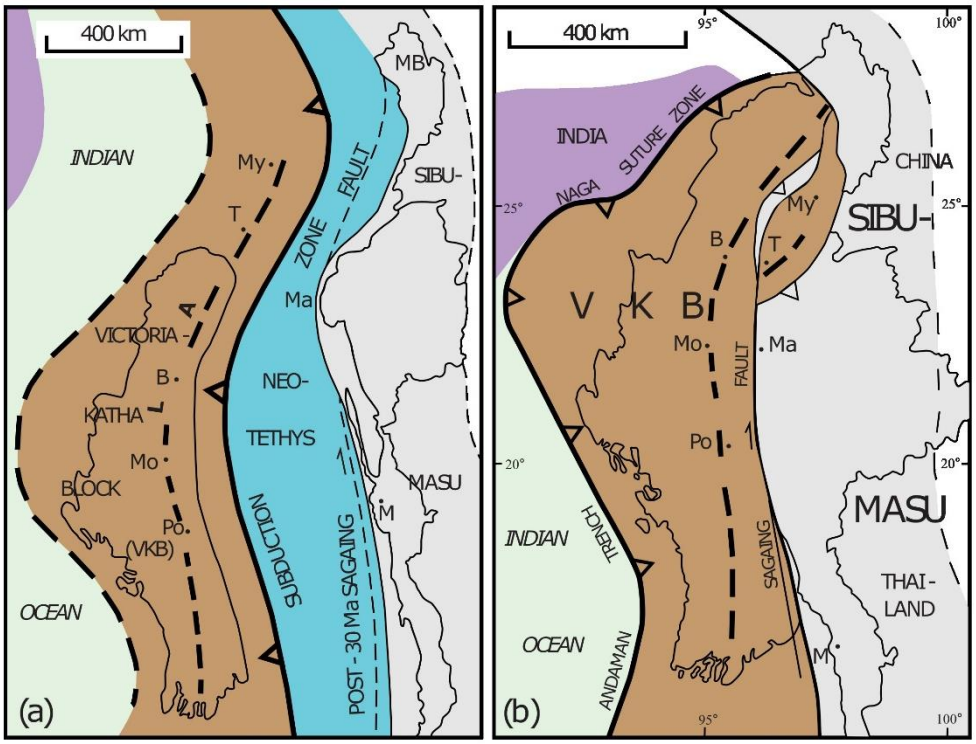

Fig. 3: Sketch maps of Myanmar and western Thailand at (a) ca 95 Ma prior to closure of Neo-Tethys and dextral displacement on the Sagaing Fault, and (b) present day. The Tagaung- Myitkyina Belt (T-My) is on the Victoria-Katha Block in (a) but east of the Sagaing Fault in (b). B Banmauk, M Moulmein, Ma Mandalay, Mo Monywa, Po Mt Popa. PLA Popa-Loimye Arc. After Mitchell et al., (2018).

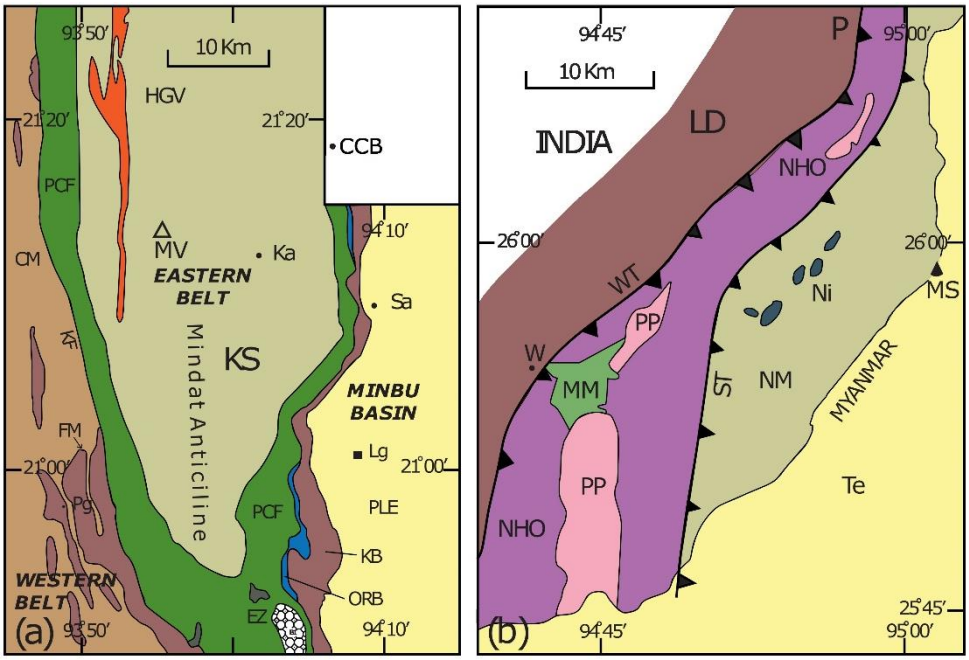

Fig. 4: Geological sketch maps, Indo-Burman Ranges. (a) Southern Chin Hills, Myanmar. CCB Che Chaung Basalts, CM Chunsung Mudstone, EZ Exotics Zone, FM Falam Fm, HGV Hilawng Volcanics, Ka Kanpetlet, KB Kabaw & Paunggyi Fms, KF Kheng Fault, KS Kanpetlet Schist, Lg Laungshe, MV Mt Victoria, ORB Orbitolina (Paung Chaung) Limestone, PCF Pane Chaung Fm or flysch, Pg Pandaung, PLE post-Lower Eocene, Sa Saw, from United Nations (1979a). (b) Part of southern Naga Hills, India and Myanmar. LD Lower Disang Fm, MM Mudstone Melange, MS Mt Saramati, NHO Naga Hills Ophiolite, Ni Nimmi Limestone, NM Naga Metamorphics, P Phokphur, PP Phokphur Fm, ST Saramati Thrust, Te Tertiary, W Waziho, WT Waziho Thrust, simplified from Aitchison et al. (2019). Locations on Fig.2.

reported by Brunnschweiler (1966). Rare chert beds occur within the Pane Chaung flysch and some other cherts contain Middle Jurassic radiolaria (Zhang et al., 2017; Zhang, Xiao, Cai, & Kyaing Sein 2020). In the northern Chin Hills the Kanpetlet Schist is not exposed and the Triassic flysch belt includes a dozen bodies of variably serpentinised ultramafic rocks. Among these United Nations (1979a,b) described the Webula Taung harzburgite-dunite body and adjacent 2 km wide amphibolite-piedmontite-quartz schist since identified as a metamorphic sole, and reported a K/Ar age of 158+- 20 Ma on low-K hornblende from a pegmatite within a serpentinite sheet in the Mindat Anticline, one of many pegmatites within serpentinites in the Chin Hills and Arakan (Rakhine) Yoma. Liu et al. (2016) obtained for plagiogranite a zircon U-Pb age of 127 Ma and for the Webula Taung amphibolitic sole, 116 Ma, the implied emplacement age of the overlying ophiolite.

Pillowed and massive basalts are here informally named Che Chaung (River) Basalts (Fig.5) from east of Mt Victoria **(Fig. 4a)** where they contain blocks of the underlying Pane Chaung flysch and are intruded by diabase and basalt dykes. To the south in the Maw Chaung a basalt body 2 km long and up to 40 m wide lies with a stratigraphic contact on flysch to the west and is overlain by mid-Cretaceous Paung Chaung Limestone which continues eastwards at the base of the Chindwin (forearc) basin succession. Over 250 km to the south in the Yethawa Chaung **(Fig. 2)** E-younging pillowed basalts up to 50 m thick overlie the flysch and pass upwards with increasing limestone intercalations into the Paung Chaung Limestone.

2.1.2. Western Belt in the Chin Hills

In the Western Belt of the southern Indo-Burman Ranges (**Figs. 4a, 5**) the oldest unit, the Falam Formation, consists of mudstones interbedded with Campanian and Maas-trichtian *Globotruncana* -bearing pelagic limestones, and containing blocks of pillowed basalt, chert, andesite and ophicalcite, exposed in the cores of upright anticlines. Limestones within the Falam Formation, the Senonian flysch of Brunnschweiler (1966), occur as boudined and coherent beds within mudstones and only locally form the supposedly exotic blocks described by Brunnschweiler (1966) and subsequent workers. The Falam Formation is overlain by Palaeocene mudstones and turbidité sandstones beneath Eocene sand-stones and limestones preserved in syncline cores which form N-trending ridges up to 2700 m elevation. To the west the Cretaceous to Eocene succession is covered by younger sedimentary rocks. The steeply-dipping Kheng Fault juxtaposes the Eastern with the Western Belt.

2.1.3. Indo-Burman Ranges in the Naga Hills

In the southern Naga Hills four main structures have been proposed **(Fig. 4b)**. The Sarameti Thrust of Aitchison et al. (2019) carries the Naga Metamorphic Complex or Naga Metamorphics of Brunnschweiler (1966) westwards over ophiolitic rocks and the mud--matrix melange of Bannert, Albert Sang Lyen & Than Htay (2011) and Aitchison et al. (2019). These are translated westwards on the Waziho Thrust, probably equivalent to the Kheng Thrust in the Chin Hills, over Aitchison et al.'s (2019) Tertiary Indo-Burman flysch. This is the Naga flysch of Brunnschweiler (1966), and correlated by Aitchison et al. (2019) with the India-derived Disang Group of Evans (1964), but we suggest that much of the Indo-Burman flysch is instead equivalent to the Falam Formation in the Chin Hills. Evans' (1964) Naga Thrust **(Fig. 2)** carries the Disang Group westwards over younger 'molasse' sediments overlying Indian basement in the Foreland Spur and is probably the continuation of the Kaladan Fault or suture zone of Yang et al. (2020) west of the Kheng Fault in the Chin Hills. Aitchison et al.'s (2019) proposed suture zone east of the Naga Metamorphics may lie within the Hpakant and Taw Maw serpentinite bodies which flank the metamorphic core in the Jade Mines area.

Aitchison et al. (2019) have shown that the Naga Metamorphics are probably post-Cambrian and that radiolarian cherts to the west have Middle and latest Jurassic and middle Early Cretaceous ages. Triassic flysch is not reported in the Naga Hills but we suspect its presence beneath the Sarameti Thrust in the melange which might include broken beds.

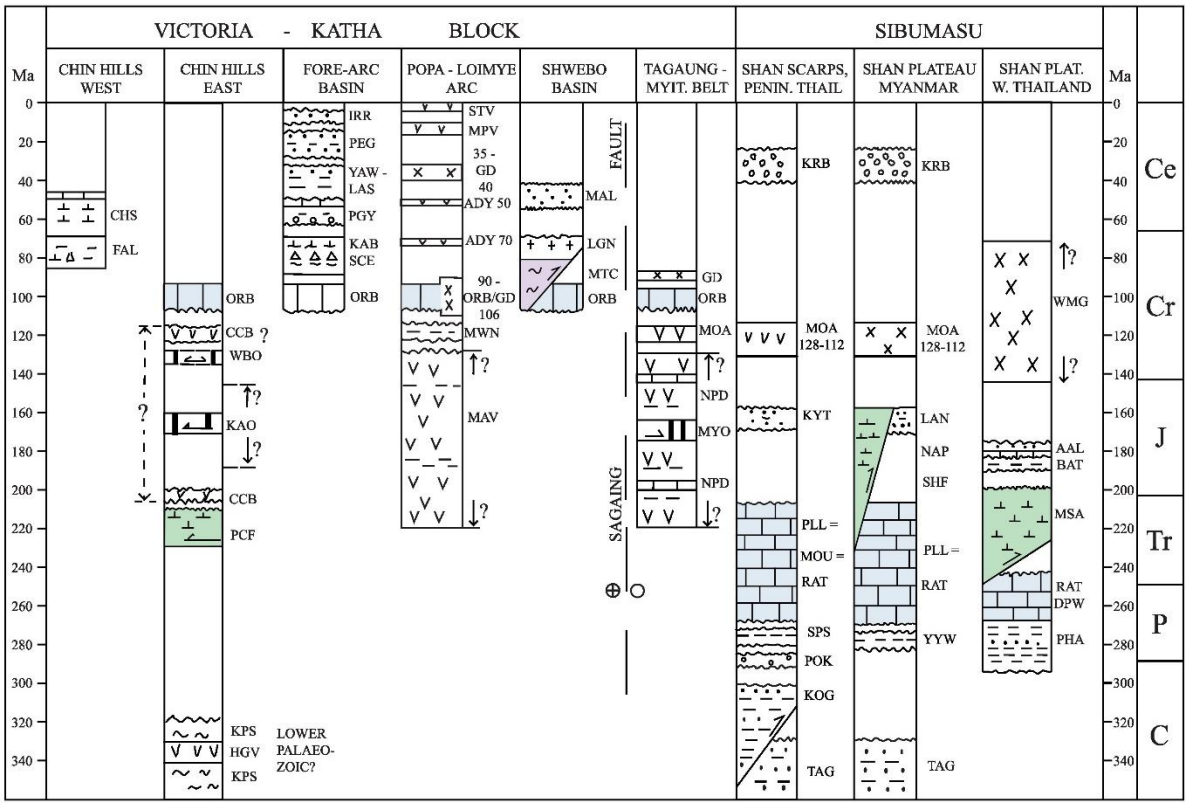

Fig. 5: Post-Devonian stratigraphic columns for structural belts in Myanmar and Thailand west of Palaeo-Tethys. AAL Aalian, ADY andesitic dyke, BAT Bathonian, CCB Che Chaung Basalts, CHS Chunsung Fm, DPW Doi Phawar Fm, FAL Falam Fm, GD granodiorite, HGV Hilawng Volcanics, IRR Irrawaddy Fm, KAB Kabaw Fm, KAO Kalemyo ophiolite, KOG Kogwe Mudstone, KPS Kanpetlet Schist, KRB Kalaw Red Beds, KYT Kyaukhsu Taung Fm, LAN Loi An Fm, LAS Laungshe Shales, LGN leucogranite, MAL Male Fm, MAV Mawgyi Volcanics, MOA Mondaung Arc, MOU Moulmein Limestone, MPV Mt Popa Volcanics, MSA Mae Sariang Fm, MTC Mayathein Complex, MWN Mawlin Fm, MYO Myitkyina ophiolite, NAP Napeng Fm, NPD Ngapyawdawchaung Fm, ORB Orbitolina Limestone, PCF Pane Chaung Flysch, PEG Pegu Gp, PGY Paunggyi Fm, PHA Pharaka Fm, PLL Plateau Limestone, POK Poklokkale Fm, RAT Ratburi Limestone, SCE Sin Chaung Exotics, SHF Shweminbon Fm, SPS Spinomartinia prolifica Shale, STV stratovolcanoes, TAG Taungnyo Gp, WBO Webula ophiolite, WMG Western Marginal Granite Belt, YAW Yaw Fm, YYW Yin Yaw Fm.

2.1.4. Structure of the Indo-Burman Ranges

United Nations (1979a) inferred that ophiolite was thrust westwards over the Pane Chaung flysch, although in the eastern limb of the Mindat Anticline they show flat-lying inverted flysch beds with W-vergent folds forming the lower limb of a regional eastward--overturned anticline with Kanpetlet Schist in the core. The E-vergent structure has not been confirmed by subsequent workers and we follow Zhang et al. (2017) who reported W--vergent folds in right-way-up beds, and Cai et al. (2020) who related 290-200 Ma detrital zircons from the Pane Chaung flysch to deposition in a submarine fan along the northern margin of Australia (**Fig. 6a)** in an analogous setting to the Tethyan Himalayan flysch. We suggest that a Victoria-Katha Block with the Pane Chaung flysch on its eastern margin then rifted from Australia, possibly in front of a back-arc basin **(Figs. 6b, 7a)** and that as proposed by Mitchell (1986) the Pane Chaung flysch was translated westwards (in present orientation) beneath an obducted ophiolite nappe (**Fig. 7b).** An Early to mid-Jurassic age for this ophiolite**,** and for many of the ultramafic bodies within the flysch belt in the northern Chin Hills, is inferred from the presence of mid-Jurassic cherts in the Ranges. Obduction of a second ophiolite **(Fig. 7 d, e**) can explain the Webula Taung ultramafic body ca 116 Ma (Liu et al., 2016). Following erosion, we speculate that the Pane Chaung

flysch was covered by Che Chaung Basalts before deposition of *Orbitolina* Limestone **(Fig. 7f, g**).

2.2 Central Lowlands:

The Myanmar Central Lowlands (Central Basin or Depression) are divided by the Popa--Loimye Arc into the fore-arc basin in the west (**Fig. 2**) and the narrower back-arc or Shwebo basin in the east.

2.2.1. Fore-arc (Salin-Chindwin and Minbu) basin and the Sin Chaung Exotics Zone

The fore-arc basin, situated between the Indo-Burman Ranges and the Popa-Loimye Arc, contains up to 17 km of sedimentary fill (Pivnic et al.,1998). The Upper Albian--Cenomanian Paung Chaung (*Orbitolina*) Limestone of the Chin and Rakhine foothills re-appears in the western flank of the Popa--Loimye Arc (**Fig. 5)** and has been intercepted in an oil exploration borehole in the Chindwin Basin. Although said to be unconformable on the Late Triassic flysch (Gramman, 1974), the Limestone commonly overlies the Che Chaung Basalts (**Fig. 5**) with an inter-layered basalt--limestone transitional zone (United Nations, 1979a).

Serpentinite sheets or sills from a few metres to a few hundred metres thick are most abundant near the eastern margin of the flysch where as noted by Chhibber (1927, *in* Chhibber, 1934) they commonly occur within *Orbitolina* Limestone and like the larger ultramafic bodies include hornblende pegmatite veins. Hydrothermal ophicalcite (listwaenite), the silicic rock of Chhibber (1934), occurs at the limestone-serpentinite contact.

Outcrops of *Orbitolina* Limestone in the southern Chin foothills are overlain in the Western Outcrops (**Fig**. **2**) by the E-dipping Kabaw Formation **(Fig. 5)** of Aung Khin & Kyaw Win (1968) and Win Swe, Thacpaw, & Nay Thaung Thaung (2010), a mudstone--turbidite-limestone association partly arc--derived (Yang et al., 2012) and equivalent to the Falam Formation west of the Mindat Anticline (**Fig. 5).** At the southern end of the Anticline, United Nations (1979a), Mitchell (1984), and Mitchell (2017, fig. 11.5) described E-dipping *Orbitolina* limestone overlain by a 2 km-wide zone of varie-coloured mudstones with rafts of Senonian micritic limestones and blocks of chert, diabase, gabbro, gabbro-clast conglomerate, basalt, ophicalcite, marble and scarce rounded cobbles of Triassic sandstone. This succession, the Sin Chaung Exotics Zone (United Nations (1979a), is over-ridden on the Kabaw Thrust (**Fig**. **7h**) by an easterly-dipping upward sequence of Triassic flysch, *Orbitolina* Limestone and Kabaw turbidites beneath conglomerates of the unconformable mid--Palaeocene to Lower Eocene Paunggyi Formation. We infer deposition of the *Orbitolina* Limestone on and east of the Che Chaung Basalts on the Victoria-Katha Block margin, followed in the Campanian and Early Maastrichtian by deposition of the Falam and Kabaw Formations on and east of the Limestone.

The fore-arc basin succession above the Kabaw Formation (**Fig. 5)** is predominatly clastic and well-exposed in the Western Outcrops **(Fig. 2).** Major unconformities occur at the bases of the Paunggyi Formation, the Oligocene Lower Pegu Group, the Lower and Middle Miocene Upper Pegu Group and the Upper Miocene to Pliocene Irrawaddy Formation (Tainsh, 1950; Ridd 2017b). The basin succession forms a synclinorium with E-vergent thrusts east of the Bago Yoma medial uplift and W-vergent to the west (Myanmar Geosciences Society, 2014).

2.2.2 Mawgyi Volcanic Group and the Popa-Loimye Arc

The Mawgyi Volcanic Group (**Figs**. **5, 7f, g)** best seen together with the younger Popa--Loimye Arc in the Wuntho-Banmauk and Monywa-Salingyi uplifts, is also known as Mawgyi Andesites, Mawgyi Basalts, or Mawgyi Volcanics. The Group consists of a thick succession of largely basaltic pillow lava and lava breccias with pervasive chlorite-epidote propylitic alteration. These are inter-bedded with volcanogenic sedimentary layers and pass up into the entirely volcaniclastic Mawlin Formation (**Fig. 5)** which is overlain by *Orbitolina* Limestone (Mitchell, 2017).

Numerous andesitic dykes, largely porphyritic hornblende-bearing and unaltered, intrude the Mawgyi Volcanic Group. Isotopic ages on the dykes are confined to K/Ar determinations of 70 and 50 Ma near Shangalon (United Nations, 1978a). Small bodies of rhyodacite intrude the Mawgyi Group, which may correlate with either the Che Chaung Basalts (**Fig. 5)** or pre-mid Cretaceous supra-subduction zone oceanic arcs inferred to have overlain the obducted upper mantle bodies in the Chin Hills (**Fig. 7d).**

In the Popa-Loimye Arc, also known as the Western Burma or Popa-Wuntho magmatic arc (Mitchell, 2017; Li et al., 2020), the older arc rocks are intrusions within the Mawgyi Volcanic Group and Mawlin Formation, all of which form inliers within Tertiary sediments (**Fig. 5)**. These intrusions include mid-and early Late Cretaceous (ca. 107 to 90 Ma) I-type biotite and biotite-hornblende granites and smaller diorites of the Kanzachaung batholith. Two-mica and foliated garnet-bearing granites form the Pinhinga Plutonic Complex north of the batholith. Younger Arc magmatic rocks are described in Section 3.7.

The arc basement (United Nations, 1979d ; Mitchell, 2017), includes amphibolites and migmatitic gneisses in the Banmauk (**Fig**. **2**) region, garnet and sillimanite schists and pegmatites at Shinmataung south of Monywa, blocks of garnet-amphibolite rock in Late Cenozoic basaltic lavas at Monywa and gneiss xenoliths at Mt Popa. Sericite and chlorite schists north of Banmauk may correlate with phyllites and argillites in the same area and with phyllite pebbles in Eocene conglomerates at Shangalon. Chlorite-albite schists northeast of Wuntho underlie the Mawgyi Volcanics and may be equivalent to those in the Tagaung--Myitkyina Belt and to the Hilawang Volcanics of the Chin Hills.

Although widely interpreted as a W-facing arc throughout its life (e.g. Mitchell, 1986; Gardiner et al., 2014, 2016; Li et al., 2020, 2018), speculative westward subduction beneath an E-facing arc (**Figs. 7f, 8a**) from ca 107 to ca 90 Ma (Mitchell et al., 2010, 2018,) allows for a Late Cretaceous closure of Neo--Tethys and either an interruption or dramatic decrease in arc magmatism until westward subduction began in the Eocene (Section 3.7).

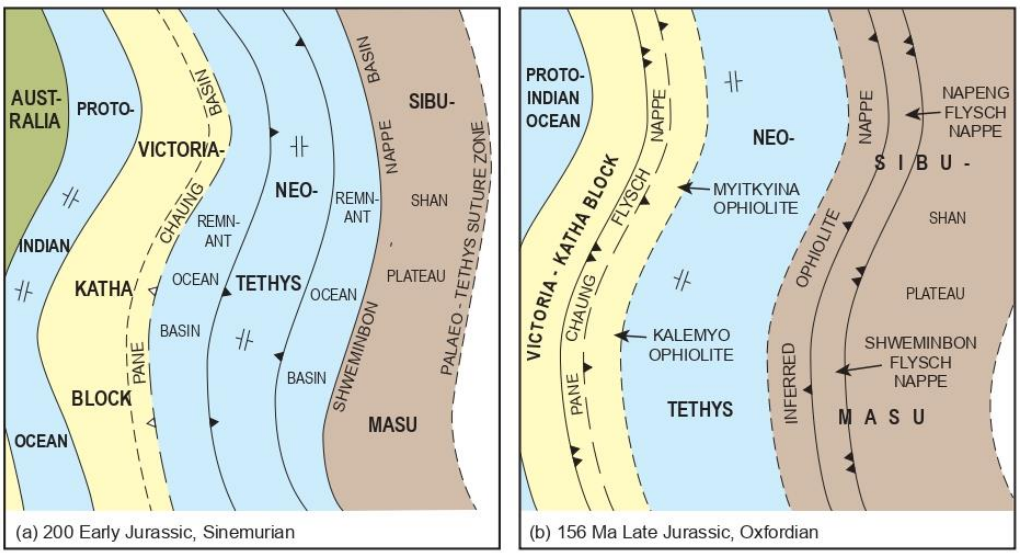

Fig. 6: Schematic sketch maps showing blocks and oceans in Myanmar and western Thailand at (a) 200 Ma Early Jurassic, Sinemurian and (b) 156 Ma Late Jurassic, Oxfordian.

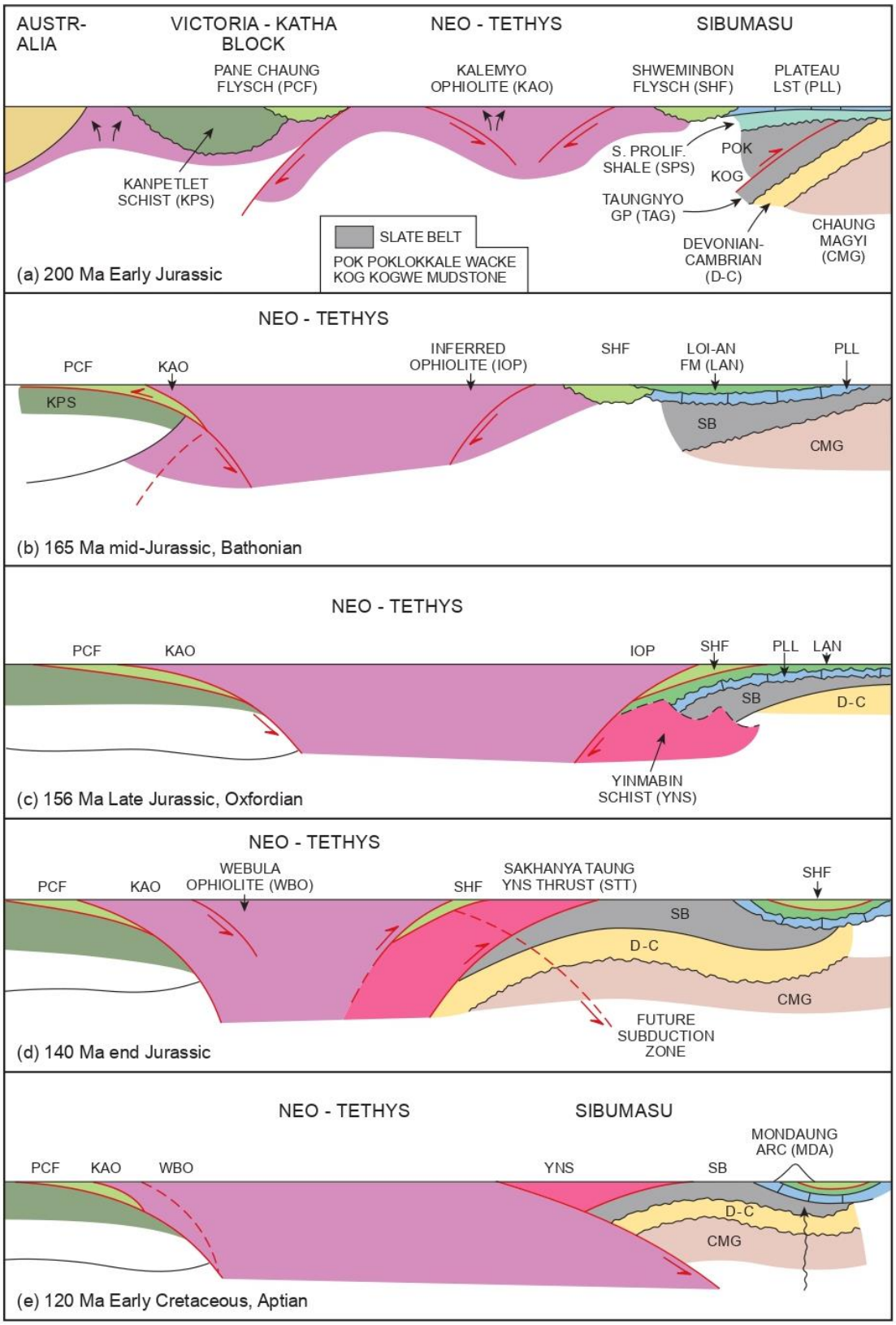

Fig. 7: Schematic E-W sequential cross-sections through north-central Myanmar and northwestern Thailand illustrating structural evolution, ocean basins and some rock units not to scale. Yinmabin Schist in (c) is metamorphosed overlying stratigraphic sequence.

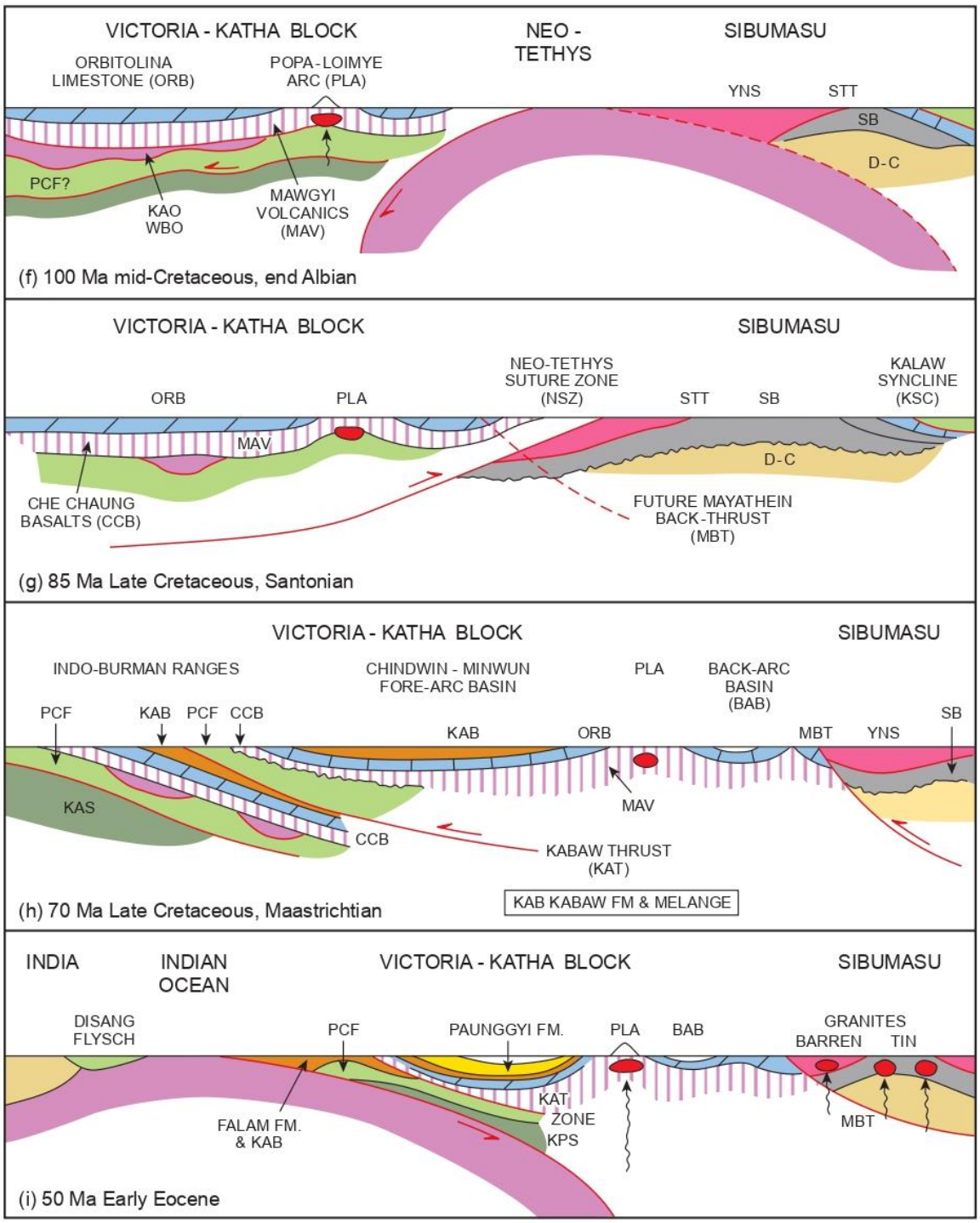

Fig. 7: Schematic E-W sequential cross-sections through north-central Myanmar and northwestern Thailand illustrating structural evolution, ocean basins and some rock units not to scale. (contd.)

2.2.3 Back-arc or Shwebo Basin

This basin attains its greatest width around latitude 22 deg 30 min N but narrows northwards to 24 deg N where granodiorite of the Popa-Loimye Arc is only 20 km west of the Sagaing Fault.

The basin is occupied largely by a succession (**Fig. 5**) of sandstones and shales with open upright folds, the Male Formation, with the Lower Eocene Tongyauk Conglo-merate at the base (Myint Thein & Maung Thein, 2014). South of Kyaukse, Neogene sedimentary rocks exten to east of the Sagaing Fault.

In the Shwebo Basin west of Tigyaing **(Fig. 2)** and a kilometre west of the Sagaing Fault a narrow inlier of diopside-phlogopite marble, skarn, amphibolite and migmatitic gneiss intruded by leucogranite forms the N-trending Mayathein Complex of United Nations (1979b, c). This is juxtaposed with the *Orbitolina*--bearing (Myint Thein, 2015) Kywethe Limestone to the west (**Fig. 5**). A few kilometres further west the Ubye serpentinite trends NNE for 15 km and is bordered on the west by basalts, phyllites, volcanogenic sediments and minor limestones forming the Ngypaw-dawchaung Formation of United Nations (1979b), correlated with the Mawgyi Volcanics in **Fig. 7f.** At the serpentinite-basalt contact pyritic quartz-haematite rock, probably listwaenite, replaces limestone.

2.3. Tagaung-Myitkyina Belt and Katha-Gangaw Range:

These features lie east of the Sagaing Fault (**Figs. 2, 3)** but their geology resembles that to the west (**Fig. 5).** The historically rather inaccessible Tagaung-Myitkyina Belt in Myanmar's Northern Shan and Kachin States consists of actinolite-epidote-albite and chlorite schists, and basaltic rocks (Than Tun & Khin Myint, unpub report, 2002) in a stratigraphic succession correlated with the Ngapyawdaw Chaung Formation (Section 2.2) west of the Sagaing Fault. The succession, well exposed in the Nan Sen Chaung east of Paladokhta and southeast of Tagaung **(Fig. 2**), comprises a thick sequence of pillowed and massive basalt lavas, pillow breccias, volcanogenic sediments, cherty mudstones and andesites, with minor coralline Triassic limestones (Dr. Thura Oo, written comm., 2005), intruded by locally sheeted basalt dykes. A similar assemblage intruded by hornblende diorites and serpentinites was described by Clegg (1941) from the Ayeyawady River south of Myitkyina. Near Myitkyina basalt, leuco-gabbro, plagiogranite and pyroxenite yield zircon U-Pb ages of 166 to 177 Ma (Yang et al., 2012), and diorites resembling plagiogranites and gabbros ages of ca 173 Ma (Liu et al., 2016). Upper Triassic flysch occurs in the west of the belt.

At Tagaung Taung (**Fig. 2)** southwest of Tigyaing United Nations (1979c) described harzurburgite and dunite with chromitites overlying a metamorphic sole of chlorite schist and quartzite thrust over cherts in which Teza Kyaw, Suzuki, & Maung Maung (2020) reported uppermost Jurassic, Hauterivian and Aptian radiolaria. At Myitsone north of Myitkyina uppermost Jurassic cherts overlie red mudstones (Maung Maung, Aung Naing Thu, & Suzuki, 2014). Throughout the Tagaung-Myitkyina Belt the mid-Cretaceous *Orbitolina* Limestone occupies synclines, is unconformable on the basalts and chert, and in the two Ayeyawady defiles northeast of Tagaung (**Fig**. **2**) shows W-dipping axial planes (Clegg, 1941; Thura Oo, oral comm., 2004).

The Katha-Gangaw Range (**Figs. 8a, 9),** part of the Victoria-Katha Block, is a sinuous ridge about 170 km long underlain by the Katha Schist, comprising garnet-mica schist and micaceous quartzites beneath talc schists, with phyllite and marble to the east. Detrital zircons from the Schist include 418 Ma (Silurian) zircon U-Pb ages and a frequency peak at 500 Ma (Zhang et al., 2018). Rocks older than the Ngapyawdaw Chaung Formation occur northwest of the Ayeyawady's second defile where serpentinite is thrust over meta-turbidites and talc schists, probably part of the Katha Schist.

3. Shan Plateau, Shan Scarps and Mon-daung magmatic arc

The Plateau, Scarps and Mondaung Arc all lie east of the Sagaing Fault.

3.1. Shan Plateau succession:

The Shan Plateau occupies eastern Myanmar and western Thailand and continues northwards as the Baoshan Block (e.g. Jin, 1996) in Yunnan. Our description of the Plateau refers to its western part.

Northeast of Mandalay the Mong Long Mica Schist and Mogok Metamorphics are overlain on an un-named fault by a southeasterly-dipping monoclinal succession with the Late Proterozoic to Early Cambrian Chaung Magyi Group at the base (**Fig. 5).** The Group, several kilometres thick, consists of slates, slatey to phyllitic sandstone turbidites and mudstones, and semi-schist or coarse-grained meta-wacke.

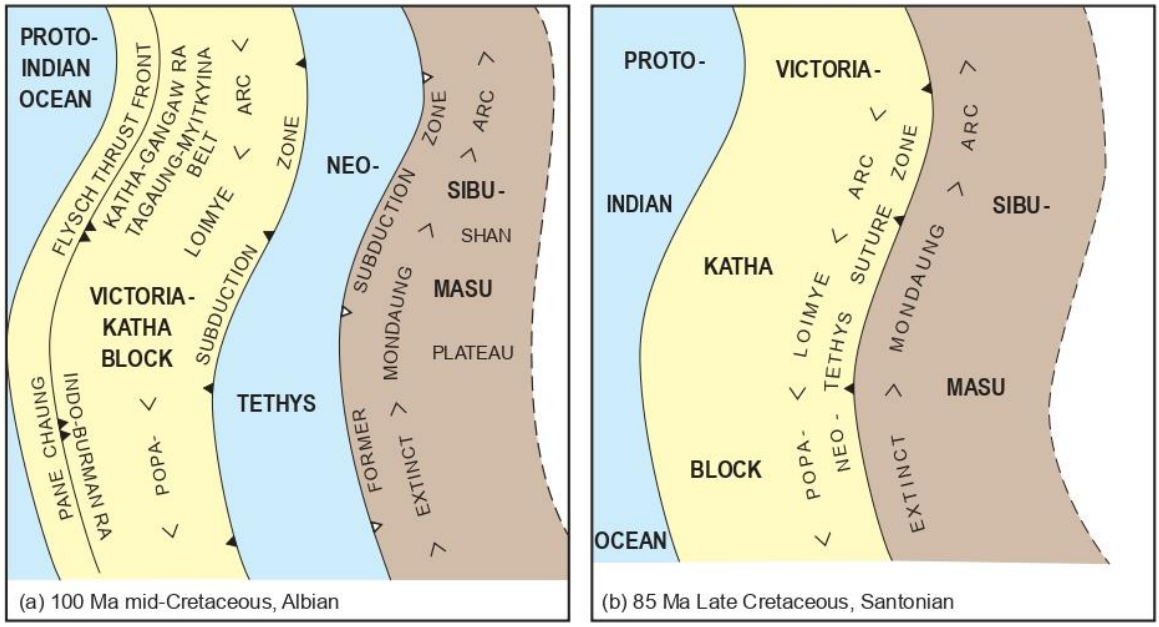

Fig. 8: Schematic sketch maps showing blocks and oceans in Myanmar and western Myanmar at (a) 100 Ma mid-Cretaceous, Albian and (b) 85 Ma Late Cretaceous, Santonian.

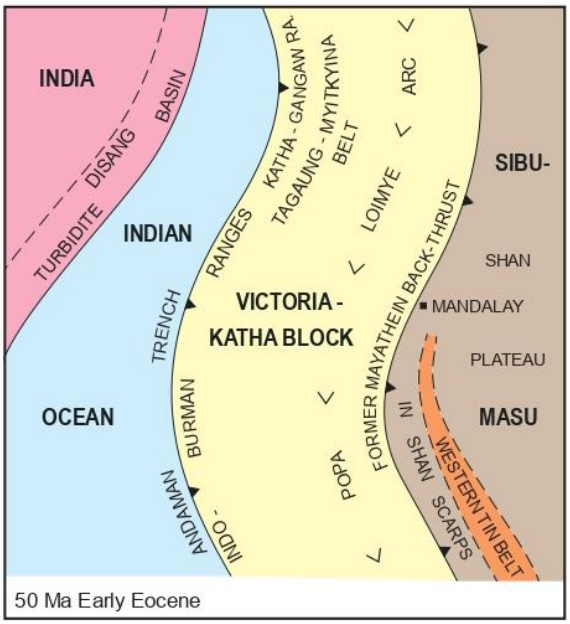

Fig. 9: Schematic sketch map showing blocks and Indian ocean at 50 Ma Early Eocene.

At its southeastern margin the Chaung Magyi is overlain probably conformably by rhyolitic pyroclastics of the Bawdwin Volcanics; both are overlain unconformably by Upper Cambrian cross-bedded quartzitic sandstones, shales and dolomitic limestones with a basal conglomerate. As recently summarised (Aye Ko Aung, 2020) the Upper Cambrian is overlain by a sequence comprising Ordovician argillaceous carbonates and shales, Silurian graptolitic shales and quartzose sandstones, and Devonian shales, dolomitic limestones and oolitic ironstones. The overlying Plateau Limestone here consists of the uppermost Permian to Triassic Nwabangyi Dolomite and Triassic Natteik Limestone. The Napeng Formation, an Upper Triassic flysch, overlies the Plateau Limestone and is said to be overlain

unconformably (Brunnschweiler, 1970) by the mid-Jurassic Tati Limestone beneath the unfossiliferous Kalaw Red Beds. East of the Shan Scarps, on the western margin of the Plateau, Plateau Limestone with the Middle and Upper Permian Thitsipin Limestone at its base continues into the mid to Late Triassic. On **Fig. 5** we show the Plateau Limestone overlain by the Bathonian to Oxfordian Loi-an Formation and the Loi-an overthrust by the complexly-folded turbidites and local limestone of the upper Triassic and lower Jurassic Shweminbon Formation, although the relationhip of the Shweminbon to the Loi-an Formation is disputed. The Shweminbon is correlated with the Napeng Formation to the north and overlain unconformably by Telu Limestone beneath Kalaw Red Beds.

3.2 The Slate Belt in the Shan Scarps, Tanintharyi and southwestern Thailand:

The Shan Scarps (**Figs. 1, 9**) were defined in the 1930s as the southward-widening belt between the Shan Plateau and Central Plain or Lowlands, extending from Mondaung south of Kyaukse to near Moulmein and bounded by the Shan Scarp in the east and alluvium east of the Sagaing Fault in the west (Myanmar Geosciences Society, 2014). The Scarps consist largely of the Slate Belt, a siliciclastic succession at least partly Late Palaeozoic in age, together with the Yinmabin Schist. The Slate Belt, absent in the Mandalay-Mogok region, re-appears in the Tengchong block (**Fig. 2**) in Yunnan and continues in Kachin State as a N--trending strip bordering China. South of the Scarps the Belt occupies most of Tanintharyi and southwestern Thailand including Phuket Island.

The lowest unit in the Slate Belt succession (**Fig. 7a)** is probably the Taungnyo Group, the Taungnyo Series of Leicester (1930), first defined in the Moulmein-Kyaikkami region (**Fig. 2**) and Late Tournaisian and Early Visean in age (Dr. Thura Oo, unpub. thesis, 2002). The Group also occurs at scattered localities along the western margin of the Shan Plateau, including Loikaw (Kyi Pyar Aung, Owens, & Metcalfe, 2014; Metcalfe & Kyi Pyar Aung, 2014) where it overlies mid-Palaeozoic strata and consists of marine sandstones, shales and minor limestones.

The Kogwe Mudstone (**Figs. 7a, 5**), the lower Formation of the Mergui Group in the Shan Scarps east of Yamethin (Mitchell et al., 2004), is probably older than and thrust over the Taungnyo Group, since the Upper Carboniferous in Sibumasu is missing (Wang et al., 2021). The Kogwe Mudstone, consisting of argillites and quartzites, is at least 2 km thick and unfossiliferous with 516 Ma detrital zircons (Kyaw Linn Zaw, Ohn Thwin, Travnor, & Thet Paing Kyaw Win, 2020) suggesting a possible source in the Bawdwin Volcanics. The Poklokkale Pebbly Wacke, the upper Formation of the Mergui Group, overlies the Kogwe Mudstone and includes thick beds of diamictite or pebbly wacke which occur through peninsular Thailand and Sumatra to Bangka Island in eastern Indonesia, and northwards through northeastern-most Myanmar into Central Lhasa and the South Qiangtang Block (**Fig. 1**) in Tibet. In South Quiangtang and south of Myanmar the distinctive pebbly wackes contain Asselian fossil assemblages (Wang et al., 2021) and in Myanmar, detrital zircons of Carboniferous, Ordovician and Precambrian age (Aung Zaw Myint et al., 2017).

The Poklokkale Wacke is overlain stratigraphically by the Sakmarian *Spinomartinia prolifica* Shale (**Fig. 5)** well exposed around Kyaukse, near Moulmein in the Zinyeik and Taungnyo Ranges and Hpa-an to the east, and east of Lebyin. South of Kyaukse the Magiye Conglomerate with clasts of Devonian to Ordovician age (refs *in* Mitchell, 2017) overlies Devonian beds and passes up into *S. prolifica* Shale beneath mid-Permian to Triassic Plateau Limestone (Thura Oo, Tin Hlaing, & Nyunt Htay (2002). On the Shan Plateau east of Nay Pyi Daw the *S. prolifica* Shale and equivalent Yin Yaw Formation of Hobson (1941) are overlain by the Plateau Limestone. In Thailand the Pharaka Formation southeast of Mae Sot and southwest of Mae Sariang **(Figs. 2, 5)** includes Sakmarian shale and is overlain by Middle Permian Limestone (Sukto, Suteethorn, Boripatgosol, Meesok &

Sareerat, 1984; Ueno & Charoentitirat, 2011). The Khao Phra Formation of Raksaskulong & Wongwanich (1993) west of Hua Hin (**Fig. 1)** includes Asselian diamictites and is therefore older than the *S. prolifica* Shale.

In northern Tanintharyi a 15 km wide belt of slates and quartzites resembling the Kogwe Mudstone is overlain by pebbly wackes dipping west beneath granite gneiss (Saw Naung et al., unpub., 1981). A similar pebbly wacke-gneiss relationship is seen at Kyaikkami near Moulmein (Nyunt Htay, Ko Ko & Ba Than, unpub. reprt, 1982). The Moulmein Limestone in Tanintharyi and the equivalent Ratburi Limestone in western and peninsular Thailand correlate with the Plateau Limestone and overlie the Slate Belt and the roughly equivalent Kaeng Krachan Group in Thailand. In the Phuket region Mitchell, Young, & Jantaranipa (1970) divided their Phuket Group, the Kaeng Krachang Formation of Javanaphet (1969) and Raksaskulong & Wongwanich (1993), into a Lower Formation with pebbly mudstones or diamictites, and a bryozoa-rich Upper Formation at least partly of Early Permian age and here correlated with the *S. prolifica* Shale, overlain by the Ratburi Limestone.

The Shan Scarps have been variously interpreted as either part of Sibumasu (e.g. Metcalfe, 1984), formerly Shan-Thai (Bunopas,1981), or a separate unit (e.g. Bender, 1983; Ridd, 2017a) or terrane with its eastern boundary in Myanmar at the W-facing Shan Scarp (**Fig. 2**). The Scarp in most places consists of Plateau Limestone and southwards from Kyaukse the westernmost outcrops of pre- Carboniferous rocks lie up to 30 km to the east. Nevertheless the *S. prolifica* Shale-Plateau Limestone succession overlies both the Asselian diamictite-bearing strata in the Slate Belt of Myanmar and western Thailand, and Devonian strata on the Shan Plateau (**Fig. 5).** This suggests that, despite a contrary view (Jin, 1996) for these belts in Yunnan, the Plateau and Shan Scarps were on the same plate through the Permian-Triassic and were not separated by an ocean basin.

The mid-Jurassic (170-172 Ma) granitic rocks intruding spinel and ruby-bearing marble at Mandalay Hill and diopside marble at Kyanikan 30 km to the north (Barley, Pickard, Khin Zaw, Rak, & Doyle, 2003), and also ca 20 Ma hornblende-biotite bearing dykes near Payangazu, lack obvious explanations.

3.3 The Shweminbon, Napeng and Mae Sariang flysch nappes:

The Upper Triassic to Lower Jurassic Shweminbon and Napeng Formations have been interpreted as passive continental margin deposits **(Figs. 6a, 7a, b)** thrust eastwards onto the Shan Plateau as an orogenic flysch **(Figs. 6a, b, 7c)** beneath an inferred and now-eroded obducted ophiolite (Mitchell et al., 2004). Cai et al. (2017) reported a 1.8 Ma peak and Permian to Triassic U-Pb ages on Shweminbon detrital zircons implying derivation from easternmost Myanmar. As noted above, the Bathonian to Oxfordian Loi-an and equivalent Kyaukhsu Taung Formations of shallow marine sediments and coals were probably deposited unconformably on Triassic Plateau Limestone and Slate Belt clastics (**Fig. 5)**, before being overthrust by the Shweminbon Formation **(Fig. 7 b, c).**

To the southeast of the Scarps in northwestern-most Thailand, Chonglokmani (2011) described the Middle and Upper Triassic Mae Sariang Formation **(Figs. 2, 5)** of cherts and pelagic limestones overlain by flysch with E-vergent folds; we correlate this with the Shweminbon Formation in Myanmar. The Mae Sariang Formation overlies siliciclastics which are underlain by the Middle and Upper Permian Doi Phawar Formation (Ueno & Charoentitirat, 2011) equivalent to the Plateau Limestone and Moulmein Limestones in Myanmar (Ridd, 2016). Curiously, ophiolitic melange thrust sheets in the Palaeo-Tethyan Changning-Menglian suture zone in Yunnan are also E-vergent (Zhong & Zhao, 2000); the exact location of the suture zone's continuation through Myanmar into northwestern Thailand **(Fig. 1**) is uncertain.

In our interpretation Jurassic emplacement of the flysch onto the Plateau was followed by generation and emplacement of the Yinmabin Schist described below.

3.4 The Yinmabin Schist in the Shan Scarps and Tanintharyi:

At its western margin the Slate Belt is overlain structurally on the Sakhanya Taung Thrust by metamorphic rocks assigned by Mitchell (2017) to the Mogok Metamorphic Group. Here we revert to the name Yinmabin Schist (Maung Thein et al., 1972, unpub.) for the metamorphics west of Yinmabin and elsewhere in the Scarps south of Mandalay. The Schist includes sillimanite schist, diopside-phlogopite marble, and migmatites, the mixed gneisses of Dutt (1942), with extensive areas of augen gneiss. It is intruded by latest Cretaceous and Palaeocene granites including the 72 Ma Nattaung Granite and a 59 Ma dyke in Bilin Quarry near Kyaukse (**Fig. 2)** town (Mitchell, Chung, Thura Oo, Lin, & Hung, 2012) which cut the main metamorphic fabric. The Schist attains a maximum width of 30 km east of Nay Pyi Taw and the Sagaing Fault (Bateson, Mitchell, & Clarke, 1972).

The locally abundant marble and calc-silicate within the Schist suggest an origin by tectonic burial of the Shan Plateau succession with its high content of Ordovician to Devonian and Permian carbonates. We infer that during and following emplacement of the Neo-Tethys-rooted Shweminbon flysch and inferred overlying ophiolite, the underlying Shan Plateau crust was shortened, metamorphosed to form the Yinmabin Schist and translated eastwards over the ophiolite, flysch and Slate Belt on the Sakhanya Taung Thrust **(Figs. 7c, d, 8a).** The Schist therefore now is structurally above the flysch, which is no longer on the western margin of Sibumasu (**Fig. 7e**) but probably correlates with Triassic flysch in the southwestern segment of the Luxi-Nujiang-Bangongco suture zone of Mo, Lu, & Shen (1993) and Chu et al. (2009) in Yunnan.

At the eastern margin of the Slate Belt south of Lebyin a narrow strip of schist, gneiss and diopside-phlogopite marble known informally as the Bon Schist can be interpreted as part of the Yinmabin Schist nappe translated eastwards on the Sakhanya Taung Thrust in the latest Jurassic or earliest Cretaceous. Uplift to the west and truncation in the east by an E-dipping extensional fault (Mitchell et al., 2021) resulted in preservation of the Schist as a klippen.

3.5 Early Cretaceous Mondaung Arc in the Shan Scarps and Plateau margin:

Rhyodacitic sills or dykes, diorites and granodiorites occur west and immediately east of the Shan Scarp in Myanmar, and comprise the Mondaung Arc of Lin, Mitchell, & Chung (2019) and Mitchell, Kyaw Min Htun, & Myint Thein Htay (2020). The Arc **(Fig. 2)** includes the Lawa or Law Chaung diorites intruding Shweminbon flysch east of Lebyin, rhyodacite dykes west of the diorites and at numerous localities between Lebyin and Mondaung, and the Yebokson Granodiorite and Yinmabin West diorite in the Slate Belt and schist near the Meiktila-Kalaw motor road. Lin et al. (2019) established that zircon U-Pb ages of these intrusions are within the 128 to 113 Ma range; the 113 Ma sample is a pebble within the Pyinyaung Formation which includes the Patchaung Volcanics of United Nations (1979c,e). Some of the intrusions form the continental margin arc of Zhang et al. (2018) who related it to eastward subduction within the Indo-Burman Ranges. We follow a proposal that subduction of Neo-Tethys (**Fig. 8a**) generated the arc after E-vergent orogeny and reversal in orogenic polarity (Mitchell et al., 2020, 2021).

Dacitic and andesitic undated dykes in the Mergui Group south of Lebyin and in the Loi-an Formation east of Kalaw, and the 121 Ma Mawpalaw Taung granite of Mi Paik & Khin Zaw (2014) southeast of Moulmein (**Fig. 2)** are probably part of the Mondaung Arc, as are Cretaceous hornblende-bearing granitic rocks to the north in Cobbing's (2011) Western Marginal Granite Belt in Thailand, I-type granites in western Tanintharyi (Cobbing, Pitfield, Derbyshire & Mallick, 1992) and rhyolites in the Mergui Archipelago. At Kyaikkami (**Fig. 2)** south of Moulmein Thet Paung Kyaw Win, Hla Kyi, & Kyaw Lin Zaw (2020) reported a zircon U-Pb age of 121 Ma on migmatite intruded by granodiorite and biotite granite. We speculate that the granite is part of the arc and that its emplacement reset the migmatite age to 121 Ma. Mondaung Arc

magmatism evidently ceased long before intrusion of the 90 Ma Mokpalin diorite (Mitchell et al., 2012) northwest of Moulmein.

3.6. Late Cretaceous closure of Neo-Tethys:

The interruption to magmatic activity in the E-facing Popa-Loimye Arc beginning ca 90 Ma (Section 2.2.2.) can conveniently be attributed to closure of Neo-Tethys and end-Cenomanian (ca 90 Ma) collision of the Victoria-Katha Block or island arc with Sibumasu on the subducting Asian plate **(Figs. 7f, g, 8a, b).** Collision-related shortening in the Sibumasu crust accompanied by regional metamorphism can explain the transformation of some Cretacous granites to augen gneiss, for example the augen-gneiss near Kyaukse town with a 114 Ma zircon U-Pb magmatic age recording its intrusion into the Yinmabin Schist. Eastward-overturned folds in *Orbitolina* Limestone northeast of Tagaung may also have resulted from the collision.

3.7 Back-thrusting and crustal granites in the Western Tin Belt:

Granites of the Western Tin Belt of Myanmar and Thailand (Mitchell, 1977) intrude the Slate Belt between Mondaung **(Fig. 2)** and Phuket Island in Thailand. These are S-type or evolved ilmenite series peraluminous and reduced fractionated granites and almost all are in the 72 to 44 Ma age range. The granites are commonly explained by either the India-Asia collision (Wang et al., 2014) or the ca 70 Ma roll-back of the supposed low-angle E-dipping subduction zone related to the Popa-Loimye Arc system (Jiang, Li, Jiang, Wang, & Wei, 2017; Sanematsu, Manaka, & Khin Zaw, 2014; Li et al., 2018, 2019). We suggest instead that following Late Cretaceous closure of Neo-Tethys and thrusting of the Victoria-Katha Block on to Sibumasu **(Fig. 7g)**, orogenic polarity reversed. A related W-directed back-thrust carried Sibumasu over the Victoria-Katha Block, resulting in crustal shortening followed by partial melting and granite generation in tectonically thickened crust of the underthrust Block (**Figs. 7h, i, 9).** The back-thrust is perhaps analogous to that proposed by Oliver, Zaw, Hotson, Meffre, & Manaka (2014) for the generation of tin granites following closure of Palaeo-Tethys and orogenic polarity reversal in the Main Range Malaysia.

We infer that in the Indo-Burman Ranges west of the main back-thrust, related W-directed thrusts translated the Falam-Kabaw Formations to their present position in the Chin Hills and generated over-pressure beneath mudstone seals within the Formations. Resulting fluidisation and disruption of the interbedded limestones and underlying sediments formed melanges or oliststromes in the Sin Chaung Exotics Zone (**Fig. 4a)** and rafts of volcanic rock in the Manipur River (United Nations, 1979a) in the northern Chin Hills. Thrusting may also have mobilised previously obducted serpentinite, allowing its ascent as sheets in the *Orbitolina* Limestone. The proposed Sin Chaung Fault (Mitchell et al., 2021) lies to the north of the Exotics Zone.

We suggest that the back-thrust is exposed in the Shwebo Basin as the N-trending fault west of the Sagaing Fault, between the Mayathein Complex and the *Orbitolina* Limestone and nearby Ubye Serpentinite (Section 2.2.3). We regard the Mayathein Complex as part of the Yinmabin Schist east of the Sagaing Fault, thrust westwards in the early Palaeocene over the Kywethe (*Orbitolina*) Limestone **(Fig. 7h, i)**. Although forming the boundary between the Victoria-Katha Block and Sibumasu, the back-thrust in most places buries the Late Cretaceous collisional suture zone. Before Oligocene and Late Cenozoic dextral dislacement on the Sagaing Fault (**Fig**. **3 a**,**b**) the Mayathein Complex, the back-thrust and the underlying Kywethe Limestone, now situated west of Tigyaing and Tagaung (**Fig**. **2**), lay south of Nay Pyi Daw and west of the Shan Scarps.

In our interpretation by ca 55 Ma the back--thrusting had migrated to the western margin of Myanmar and initiated eastward subduction of the proto-Indian Ocean (**Fig**. **9**) with renewed magmatism in the Popa-Loimye Arc, forming Late Eocene plutons at Shangalon (e.g. United Nations, 1978 a,b; Mitchell, 2017), 14 Ma quartz andesite porphyries and rhyolites at Monywa, and ca 14 Ma rhyolites now beneath the Mt Popa (Stephenson & Marshall, 1984; Lee,

Chung, & Yang, 2016,) stratovolcano **(Fig. 5)**. Many of these rocks either intrude or overlie the Cretaceous arc plutons, although Taungthonlon stratovolcano lies west of the old arc axis.

4. Mogok Metamorphic Belt

The sickle-shaped Mogok Metamorphic Belt extends northwards from Mandalay hill through Mogok to northernmost Myanmar. The Belt consists of sillimanite-bearing migmatites, calc-silicates, schists and marbles (Iyer, 1953; Searle & Ba Than Haq, 1964) in upward succession with a metamorphic grade up to granulite facies (Searle et al., 2020). The most distinctive rocks are diopside-phlogopite-graphite marbles which commonly include gem-quality spinel or locally ruby. The metamorphic rocks are intruded by Upper late Oligocene to Lower early Miocene biotite granites, and leucogranite sheets occur in the migmatites. Intrusions of nepheline syenite (e.g. Iyer, 1953) and charnockite, mostly sheet-like, are present in the Mogok gemstone district and are probably Jurassic (Searle et al., 2020) and mid-Miocene (Shi et al., 2021), both older and younger than the late Eocene-Oligocene (Lamont et al., 2021) or Oligocene-early Miocene (Myint Myat Phyo et al., 2020) high-grade metamorphism.

At Nanyaseik (**Fig. 2**) west of the main splay of the Sagaing Fault, inliers in alluvium expose a 12 km wide biotite granite in which bodies of diopside-phlogopite marble, probably roof pendants (Dr. M.J. Crow, oral comm. 2021), contain ruby and spinel and resemble marble from the Mogok Metamorphic Belt. This has arguably been translated northwards on the Sagaing Fault from an original position southwest of Mandalay.

Clegg (1941) proposed that the Mogok Metamorphic Belt is the metamorphosed equivalent of the *Orbitolina* limestone and older formations on the Shan Plateau. This equi-valence, excluding the *Orbitolina* limestone, is supported by the structural position of the Mogok Metamorphics dipping southeast under the Mong Long Mica Schist and Chaung Magyi Group (**Fig. 10**). We suggest that the Mogok Belt and Yinmabin Schist both formed by metamorphism of a Shan Plateau succession protolith and had a similar early tectonic and metamorphic history, but that the Mogok Belt underwent longer-lasting uplift than the Schist. The north-eastward continuation of the Mayathein back-thrust may be the steep SE--dipping Kyaukpyu Fault between the Mogok Metamorphic Belt and Tagaung-Myitkyina Belt (**Figs. 2, 11**). Part of the Mogok Belt's uplift and exhumation may have taken place in the footwall of the un-named extensional fault (Mitchell et al., 2021), perhaps a re-activated thrust, inferred at the base of the Chaung Magyi Group. Displacement here perhaps contributed to prolonged uplift with deeper, younger and higher-grade peak metamorphism in the Mogok Metamorphics than in the Yinmabin Schist.

5. Mineral deposit and gemstone formation in western Myanmar-Thailand

Episodes of mineralisation and gemstone formation from the Jurassic to Pliocene (**Fig. 11**) are an essential part of the region's evolution. The oldest potentially economic hydrothermal deposits are the stratiform volcanogenic copper-gold occurrences situated near the top of the Mawgyi Volcanics north of Shangalon, and discovered ca 2012. The mineralisation, conformable with the Mawgyi basalt host rocks, is poorly constrained as Triassic to Early Albian.

Possibly the next oldest deposits are the orogenic quartz-gold vein systems in the Slate belt of the Shan Scarps where Modi Taung has produced an estimated ten tonnes of gold from12 km of underground workings. Veins are cut by dacitic and andesitic dykes thought to be part of the 128 to 113 Ma Mondaung Arc. The veins are no older than the maximum late Early Permian age for deformation in the Slate Belt, but we speculate that veining followed Late Jurassic emplacement of the Shweminbon flysch. Numerous similar auriferous veins are present elsewhere in the Scarps and include occurrences in the Slate Belt of Tanintharyi and near Hua Hin (**Fig. 1**) in Thailand. Orogenic quartz-gold veins in the Late Precambrian to earliest Cambrian Chaung Magyi slates (**Fig. 11**) could be co-eval with those within the Slate Belt.

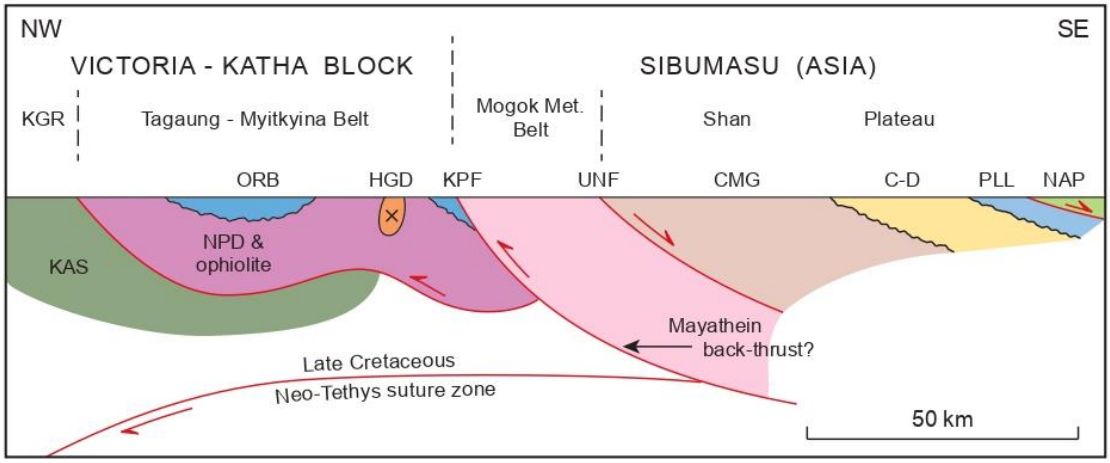

Fig. 10: Schematic NW-SE cross-section, Mogok region. CD Cambrian-Devonian, CMG Chaung Magyi Group, HGD hornblende-biotite granodiorite, KAS Kanpetlet Schist, KGR Katha-Gangaw Range, KPF Kyaukpyu Fault or thrust, NAP Napeng flysch, NPD Ngapyawdawchaung Fm., ORB Orbitolina Limestone, UNF un-named fault. Location on Fig.2.

Gold-copper skarn ores are mined from marbles and Lower Cretaceous diorite stocks and dykes of the Mondaung Arc at Shwe-minbon immediately east of Lebyin and at Paladokhta near Tagaung in the Tagaung--Myitkyina Belt. Jadeite veins in northwestern Myanmar are in serpentinites which probably ascended from deeply subducted rocks of the Victoria-Katha Block (Mitchell et al., 2021) and were exhumed by mid-Cretaceous time but most of the extraordinarily high production of gem-quality jade is from vein-derived fossil placers, probably of Late Cenozoic age at Hpakant and Palaeogene at Khamti.

In the Western Tin Belt mineralisation is associated with the reduced crustal granites (Section 7) within the Slate Belt which forms a world-class Sn-W-Ta and also an orogenic Au metallotect. Clegg (1944) described 400 Sn-W workings in the Myanmar segment where some veins yield more tungsten than tin, described with isotopic ages in many recent publications. Niobium-tantalum is recovered from concentrates from the Thai segment. The veins and pegmatites with Sn-W-Ta occur in granite apices and host rocks which are invariably hornfelsed, but apparently identical granites in the Yinmabin Schist lack mineralisation. The tin, and also the granites, may have originated in the Victoria-Katha Block beneath the Mayathein back-thrust.

Several types of mineralisation are undoubtedly related to hydrothermal systems associated with the post-Cretaceous W-facing Popa-Loimye Arc. These include chalcopyrite-bornite veins in the 40-33 Ma granodioritic stocks and dykes at Shangalon, frequently cited as a porphyry system but with distinctive quartz stockworks and probable potassic alteration. Low sulphidation epithermal gold veins are widespread in the Mawgyi Volcanics, a gold metallotect, but are probably genetically related to unexposed deep intrusions in the Popa-Loimye Arc. Epithermal gold veins at Kyaukpahto (Ye Myint Swe, Cho Cho Aye, & Khin Zaw, 2017) are hosted by Eocene sedimentary rocks which are underlain by Mawgyi or probably equivalent Ngapyaw-dawchaung basalts. The basaltic rocks may form a structural high and suggest that the veins in the Mawgyi metallotect are also post-Eocene. Antimony deposits (e.g. Lebyin, and Thabyu near Moulmein) are associated with quartz-pyrite alteration zones implying epithermal systems, and occur in or on anticlinal uplifts within Late Palaeozoic sedimentary carbonaceous host rocks situated behind the Popa-Loimye Arc.

Porphyritic quartz andesites and adjacent sedimentary rocks host the ca 14 Ma high suphidation epithermal chalcocite-covellite copper deposits at Monywa. Pre-mining reserves

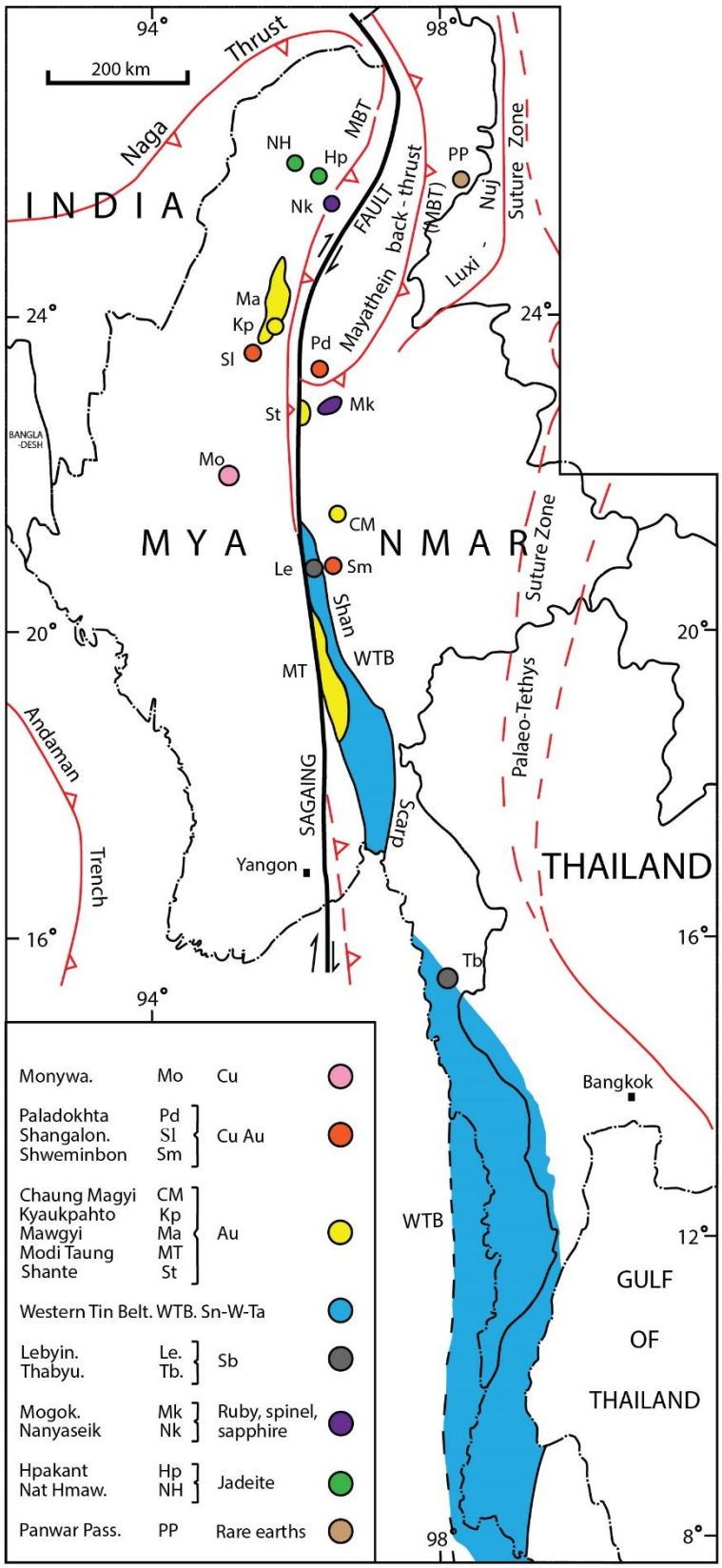

Fig. 11: Map of Myanmar and part of Thailand showing mineral deposits or metallotects and selected regional structural features described in text.

of 7 mt copper are probably the largest of any producing copper mine in Southeast Asia. Minor low sulphidation quartz-gold veins at Monywa are hosted by hornfelsed mud-stones and rhyolites and no older than the copper deposits. Perhaps of similar age are advanced argillic silicic lithocaps at Mt Popa, and north of Pinlebu where they overlie copper mineralisation at depth.

The second-youngest economic minerals are the famous gem-quality ruby and spinel found mainly in the Mogok region and considered to be related to retrograde metamorphism not younger than early Miocene. Here sapphire-bearing nepheline syenite has yielded SIMS U-Pb ages ca 13.5 Ma (Shi et al., 2021). Gemstone formation was succeeded by emplacement of high-grade auriferous veins in the Shante gold district in the Mogok Metamorphic Belt southwest of Mogok, with evidence of both low sulphidation epithermal (e.g. Mitchell, 2017) and orogenic epizonal (e.g. Aung Zaw Myint, Wagner, & Khin Zaw, 2022) gold systems.

6 Conclusions

Our proposed tectonic events include obduction of Neo-Tethyan ophiolite and flysch over the Asian and Victoria-Katha Block margins, ocean closure, back-thrusting in the collision belt and reversal of the E-facing Popo-Loimye Arc. These events while in some cases speculative, provide new and reasonably satisfactory explanations for many aspects of the geology and for some of the major mineral deposits in the region considered. Late Cretaceous closure of Neo-Tethys by southward (now rotated to westward) subduction provides a possible mechanism for transporting the island arc of Westerweel et al. (2019) and Licht et al. (2020), our Popa-Loimye Arc, from mid-Tethys to the Asian margin after 95 Ma.

Our re-interpretation of the Falam Formation melanges suggests the possibility, not explored in this paper, that the Late Cretaceous Falam and Kabaw Formations and Naga flysch are an orogenic flysch deposited in a narrow ocean basin opened between the Indo-Burman Ranges and the Popa- Loimye arc. With basin closure the flysch was expelled westwards before deposition of the Paunggyi Formation began in the mid-Palaeocene.

E-vergent Triassic flysch in northwestern Thailand correlates with that to the northwest, east of the Shan Scarps in Myanmar, and implies a tectonic boundary or overlap with the established W-vergent structures in Thailand's Inthanon Zone to the east. Before its closure in the Late Cretaceous, Neo-Tethys was probably continuous with the Luxi-Nujiang-Bangongco Ocean in Yunnan and Tibet. However our proposed convergent Jurassic subduction zones beneath Neo-Tethys have not yet been reconciled with the widely accepted closure of Tibetan Neo-Tethys by divergent subduction.

Our adoption of interpretations of the Indo-Burman Ranges or Kalemyo ophiolites and radiolarian cherts as the former southwestward continuation of those in the Tagaung-Myitkyina Belt, all relicts of a single Neo-Tethys now offset by dextral displacment on the Sagaing Fault, is not in conflict with the field observations. The reports we cite of the youngest cherts (Lower Cretaceous) in the Tagaung segment of the ocean, younger than those (Upper Jurassic) in the Indo-Burman Ranges segment, neither support nor disprove our interpretation, but do reduce the credibility of the widespread opinion that the suture zone in the Indo-Burman Ranges is younger than that in the Tagaung-Myitkyina Belt.

Acknowledgements

We thank U Htun Lynn Shein for permission to refer to gold and jadeite deposits mined by Myanmar Precious Resources Group. We thank reviewers for suggestions which improved the manuscript, particularly that on the ages of Permian rocks, and for recommending an expansion of the Conclusions.

References

Aitchison, J.C., Aliba, A., Bhowmik, S., Clarke, G.L., Ireland T.R., Kachovich, S., … Zhou, R. (2019). Tectonic evolution of the western margin of the Burma microplate based on new fossil and radiometric age constraints. *Tectonics*, 10.1029/2018TC005049.

Aung Khin & Kyaw Win (1968). Preliminary studies of the palaeogeography of Burma during the Cenozoic. *Union of Burma Journal of Science and Technology*, 2, 53-81.

Aung Zaw Myint, Khin Zaw, Ye Myint Swe, Yonezu, K., Cai, Y., Takayuki, M., & Watanabe, K. (2017). Geochemistry and geochronology of granites hosting the Mawchi Sn-W deposit, Myanmar: implications for tectonic setting and emplacement. In A.J. Barber, Khin Zaw & M.J. Crow (Eds.), *Myanmar: Geology, Resources and Tectonics* (pp. 385-400). London: Geological Society, Memoirs 48.

Aung Zaw Myint, Wagner, T., & Khin Zaw (2022). Telluride-bearing Au-Ag mineralisation in the Singu-Thabeikkyin gold district, Mogok Metamorphic Belt, Myanmar: new constraints on an intermediate sulphidation epizonal orogenic ore system. *Journal of Asian Earth Sciences*, 227. https://doi.org/10.1016/j.jseaes.2022.105120.

Aye Ko Aung (2020). A review of Palaeozoic stratigraphy in the western part of Southern Shan State, Myanmar. In *GeoMyanmar 2020, Fourth International Congress on Geosciences of Myanmar and Surrounding Regions Plus IGCP 668 & IGCP 679 (*pp. 1-4). Yangon: Myanmar Geosciences Society, Abstracts.

Bannert, D., Albert Sang Lyen, & Than Htay (2011). *The Geology of the Indoburman Ranges in Myanmar. Hannover:* Natural History Book Service, Geologisches Jahrbuch, B101, 101pp.

Barber, A.J., Khin Zaw, & Crow, M.J. (2017). The pre-Cenozoic tectonic evolution of Myanmar. In A.J. Barber, Khin Zaw and M.J. Crow (Eds.), *Myanmar: Geology, Resources and Tectonics (*pp. 689-714*).* London: Geological Society, Memoirs 48.

Barley, M.E., Pickard, A.L., Khin Zaw, Rak, P., & Doyle, M.G. (2003). Jurassic to Miocene magmatism and metamorphism in the Mogok metamorphic belt and the India-Eurasia collision in Myanmar. *Tectonics*, 22, 1-11.

Bateson, J.H., Mitchell, A.H.G., & Clark, D.A. (1972). *Geological and Geochemical Reconnaissance of the Seikphyudaung-Padatgyaung Area of Central Burma.* Overseas Division Report No. 25, Institute of Geological Sciences, London: HMSO.

Bender, F. (1983). *Geology of Burma*. Berlin: Borntraeger.

Brunnschweiler, R.O. (1966). On the geology of the Indoburman Ranges. *Journal of the Geological Society, Australia,* 13 (1), 137-194.

Brunnschweiler, R.O. (1970). Contributions to the post-Silurian geology of Burma (Northern Shan States and Karen State). *Journal of the Geological Society, Australia*, 17, 59-79.

Bunopas, S. (1981). *Palaeogeographic History of Western Thailand and Adjacent Parts of South- East Asia: a Plate Tectonics Interpretation*. Geological Survey Paper No. 5 Special Issue, Bangkok: Department of Mineral Resources.

Cai, F., Ding, L., & Yao, W. (2020). Late Triassic palaeogeographic reconstruction along the Neo-Tethyan ocean margins, southern Tibet and Myanmar. In *GeoMyanmar 2020, Fourth International Congress on Geosciences of Myanmar and Surrounding Regions Plus IGCP 668 & IGCP 679 (*p. 39). Yangon: Myanmar Geosciences Society, Abstracts.

Cai, F., Ding, L., Yao, W., Laskowski, A.K., Xu, Q., Zhang, J., & Kyaing Sein (2017). Provenance and tectonic evolution of Lower Palaeozoic-Upper Mesozoic strata from Sibumasu terrane, Myanmar. *Gondwana Research*, 41, 326-66, http://dx.doi.org/10.1016/j.gr.2015.03.005.

Cai, L. & Li, X. (2001). Geology of Yunnan Province. In L. Ma (Ed.), *Geology Atlas of China (*pp. 293-300). Beijing.

Chhibber, H.L. (1934). *The Geology of Burma.* London: Macmillan.

Chonglokmani, C. (2011). Triassic, In M. F. Ridd, A.J. Barber, & M.J. Crow (Eds.), *Geology of Thailand* (pp. 137-150). London: Geological Society.

Chu, Z.Y., Wang, W., Chen, F.K., Wang, X.L., Li, X.H., & Ji, J.Q. (2009). Os-Nd-Pb-Sr isotopic compositions of the Santaishan ultramafic rock in western Yunnan and its geological significances. *Acta Petrologica Sinica*, 25, 3221-3228 (in Chinese with English abstract).

Clegg, E.L.G. (1941). *The Cretaceous and associated rocks of Burma*. Geological Survey of India Memoirs 74, 101p.

Clegg, E.L.G. (1944). *Bulletin No 15. Notes on Tin and Wolfram with a Description of the Tin and Wolfram Deposits of India and Burma.* Kolkata: Geological Survey of India, Records, 76, 120 p.

Cobbing, E.J. (2011). Granitic rocks. In M.F. Ridd, A.J. Barber, & M.J. Crow (Eds.), *Geology of Thailand* (pp. 441-457). London: Geological Society.

Cobbing, E.J., Pitfield, P.E.J., Derbyshire, D.P.F., & Mallick, D.I.J. (1992). *The Granites of the Southeast Asian Tin Belt.* British Geological Survey, Overseas Memoir, 10 (pp.369). London: HMSO.

Deng, J., Wang, Q., Li, G., Li, C., & Wang, C. (2014). Tethys tectonic evolution and its bearing on the distribution of important mineral deposits in the Sanjiang region, SW China. *Gondwana Research,* 26, 419-37.

Dutt, A.B. (1942). *The Mineral Resources of the Shan Scarps included in the Kyaukse, Meiktila and*

Yamethin districts and the Yengan State. Geological Survey of India, Records, 77, Pref. Paper 10, 55 p.

Evans, P. (1964). The tectonic framework of Assam. *Journal of the Geological Society of India*, 5**,** 80-96.

Gardiner, N.J., Robb, L.J., & Searle, M.J. (2014). The metallogenic provinces of Myanmar. *Transactions of the Institution of Mining & Metallurgy*, B 123 (1), 25-38. https://doi.org/10.1179/1743275814Y.0000000049.

Gardiner, N.J., Robb, L.J., Morley, C.K., Searle, M.P. , Cawood, P.A., Whitehouse, M.J., … Tin Aung Myint (2016). The tectonic and metallogic framework of Myanmar: a Tethyan mineral system. *Ore Geology Reviews*, 79, 26-45.

Gardiner, N.J., Searle, M.P., Morley, C.K., Robb, L.J., Whitehouse, M.J., Roberts, N.M.W., …Spencer, C.J. (2018). The crustal architecture of Myanmar imaged through zircon Pb, Lu-Hf and O isotopes: tectonic and metallogenic implications. *Gondwana Research*, https://doi.org/10.1016/j.gr.2018.02.008.

Garson, M.S., Amos, B.J., & Mitchell, A.H.G. (1976). *The Geology of the area around Neyaungga and Ye-ngan, Southern Shan States, Burma*. Institute of Geological Sciences, Overseas Division, Memoir 2. London: HMSO.

Gramman, F. (1974). Some palaeontological data on the Triassic and Cretaceous of the western part of Burma (Arakan Islands, Arakan Yoma, western outcrops of Central Basin). *Newsletter Stratigraphy*, 3, 272-290.

Hobson, G.V. (1941). *Report on a Geological Survey in Part of Karenni and Southern Shan State*. Geological Survey of India, Memoir, 74, Part 2, 103--209.

Iyer, L.A.N. (1953). *The geology and gemstones of the Mogok stone tract, Burma.* Geological Survey of India Memoir, 82, 100.

Javanaphet, J.C. (1969*). Geological Map of Thailand, Scale1:1,000,000.* Bangkok: Department of Mineral Resources.

Jiang, H., Li, W.Q., Jiang, S.Y., Wang, H., & Wei, X.P. 2017. Geochronological, geochemical and Sr-Nd-Hf isotopic constraints on the petrogenesis of late Cretaceous A-type granites from the Sibumasu block, southern Myanmar. *Lithos*, 268-271, 32-47, https://doi.org/10.1016/j.lithos.2016.11.005.

Jin, X. (1996). Tectono-Stratigraphic Units of Western Yunnan, China and their counterparts in Southeast Asia. *Continental Dynamics*, 1, 12-133.

Kyaw Linn Zaw, Ohn Thwin, Travnor, J., & Thet Paing Kyaw Win (2020). Origin and evolution of the ore-forming fluids in Shwesin Vein System, central Myanmar: constraints from structure, wall rock alteration and mineral chemistry. In *GeoMyanmar 2020, Fourth International Conference on Geosciences of Myanmar and Surrounding Regions Plus IGCP 668 & IGCP 679 (*p.78). Yangon: Myanmar Geosciences Society, Abstracts.

Kyi Pyar Aung, Owens, R., & Metcalfe, I. (2014). New evidence of the Carboniferous age of the Taungnyo Group exposed in the Loikaw area , Kayah State. In Win Swe, Soe Thura Tun, Myo Thant, & Khin Zaw (Eds.), *Geomyanmar 2014, GEOSEA 13, Thirteenth Regional Congress on Geology, Mineral and Energy Resources of Southeast Asia (*pp.34-35*).* Yangon: Myanmar Geosciences Society, Abstracts

Lamont, T.N., Searle, M.P., Hacker, B.R., Kyi Htun, , Kyaw Min Htun, Morley, C.K., …White, R.W. (2021). Late Eocene-Oligocene granulite facies garnet-sillimanite migmatites from the Mogok Metamorphic belt, Myanmar, and implications for timing of slip along the Sagaing Fault. *Lithos*, https://doi.org/10.1016/j.lithos.2021.106027.

Lee, H.Y., Chung, S.L., & Yang, H.-M. (2016). Late Cenozoic volcanism in central Myanmar: geochemical characteristics and geodynamic significance. *Lithos*, 245, 174-190.

Leicester, P. (1930). Geology of Amherst District. Geological Survey of India, Records, 63, 1.

Li, J-X, Fan, W-M, Zhang, L-Y, Evans, NJ, Sun, Y-L, Ding, I, … Kyaing Sein (2019). Geochronology, geochemistry and Sr-Nd-Hf isotopic compositions of Late Cretaceous-Eocene granites in southern Myanmar: petrogenetic, tectonic and metallogenic implications. *Ore Geology Reviews*, 112, 1-16.

Li, J.X., Fan, W.M., Zhang, L.Y., Peng, T.P., Sun, Y.L., Ding, L., … Kyaing Sein (2020). Prolonged Neo-Tethyan magmatic arc in Myanmar: evidence from geochemistry and Sr-Nd-Hf isotopes of Cretaceous mafic-felsic intrusions in the Banmauk-Kawlin area. *International Journal of Earth* Sciences https://doi.org/10.1007/s00531-020-01824-w.

Li, J.X., Zhang, L.Y., Fan, W.M., Ding, L., Sun, Y.L.,Peng, T.P….Kyaing Sein (2018). Mesozoic-Cenozoic tectonic evolution and metallogeny in Myanmar: evidence from zircon/ cassiterite U-Pb and molybdenite Re-Os geochronology. *Ore Geology Reviews*, 102, 829-845. https://doi.org/10.1016/j.oregeorev.2018.10.009.

Licht, A., Zaw Win, Westerweel, J., Cogne, N., Morley, C.K., Chantraprasert, S., … Dupont-Nivet, G. (2020). Magmatic history of central Myanmar and implications for the evolution of the Burma Terrane. *Gondwana Research*, 87, 303-319.

Lin, T.H., Mitchell, A.H.G., & Chung, S.L. (2019). Early Cretaceous Mondaung-Lawa arc in Myanmar and its plausible correlation with Yunnan. In *Goldschmidt 2019, Poster Presentation*, Abstract.

Liu, C.Z., Chung, S.L., Wu, F.Y., Zhang, C., Xu, Y., Wang, J.G….. Guo, S. (2016). Tethyan suturing in

Southeast Asia: zircon U-Pb and Hf-0 isotopic constraints from Myanmar ophiolites. *Geology*, 44, 311-314.

Maung Maung, Aung Naing Thu, & Suzuki, H. (2014). Latest Jurassic radiolarian fauna from the Chinghkran area, Myitkyina Township, Kachin State, northern Myanmar. In Win Swe, Soe Thura Tun, Myo Thant and Khin Zaw (Eds.), *GeoMyanmar 2014, GEOSEA 13, Regional Congress on Geology, Mineral and Energy Resources of Southeast Asia (*pp. 38-39). Yangon: Myanmar Geosciences Society, Abstracts,

Metcalfe, I. (1984). Stratigraphy, palaeontology and palaeogeography of the Carboniferous of Southeast Asia. *Memoires de la Society Geologue de France*, 147, 107-118.

Metcalfe, I. (2011). Mesozoic history of SE Asia. In R. Hall, M.A. Cottam, & M.E.J. Wilson (Eds.), *The SE Asian Gateway: History and Tectonics of the Australia-Asia Collision*. Special Publications, 355, 7-35, http://dx.doi.org/10.1144/SP355.2. London: Geological Society.

Metcalfe, I. (2013). Gondwana dispersion and Asian accretion: tectonic and palaeogeographic evolution of eastern Tethys. *Journal of Asian Earth Sciences*, 66, 1-33.

Metcalfe, I., & Kyi Pyar Aung (2014). Late Tournaisian conodonts from the Taungnyo Group near Loi Kyaw, Myanmar (Burma): implications for Shan Plateau stratigraphy and evolution of the Gondwana-derived Sibumasu terrane. *Gondwana Research,* 26, 1159-1172.

Mi Paik & Khin Zaw (2014). Age, petrology and geochemistry of granitoid rocks in the Mawpalaw Taung area, Thanbyuzayat Township: constraints on their magma genesis and tectonic setting. In Win Swe, Soe Thura Tun, Myo Thant, and Khin Zaw (Eds.), *GeoMyanmar 14, GEOSEA 13, Regional Congress on Mineral and Energy Resources of Southeast Asia (*pp. 54-55). Yangon, Myanmar Geosciences Society, Abstracts.

Mitchell, A.H.G. (1977). Tectonic settings for emplacement of Southeast Asian tin granites. *Geological Society of Malaysia Bulletin*, 9, 123-140.

Mitchell, A.H.G. (1979). Guides to Metal Provinces in the Central Himalayan Collision Belt; the Value of Regional Stratigraphic Correlations and Tectonic Analogies. *Geological Society of China, Memoir* no.3, 167-194.

Mitchell, A.H.G. (1984). Post-Permian events in the Zangbo 'suture' zone, Tibet. *Journal of the Geological Society of London*, 141, 129-136.

Mitchell, A.H.G. (1986). Mesozoic and Cenozoic regional tectonics and metallogenesis in mainland SE Asia. In *GEOSEA V Proceedings, vol.II.* (pp. 221--239). Geological Society of Malaysia Bulletin, 20.

Mitchell, A.H.G. (2017). *Geological Belts, Plate Boundaries and Mineral Deposits in Myanmar*. Amsterdam: Elsevier.

Mitchell, A.H.G., & Garson, M.S. (1981). *Mineral Deposits and Global Tectonic Settings.* London: Academic Press.

Mitchell, A.H.G., Young, B., & Jantaranipa, W. (1970). The Phuket Group, Peninsular Thailand: a Palaeozoic? geosynclinal deposit. *Geological Magazine*, 107, 411-428.

Mitchell, A.H.G., Ausa, C.A., Deiparine, L., Tin Hlaing, Nyunt Htay, & Aung Khine (2004). The Modi Taung-Nankwe gold district, Slate belt, central Myanmar: mesothermal veins in a Mesozoic orogen. *Journal of Asian Earth Sciences*, 23, 321-341.

Mitchell, A.H.G., Tin Hlaing, & Nyunt Htay (2010). The Chin Hills segment of the Indo-Burman Ranges: not a simple accretionary wedge. In S. Ibotomboi (Ed.), *Indo-Myanmar Ranges in the Tectonic Framework of the Himalaya and Southeast Asia (*pp. 3-24). Golden Jubilee Volume, Memoir No 75, Bangalore: Geological Society of India.

Mitchell, A.H.G., Chung, S.L., Thura Oo, Lin, T.H., & Hung, C.H. (2012). Zircon U-Pb ages in Myanmar: metamorphic events and the closure of a neo-Tethys ocean? *Journal of Asian Earth Sciences*, 56, 1-23.

Mitchell, A.H.G., Myint Thein Htay, & Kyaw Min Htun (2018). The Popa-Loimye arc, its mineralisation and arc reversal. In *GeoMyanmar 2018, Third International Congress on Geology, Resources, Geohazards of Myanmar and Surrounding Regions (*p.6). Yangon: Myanmar Geosciences Society, Abstracts.

Mitchell, A.H.G., Kyaw Min Htun, & Myint Thein Htay (2020). Mondaung-Lawa and Popa-Loimye arcs and other belts, their mineral deposits and other settings. In *GeoMyanmar 2020, Fourth International Congress on Geosciences of Myanmar and Surrounding Regions Plus IGCP 668 & IGCP 679 (*pp. 5-7). Yangon: Myanmar Geosciences Society, Abstracts.

Mitchell, A., Myint Thein Htay, & Kyaw Min Htun (2021). Middle Jurassic arc reversal, Victoria- Katha Block and Sibuma Terrane collision, jadeite formation and Western Tin Belt generation, Myanmar. *Geological Magazine* https://doi.org/10.1017/.S0016756821000066.

Mo, X.X., Lu, F.X., & Shen, S.Y. (1993*). Sanjiang Tethyan Volcanism and Related Mineralisation*. Beijing: Geological Publishing House, in Chinese with English Abstract.

Morley, C.K., & Arboit, F. (2019). Dating the onset of motion on the Sagaing Fault: evidence from detrital zircon and titanite U-Pb geochronology from the North Minwun Basin, Myanmar. *Geology*, 47, 581--585.

Morley, C.K., Chantraprasert, S., Kongchum, J., & Chenoll, K. (2021). The West Burma Terrane, a review of recent palaeo-latitude data, its geological implications and constraints. *Earth-Science Reviews*, 220, 1-16. htpps://doi.org/10.1016/.earseirev.2021. 103722.

Myanmar Geosciences Society (2014*). Geological Map of Myanmar (2014), 1:2,250,000.* Yangon*:* Myanmar Geosciences Society.

Myint Myat Phyo, Wang, H.A.O, Guillong, M., Berger, A., Franz, L., Balmer, W.A., & Krzemnicki, M.S. (2020). U-Pb dating of zircon and zirconlite inclusions in marble-hosted gem-quality ruby and spinel from Mogok, Myanmar. *Minerals*, 10, 195, doi:10.3390/min10020195.

Myint Thein (2015). The Pre-Tertiary carbonate rocks exposed at the NE margin of the Central Myanmar Basin and their developmental history. *Journal of the Myanmar Geosciences Society*, 6, 1-26.

Myint Thein & Maung Thein (2014). The Eastern Basin of Central Myanmar: its basement rocks, lithostratigraphic units, palaeocurrents, provenance and development history. In Win Swe, Soe Thura Tun, Myo Thant, and Khin Zaw *(*Eds.), *GeoMyanmar 2014*, *GEOSEA 13*, *Regional* C*ongress on Geology, Mineral and Energy Resources of Southeast Asia* (pp.41-42). Yangon: Myanmar Geosciences Society, Abstracts.

Oliver, G.J.H., Zaw, K., Hotson, M.D., Meffre, S., and Manaka, T. (2014). U-Pb zircon geochronology of Early Permian to Late Triassic rocks from Singapore and Johor: a plate tectonic re-interpretation. *Gondwana Research*, 26, 132-143.

Peng, S., Peng, T., Fan, W., Zhao, G., Dong, X., Liu,Y.,…Me Me Aung (in press). Initial opening of the Neotethyan Ocean in SE Asia: constraints from Triassic magmatism and sedimentation. *Geological Society of America Bulletin.*

Pivnic, D.A., Nahm, J., Tucker, R.S., Smith, G.O., Nyein, K., Nyunt, M., & Maung, P.M. (1998). Polyphase deformation in a fore-arc/ back-arc basin, Salin Sub-basin, Myanmar (Burma). *American Association of Petroleum Geologists Bulletin*, 82, 1837-1856.

Raksaskulong, L., & Wongwanich, T. (1993). *Stratigraphy of the Kaeng Krachan Group in Peninsular and Western Thailand*. Geological Survey Division, Bangkok: Department of Mineral Resources (in Thai).

Ridd, M.F. (2016). Should Sibumasu be renamed Sibuma? The case for a discrete Gondwana- derived block embracing western Myanmar, upper Peninsular Thailand and NE Sumatra. *Journal of the Geological Society, London*, 173, 249-264.

Ridd, M.F. (2017a). Karen-Tenasserim Unit. In A.J. Barber, Khin Zaw & M.J. Crow (Eds.), Myanmar: Geology, Resources and Tectonics, Memoir 48 (pp. 365-384). London: Geological Society.

Ridd, M.F. (2017b). Central Burma Depression and Its Petroleum occurrences. In Mitchell, A.H.G., *Geological Belts, Plate Boundaries and Mineral Deposits in Myanmar* (pp. 325-341). Amsterdam: Elsevier.

Sanematsu, K., Manaka, T., & Khin Zaw (2014). Geochemical and geochronological charactersistics of granites and Sn-W-REE mineralisation in the Tanintharyi region, southern Myanmar. In Win Swe, Soe Thura Tun, Myo Thant, and Khin Zaw (Eds.), *GeoMyanmar 14, GEOSEA 13, Regional Congress on Geology, Mineral and Energy Resources of Southeast Asia* (pp.19-20). Yangon*:* Myanmar Geosciences Society, Abstracts.

Searle, D.I. & Ba Than Haq (1964). The Mogok belt of Burma and its relationship to the Himalayan orogeny. In *Proceedings of the 22nd International Geological Conference* 11, pp.132-161, Delhi.

Searle, M.P., Garber, J.M., Hacker, B.R., Kyi Htun, Gardiner, N.J., Waters, D.J. & Robb, L.J. (2020). Timing of syenite-charnockite magmatism and ruby and sapphire metamorphism in the Mogok Valley region, Myanmar. *Tectonics*, 10.1029/2019TC00 5998.

Shi, G., Zhang, X., Wang, Y., Li, Q., Wu, F., and He, H. (2021). Age determination of oriented rutile inclusions in sapphire and moonstone from the Mogok metamorphic belt, Myanmar. *American Mineralogist*, 106, 1852-1859.

Stephenson, D. & Marshall, T.R. (1984). The petrology and mineralogy of Mt Popa Volcano and the nature of the late-Cenozoic Burma Volcanic Arc. *Journal of the Geological Society of London*, 141, 747-762.

Sukto, P., Suteethorn, V., Boripatgosol, S., Meesok, A. & Sareerat, S. (1984). *Geologic Map of Moulmein (Sheet NE 47-14, Scale 1:250,000*). Geological Survey Division, Department of Mineral Resources, Bangkok.

Tainsh, H.R. (1950). Tertiary geology and principle oilfields of Burma. *Bulletin of the American Association of Petroleum Geologists*, 34, 823-855.

Teza Kyaw, Suzuki, H. & Maung Maung (2020). Radiolarian ages of the That-Tu bedded chert of Tagaung area with respect to the oceanic plate stratigraphy. In *GeoMyanmar 2020, Fourth International Congress on Geosciences of Myanmar*

*and Surrounding Regions Plus IGCP 668 & IGCP 679 (*pp. 64-65). Yangon: Myanmar Geosciences Society, Abstracts.

Theobald, W. (1871). The Axial Group in western Prome, British Burma. *Geological Survey of India, Records*, 4, 33-44.

Thet Paung Kyaw Win, Hla Kyi & Kyaw Linn Zaw (2020). Petrological and geochronological characteristics of migmatites at Kyaikkhami-Setse Township, Mon State, Myanmar. In *Geo- Myanmar 2020, Fourth lnternational Congress on Geosciences of Myanmar and Surrounding Regions Plus IGCP 668 & IGCP 679 (*p.77). Myanmar Geosciences Society, Abstracts.

Thura Oo, Tin Hlaing, & Nyunt Htay (2002). Permian of Myanmar. *Journal of Asian Earth Sciences*, 20, 683-689.

Ueno, K. & Charoentitirat, T. (2011). Carboniferous and Permian. In M.F. Ridd, A.J. Barber & M.J. Crow (Eds.), *The Geology of Thailand* (pp. 71-136). London: Geological Society.

United Nations (1978a). *Geology and Mineralisation of the Shangalon Copper Prospect and Surroundings, Technical Report No.1*. Geological Survey and Exploration Project, United Nations Development Programme, DP/UN/BUR-72-002, New York: United Nations.

United Nations (1978b). *Geology and Exploration Geochemistry of the Pinlebu-Banmauk area, Sagaing Division, northern Burma, Technical Report No. 2.* Geological Survey and Exploration Project, United Nations Development Programme, DP/UN/BUR-72-002, 69 p., New York: United Nations.

United Nations (1979a). *Geology and Exploration Geochemistry of Part of the Northern and Southern Chin Hills and Arakan Yoma, Western Burma, Technical Report No. 4.* Geological Survey and Exploration Project, United Nations Development Programme, DP/UN/BUR-72-002, 59 p., New York: United Nations.

United Nations (1979b). *Mineral Exploration in Selected Areas, Burma, Technical Report No.6.* Geological Survey and Exploration Project, United Nations Development Programme, DP/UN/BUR-72-002, 86p., New York: United Nations.

United Nations (1979c). *Geological Mapping and Geochemical Exploration in Mansi-Manhton, Indaw-Tigyaing, Kyindwe-Longyi, Patchaung-Yane and Yezin Areas, Burma, Technical Report No.16.* Geological Survey and Exploration Project, United Nations Development Programme, DP/UN/ BUR-72-002, 13 p., New York: United Nations.

United Nations (1979d). *Geology and Exploration Geochemistry of the Salingyi-Shinmataung area, Central Burma, Technical Report No. 5*. Geological Survey and Exploration Project, United Nations Development Programme, UN/BUR-72-002, 38 p., New York: United Nations.

United Nations (1979e). *Geology and Exploration Geochemistry of the Shan Scarps area, east of Kyaukse, Thazi and Tatkon, central Burma, Technical Report No. 3*. Geological Survey and Exploration Project, United Nations Development Programme, DP/UN/BUR-72-002, 68 p., New York: United Nations.

Wang, C., Deng, J., Carranza, E.J.M., & Santosh, M. (2014). Tin metallogenesis associated with granitoids in the southwestern Sanjiang Tethyan Domain: nature, deposit types and tectonic setting. *Gondwana Research*, 26, 576-593.

Wang, X.-D., Hu, K.-Y, Shi, Y.-K., Chen, J.-T., Yang, S.-R., Ye, X.- Y.,… Shen, S.-Z. (2021). The missing upper Carboniferous in the Cimmerian continent: a critical review. *Earth Science Reviews*, 217, 103627.

Westerweel, J., Roperch, P., Licht, A., Dupont-Nivet, G., Zaw Win, Poblete, F.,… Day Wa Aung (2019). Burma Terrane part of the Trans-Tethyan arc during collision with India according to palaeomagnetic data. *Nature Geoscience*, https:/doi.org/10.1038/s41561-019-0443-2.

Win Swe, Thacpaw, C., & Nay Thaung Thaung (2010). Upper Cretaceous fossils from the lower part of the Western Outcrops of the Chindwin Basin, Central Myanmar Belt. *Journal of the Myanmar Geosciences Society, 3*, 20-32.

Yang, J.S., Xu, Z.Q., Duan, X.D., Li, J., Xiong, F.H., Liu, Z…., Li, H.Q. (2012). Discovery of a Jurassic SSZ ophiolite in the Myitkyina region of Myanmar. *Acta Petrologica Sinica*, 28, 1710-1730.

Yang, L., Xiao, W., Rahman, M.J.J., Windley, B.F., Schulman, K., Ao, S.,… Dong, Y. (2020). Indo-Burma passive amalgamation along the Kaladan Fault: insights from zircon provenance in the Chittagong-Tripura Fold Belt (Bangladesh). *Geological Society of America Bulletin*, https://dog.org/10.1130/B35429.1.,

Ye Myint Swe, Cho Cho Aye & Khin Zaw (2017). Gold deposits of Myanmar. In A.J. Barber, Khin Zaw and M.J. Crow (Eds.*), Myanmar: Geology, Resources and Tectonics.* Geological Society, London, Memoir 48.

Zhang, J.E., Xiao, W.J., Windley, B., Cai, F.L., Kyaing Sein, & Naing, S. (2017). Early Cretaceous wedge extrusion in the indo-Burma Range accretionary complex: implications for the Mesozoic subduction of Neotethys in SE Asia. *International Journal of Earth Sciences*, 106, 1391-1408.

Zhang, J., Xiao, W., Windley, B.F., Wakabayashi, J., Cai, F., Kyaing Sein, & Soe Naing (2018). Multiple

alternating forearc and backarc-ward migration of magmatism in the Indo-Myanmar Orogenic Belt since the Jurassic: documentation of the orogenic architecture of eastern NeoTethys in SE Asia. *Earth Science Reviews*, 185, 704-731.

Zhang, J., Xjao, W., Cai, F., & Kyaing Sein (2020). Wedge extrusion in the Indo-Burma Range accretionary complex and implication for orogenic architecture of Neo-Tethys in SE Asia. In *GeoMyanmar 2020, Fourth International Congress on Geosciences of Myanmar and Surrounding Regions plus IGCP 668 & IGCP 679 (*p. 46). Myanmar Geosciences Society, Abstracts.

Zhong, D. & Zhao, J. (2000). The Changing-Menglian tectonic belt. In D. Zhong (Ed.), *Palaeo-Tethysides* (pp. 122-123). Beijing: Science Press.

THAI GEOSCIENCE JOURNAL

If you are interested in earth sciences
Support geoscience with a subscription to

Thai Geoscience Journal

The **Thai Geoscience Journal** publishes original research
And review articles from the international community in all
Fields of geological sciences such as

- Engineering Geology
- Petrology
- Paleontology
- Economic Geology
- Geophysics
- Tectonics
- Structural Geology
- Geochemistry

All articles published by the **Thai Geoscience Journal**
are made freely and permanently accessible online
Immediately upon publication, **without subscription charges or registration barriers.**

Please scan for

VISIT US

ARTICLES SUBMISSION

SUBSCRIPTION TO TGJ

AND MORE INFORMATION

Contact
Mineral Resources Research and Development Center
Department of Mineral Resources 75/10 RAMA VI Road,
Ratchatewee, Bangkok 10400 Phone: +66 2-6219731
Website : https://www.dmr.go.th/tgjdmr/
E-mail : tgj.2020@gmail.com

Published by

CONCEPT DESIGN

This logo composes of Abbreviations of Thai Geoscience Journal

T = THAI G = GEOSCIENCE J = JOURNAL

Coexistence of 3 abbreviations design in a concept of modernity blend with a Thainess
Modification of G alphabet in a shape of ammonoid shows relevance to geology
and infinite development of Thai Geoscience Journal

- **SCOPE AND AIM OF THAI GEOSCIENCE JOURNAL (TGJ):** TGJ is an international (Thai and English) journal publishing original research articles dealing with the geological sciences. It focuses, mainly but not exclusively, on: Sedimentology and Geomorphology, Palaeontology, Quaternary, Geology and Environment Change, Geological Hazards, Environmental Geosciences, Geophysics, Mineral and Petroleum Geology, Tectonics and Structural Geology, Geochemistry and Geochronology, Metamorphic Geology and Volcanic and Igneous Geology. Two types of articles are published in the Journal: Research Articles and Reviews. Research Articles are new original articles, normally not exceeding 25 pages. Review Articles are those papers that summarize the current state of knowledge on specific fields or topics of geosciences. They analyze and discuss previously published research results, rather than report new results. TGJ Aim is to provide valuable geoscience knowledge and information and push more inspiration for readers and researchers to produce treasure research in the future.
- **FEEDBACK AND CONTACT:** We welcome your feedback, comments and suggestions for the development of TGJ

Please contact: Dr. Apsorn Sardsud (Editor-in-Chief, TGJ)
Department of Mineral Resources
75/10 RamaVI Road Ratchathewee Bangkok 10400, Thailand

Phone: +66 (0)2 6219731

Email: tgj.2020@gmail.com

Website: http://www.dmr.go.th/tgjdmr

TGJ Contributors

Assoc. Prof. Dr. Apichet Boonsoong	Chiang Mai University, Thailand
Dr. Apsorn Sardsud	Department of Mineral Resources, Thailand
Prof. Dr. Che Aziz bin Ali	Universiti Kebangsaan Malaysia, Malaysia
Prof. Dr. Clive Burrett	Mahasarakham University, Thailand
Assoc. Prof. Dr. Danupon Tonnayopas	Prince of Songkla University, Thailand
Dr. Dhiti Tulyatid	Coordinating Committee for Geoscience Programmes in East and Southeast Asia (CCOP), Thailand
Dr. Ian Watkinson	University of London, England
Mr. Jittisak Premmanee	Department of Mineral Resources, Thailand
Prof. Dr. Katsumi Ueno	Fukuoka University, Japan
Prof. Dr. Katsuo Sashida	Mahidol University, Kanchanaburi campus, Thailand
Prof. Dr. Ken-Ichiro Hisada	University of Tsukuba, Japan
Assoc. Prof. Dr. Kieren Howard	Kingsborough Community College, City University of New York, USA
Prof. Dr. Koji Wakita	Yamaguchi University, Japan
Assoc. Prof. Dr. Kriengsak Srisuk	Khon Kaen University, Thailand
Assoc. Prof. Dr. Lindsay Zanno	North Carolina State University, USA
Dr. Mallika Nillorm	Department of Mineral Resources, Thailand
Dr. Martin Smith	Global Geoscience, British Geological Survey, UK
Adj. Prof. Dr. Michael Ryan King	Western Colorado University, Thailand
Prof. Dr. Montri Choowong	Chulalongkorn University, Thailand
Assoc. Prof. Dr. Mongkol Udchachon	Mahasarakham University, Thailand
Prof. Dr. Nigel C. Hughes	University of California, Riverside, USA
Mr. Niwat Boonnop	Department of Mineral Resources, Thailand
Asst. Prof. Nussara Surakotra	Khon Kaen University, Thailand
Asst. Prof. Dr. Passkorn Pananont	Kasetsart University, Thailand
Dr. Phumee Srisuwan	Department of Mineral Fuels, Thailand
Prof. Dr. Pitsanupong Kanjanapayont	Chulalongkorn University, Thailand
Dr. Pol Chaodumrong	Geological Society of Thailand, Thailand
Dr. Pradit Nulay	Department of Mineral Resources, Thailand
Dr. Prinya Putthapiban	Mahidol University Kanchanaburi Campus, Thailand
Prof. Dr. Punya Charusiri	Department of Mineral Resources, Thailand
Asst. Prof. Dr. Rattanaporn Hanta	Suranaree University of Technology, Thailand
Assoc.Prof. Rungruang Lertsirivorakul	Khon Kaen University, Thailand
Assoc. Prof. Dr. Sachiko Agematsu-Watanabe	University of Tsukuba, Japan
Dr. Sasiwimol Nawawitphisit	Department of Mineral Resources, Thailand
Dr. Seung-bae Lee	Korea Institute of Geoscience and Mineral Resources, Republic of Korea
Dr. Siriporn Soonpankhao	Department of Mineral Resources, Thailand
Asst. Prof. Dr. Sombat Yumuang	Geo-Informatics and Space technology Development Agency, Ministry of Science and Technology (GISTDA), Thailand
Mr. Somchai Chaisen	Department of Mineral Resources, Thailand
Dr. Surin Intayos	Burapha University, Chanthaburi Campus, Thailand
Mr. Sutee Chongautchariyakul	Department of Mineral Resources, Thailand
Dr. Tawatchai Chualaowanich	Department of Mineral Resources, Thailand
Mr. Thananchai Mahatthanachai	Department of Mineral Fuels, Thailand
Assoc. Prof. Dr.Thasinee Charoentitirat	Chulalongkorn University, Thailand
Dr. Toshihiro Uchida	Retired geophysicist, Japan
Mr.Tritip Suppasoonthornkul	Department of Mineral Fuels, Thailand
Dr. Weerachat Wiwegwin	Department of Mineral Resources, Thailand
Assoc. Prof. Dr. Yoshihito Kamata	University of Tsukuba, Japan

Thai Geoscience Journal
Vol. 3 No. 4
July 2022
ISSN 2730-2695

CONTENTS

Published by
Department of Mineral Resources
Geological Society of Thailand
Coordinating Committee for Geoscience Programmes in East And Southeast Asia (CCOP)